論文 / 著書情報
Article / Book Information

題目(和文)	
Title(English)	Control of the Magnetic Properties by Nitrogen Incorporation in CoPt Layers of CoPt/TiN Heterostructures
著者(和文)	ペトルスカエサリオ
Author(English)	Petrus Caesario
出典(和文)	学位:博士(工学), 学位授与機関:東京工業大学, 報告番号:甲第11287号, 授与年月日:2019年9月20日, 学位の種別:課程博士, 審査員:史 蹟,中村 吉男,須佐 匡裕,木村 好里,林 幸,中川 茂樹
Citation(English)	Degree:Doctor (Engineering), Conferring organization: Tokyo Institute of Technology, Report number:甲第11287号, Conferred date:2019/9/20, Degree Type:Course doctor, Examiner:,,,,,
学位種別(和文)	博士論文
Type(English)	Doctoral Thesis

TOKYO INSTITUTE OF TECHNOLOGY

DOCTORAL THESIS

Control of the Magnetic Properties by Nitrogen Incorporation in CoPt Layers of CoPt/TiN Heterostructures.

Author:
Petrus CAESARIO

Supervisor:
Prof. Ji SHI
Prof. Yoshio NAKAMURA

A thesis submitted in fulfillment of the requirements for the degree of
Doctor of Engineering
in the

Nakamura-Shi Laboratory
School of Materials and Chemical Technology

August 19, 2019

Declaration of Authorship

I, Petrus CAESARIO, declare that this thesis titled, "Control of the Magnetic Properties by Nitrogen Incorporation in CoPt Layers of CoPt/TiN Heterostructures." and the work presented in it are my own. I confirm that:

- This work was done wholly or mainly while in candidature for a research degree at this University.
- Where any part of this thesis has previously been submitted for a degree or any other qualification at this University or any other institution, this has been clearly stated.
- Where I have consulted the published work of others, this is always clearly attributed.
- Where I have quoted from the work of others, the source is always given. With the exception of such quotations, this thesis is entirely my own work.
- I have acknowledged all main sources of help.
- Where the thesis is based on work done by myself jointly with others, I have made clear exactly what was done by others and what I have contributed myself.

Signed:

_____

Date:

_____

TOKYO INSTITUTE OF TECHNOLOGY

Abstract

Faculty Name

School of Materials and Chemical Technology

Doctor of Engineering

Control of the Magnetic Properties by Nitrogen Incorporation in CoPt Layers of CoPt/TiN Heterostructures.

by Petrus CAESARIO

This study focuses on the fabrication of magnetic recording media oriented CoPt thin films with perpendicular magnetic anisotropy and ease of writability. It has been found that Nitrogen gas incorporation during the deposition leads to an improvement in perpendicular coercivity by magnitude of 10 and the reduction in ordering temperature by 200 ^{o}C. The increased number of vacancies inside the CoPt lattice is believed to be improving the diffusion speed of Co and Pt atoms during the ordering transformation. On the other hand, when depositing CoPt films on TiN/MgO(100) underlayer, a good PMA has been observed at 400 ^{o}C. It has been assumed that the lattice mismatch between TiN and CoPt strains the lattice of A1-CoPt, breaking the symmetry and giving rise to high PMA. Finally, by coupling a magnetically soft CoPt layer on top of the magnetically hard CoPt layer, a 50% reduction in switching field has been achieved in a relatively simple equipment. This study shows a good method to manufacture CoPt films for future high density magnetic recording media.

Acknowledgements

I would like to express my deepest gratitude to my professor and mentor, Ji Shi, who had guided and tutored me throughout my doctoral study. Thank you for agreeing to be my mentor and letting me learn in his laboratory. Your kindness and care for your students are remarkable and I thank you for giving me a a place to study in one of the most prestigious universities in Japan which helped me a lot in getting in the Scholarship Program in Japan. It is an honour to be supervised by you and I thank you for giving me the best experience in research in your laboratory.

Special thanks to my supervisor, Professor Yoshio Nakamura. Your deep knowledge on microstructure analysis of crystal helped me realizes many things and develop new methods for experiments. Your kindness during the seminar and helpful input also made me able to complete this work on time.

I would also like to express my sincere thank to Associate Professor Takashi Harumoto. Your attention and efforts to spend the extra hours just to teach me everything from the basic and showed me the steps are the reason I can finish this thesis on time and with good results. I would never be able to learn so much during my study without your help.

Last but not least, I want to thank my family, my friends, all my lecturers, and my best friend Happy Permatasari. Without all your support, kindness, and effort, I would not be able to attend this university and experience an excellent level of education.

Contents

List of Figures

List of Tables

Chapter 1

Introduction

1.1 Hard Disk Drives

In the last five decades, hard disk drive (HDD) is the main storage device for computers. A remarkable development in HDD had seen its areal density increases significantly in the late 1990s, doubling the areal density per year. Until 2003, the areal density has multiplied by eight while the cost per bit has dropped to almost one eighth of the original price. This has made the production of smaller HDDs with large capacity at a cheap cost possible. Consequently, HDD found its way into smaller electronics devices such as MP3 players, digital cameras, portable game consoles, and many other devices. Even though the introduction of flash memory has shaved the use of HDD in low capacity electronic devices, the increase of information data with the popularity of cloud storage opens up a new growth area for HDD.[1]

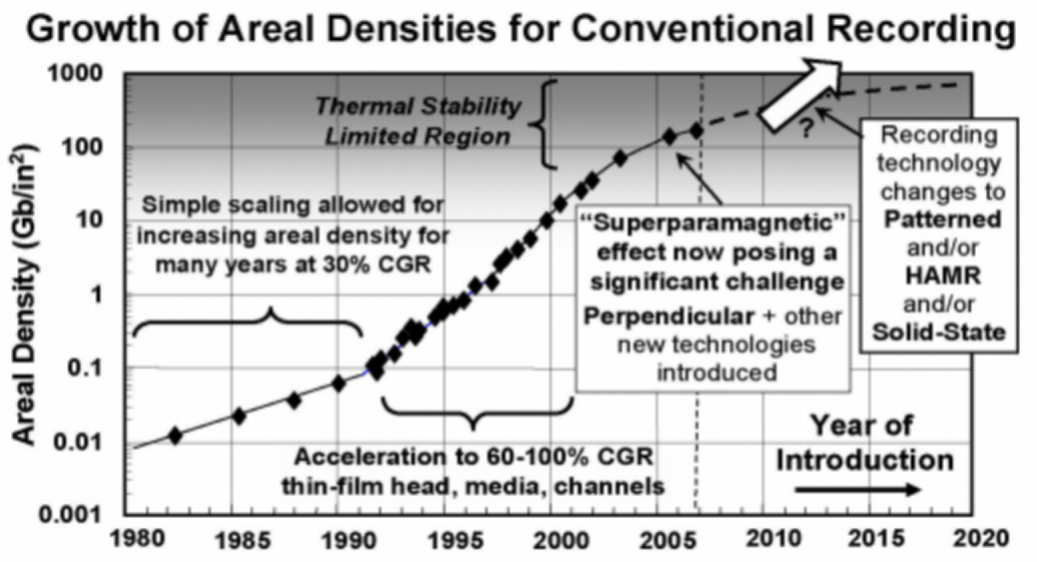

FIGURE 1.1: Future plan for hard disk drive. Image is adapted from [2].

1.2 Longitudinal Recording

Current hard disk drives are utilizing thin film media, which are usually sputtered using dc magnetron sputtering. It consists of a magnetic layer(s) and some other layers to control the growth of the magnetic layer which are polycrystalline in nature. This polycrystalline nature means that the grains inside the magnetic layer are randomly aligned with respect to the plane of the film. Due to this random nature of the grains itself, a single grain cannot be used as a single bit to store information; instead, several grains are grouped together as one bit in order to store the information. This resulted in a problem called the signal-to-noise ratio (SNR). SNR is dependent on the number of grains used as a single bit, thus the ability to reduce the grain size and achieve a uniform grain size distribution is required to minimize the SNR. Several groups have developed methods using seedlayers or underlayers with smaller grain size to try to control the grain size of the magnetic layer [3, 4]

Another important thing to note in magnetic recording is the anisotropy energy K_uV, where K_u is the anisotropy constant of a material while V is the volume of the grain. K_uV reflects the energy necessary to flip the direction of the magnetization of a particle, or in another word, the energy barrier to change the magnetization in a particle. Within the same material, the K_u is usually kept constant and thus the energy

barrier depends solely on the volume of the grain. However, in order to increase the areal density of a magnetic recording media, the grain volume of the magnetic media needs to be reduced. Therefore, along with the reduction of the grain size, a reduction in the anisotropy energy could not be avoided. In this case, the thermal energy which is described as kBT (where kB is the Boltzmann constant and T is the temperature) starts to become significant and may compete with the anisotropy energy. When this happens, the magnetization may be thermally excited and reversed. This phenomenon is called superparamagnetism, where the magnetization of a particle could be reversed without the influence of any external field.

Due to the random nature of the grain growth inside a magnetic recording medium, the grain size distribution would not be uniform, such that some grains will be smaller than the average and thus will be more susceptible to superparamagnetism. The issue with thermal stability can be solved by increasing the anisotropy constant K_u, to increase the energy barrier. However, when the K_u is too large it would be too difficult to reverse the magnetization. In other words there would be a problem with the writability of the material because there is a limit to the magnetic field that can be produced by the write-head material.

This leads to the infamous magnetic recording trilemma, the SNR, thermal stability, and the writability. These three aspects affected each other in a way that when one issue is solved, the other will arise. With that said, longitudinal recording has reached the superparamagnetic limit and must be replaced with a new technology.

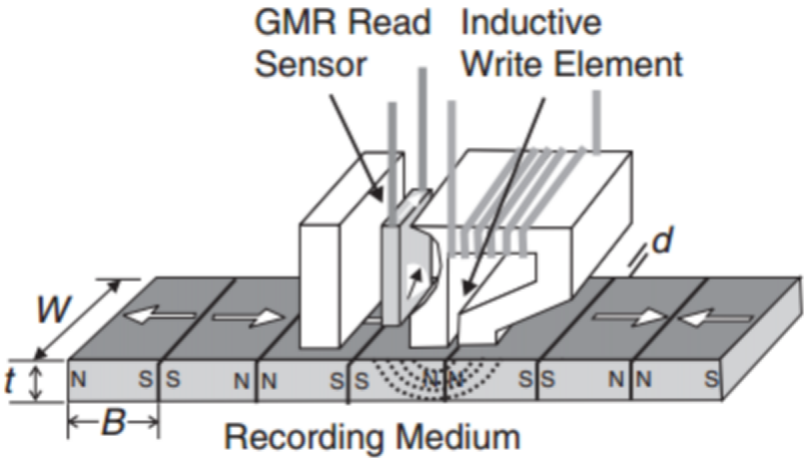

FIGURE 1.2: Schematic drawing of a longitudinal recording system. B is the bit length, W is the track width and t is the medium thickness. d is the flying height of the head above the medium. Figure is adapted from [1].

1.3 Perpendicular Recording

The foundations of perpendicular magnetic recording (PMR) was introduced by Iwasaki et al. in the 1970s as a way to solve the issue with the superparamagnetic limit of longitudinal magnetic recording. Several materials were chosen as the basis of perpendicular magnetic recording including the CoCr alloy with perpendicular magnetic anisotropy [5–7]. Along with the CoCr based recording media, double-layered recording media with NiFe as the soft underlayer (SUL) and various head designs, including the single pole head design are developed to support this new perpendicular recording technology. The combinations of these new technology signalled the coming of a new age of recording technology, as the perpendicular recording media could potentialy outperform the previous longitudinal recording media. After about three decades of development, perpendicular recording finally started to cement its place in hard disk drives as the main magnetic recording technology. This section will explore more about the development of perpendicular recording media.

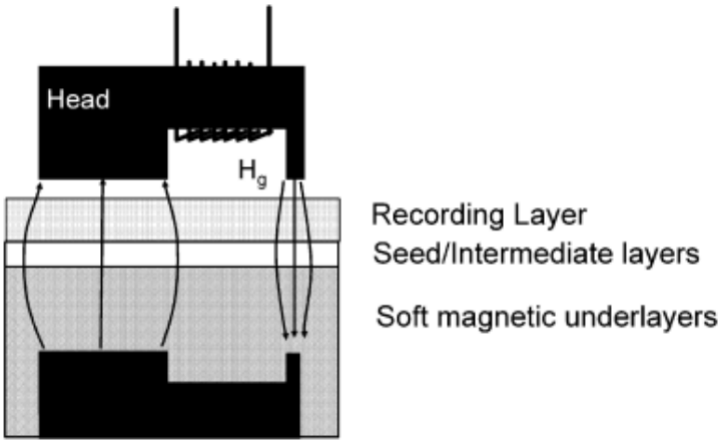

FIGURE 1.3: Schematic illustration of various layers of perpendicular recording media and the writing process. Figure is adapted from [1].

Fig. 1 demonstrates a number of utilized layers including the soft underlayer (SUL) and the recording layer (RL) inside a normal double-layered perpendicular recording media, along with the writing mechanism. In real life applications, there several layers included in every functional parts, however, for the sake of simple demonstration, only one layer is illustrated in each functional layer. Recording layer could also be deposited on AlMg alloy or glass substrate with a proper dimension for its intended application. These functional layers inside the hard disk are mainly deposited by using the sputtering process. First, adhesion or interface layer are deposited directly on the substrates. This layer is mainly made of Ta, Ti, or an alloy of these materials. The function of such layer is to help improve the adhesion of the SUL or other layers with the substrate. Next comes the soft magnetic underlayer on top of the interface layer. This layer is deposited with the intention to aid in the writing process by directing the flux coming out from the writing head to the receiving pole. One way or another, the SUL also behave as a magnetic mirror, meaning that when the writing head projects the "north" pole, the opposite "south" pole will be formed on the upper surface of the SUL. The polarity of the writing head and the SUL enabled the media to be kept between the pole gaps (the real pole and one "image" pole), close to the head gap which is capable of producing more field than the fringing field that is utilized in the longitudinal recording technology. This is the main reason behind the supremacy of perpendicular recording over longitudinal recording.

One of the problem with SUL was reported in the 1980s that using SUL might generate noise substantial enough to be deemed an issue [6]. It was not until around 2003 that several designs of SUL were developed and studied to counter this noise issue. One of the most effective way of reducing the noise is by pinning the magnetization of the SUL along the radial direction. Such pinning could be facilitated by depositing a hard magnetic layer or an antiferromagnetic pinning layer (such as IrMn), or with the help of a magnetic field which was applied along the in-plane direction during the deposition of SUL [8]. In special cases, a combination of these techniques may be required to reduce the noise issue. Another way to tackle the noise problem is by using anti-parallel coupled soft magnetic underlayer (APC-SUL) [9].

After depositing the SUL, some intermediate layers may be sputtered on top of the SUL with or without the help of seedlayers. Intermediate layers serve at least two functions in the hard disk drive. First, it decouples the exchange coupled SUL and RL. Second, it provides the proper condition for epitaxial growth of the RL. For Co based perpendicular recording media, it is necessary to obtain Co grains with a (0002) orientation normal to the plane. Presently, one of the most utilized element for intermediate layer is Ru. Additionally, seedlayers may be deposited on SUL before the intermediate layers to enhance the preferred growth orientation. The importance of the seed layer materials have been studied and proved to be significant in enhancing the preferred growth of intermediate layer.[10, 11]

In recent times, intermediate layers are proven to facilitate the grain size reduction in the RL. For the said purpose, sometimes additional Ru alloy layer is sputtered at high pressure and in reactive gas (such as oxygen) atmosphere. The RL is mainly a Co based hcp alloy. The main function of the RL is as the information storage location for an extended period of time (of around 10 years) and to generate some kind of signal when the information is read back. One of the commonly used material is the CoCrPt alloys along with several forms of oxide. The oxide could be sputtered from oxide targets such as Si, Ti or Ta, or by sputtering under the oxygen atmosphere to form Cr oxides. One additional advantage of using this method is that a mixture of oxides may be segregated into the grain boundary, helping to decouple the grains and reduce the noise [12]. Adding Pt into the target is intended to increase the anisotropy constant of the grain while changing the concentration of

oxides could help to control the grain size [13]. Improving the thermal stability has been one of the issues since the longitudinal recording era. In this system, it can be solved by depositing two or more layers of RL with different functions. With three layers, the first layer can be used to get finer grains, while the upper layer can be optimized to achieve high thermal stability [14]. Mechanical and chemical resistance of the layers can also be added by coating them with carbon overcoats or lubricants.

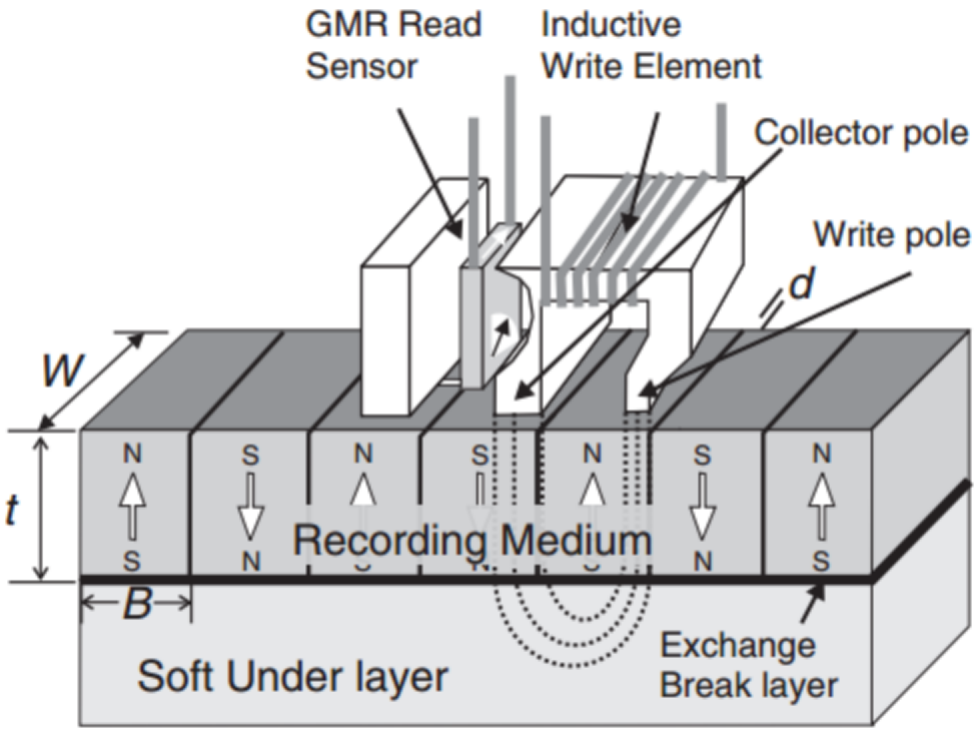

FIGURE 1.4: Schematic drawing of a type 1 perpendicular recording system with SUL and a single pole head. Figure is adapted from [1].

1.4 CoPt Media

The development of CoCrPt/oxide based perpendicular recording media reached a ceiling as the hard disk drives are attempting at reaching an areal density larger than 500 or 600 GB/inches^2. Even with the help of newer concept such as ECC (exchange coupled composite) media, it was perceived that the CoCrPt/oxide media may had reached its limit and thus it is impossible to get areal density of more than 1 TB/inches^2.

In order to counter this problem, a new media other than CoCrPt/oxide must be

found or a new recording technology had to be founded. Regarding the thermal stability limit of magnetic recording, each issue has something to do with the formula $K_u V/kBT$. Thus in order to get better stability, researches have focused on increasing the K_u and using heat localized on each bit to flip the magnetization (Heat assisted magnetic recording, HAMR), or on the V by using patterned media.

In the case of HAMR, materials with large magnetic anisotropy K_u are desired. One promising material for such application is the $L1_0$ form of FePt or CoPt. This ordered form of CoPt can reach thermal stability even in such a small grain size of around 3nm [15]. If such small grain sizes could be materialized and applied in real life application, and if the media could store information and allow to be rewritten, then producing hard disk drives with areal density of over 1 TB/inches^2 would be possible. The ultimate question is how to condition the deposition of such CoPt based magnetic recording media to suit the necessary requirements for the technology.

One of the main concerns of using CoPt based media is controlling the grain size of the material. To achieve the 1 TB/inches^2 areal density, average grain size of the material should be lower than 4 nm, moreover, the standard deviation in the grain size should not exceed 0.4 nm. In reality, it is extremely difficult to achieve such feat. CoPt deposited using chemical method may have small grain size of about 4 nm, nevertheless increasing the temperature would lead to recrystallization and grain growth inside the material which also lead to larger grain size. Beam deposition techniques had also been utilized to deposit the $L1_0$ CoPt nanoparticles, however this technique also fell short because the nanoparticles produced are not in the ordered phase. Another research also tried to use in-situ annealing during the deposition to get the $L1_0$ CoPt phase, however the resulted particles have coercivity of just a few thousand Oe. Another problem to note beside the small grain size and the distribution is how to orientate the easy axis of these particles in the direction desired. A research group made an attempt to make the nanoparticles cubic to get an easily controllable easy-axis orientation [16]. However this technique is far from being applicable in the real life applications and thus improving the sputtering process is the only way to manufacture the recording media. By using RuAl underlayer, the smallest grain size of around 6.6 nm was achieved [17]. The small grain size of RuAl is the

main factor in obtaining this small grain size in the media. This proved that controlling the underlayer grain size is an effective method to reduce the grain size of the upper RL, which is similar to the approach in the longitudinal recording [18]. Another way to control the grain size of CoPt media is by adding doping materials such as Ag, Cu, and C. By adding carbon of around 50% the total concentration, grain size as small as 4 nm could be obtained [19]. Nevertheless, this material showed an easy axis lying along the plane direction. This also showed that extreme doping of carbon elements may harm the perpendicular anisotropy and turn it into the in-plane direction. Adding C elements into the material may have isolated some grains due to the segregation effect, however a TEM observation showed that such case occurred in a much more complex nature [20]. By doping the media with C, two layers would form inside the material. One layer at the bottom is a continuous layer, while the upper layer is a segregated granular layer. Thus, it could be concluded that adding materials into the recording media may not be the best approach to reduce the grain size. However, obtaining the perfect doping material to reduce the grain size could be a potential research field. Piramanayagam and Srivinasan have reported an attempt of using synthetic nucleation layer (SN layer) in order to reduce the grain size in CoCrPt/oxide media. However, in their case the deposition of recording media of those materials were done at room temperature [21]. For $L1_0$ based media like CoPt and FePt, the RL has to be prepared at elevated temperature to overcome the energy barrier needed to get the ordering transformation. When deposited at room temperature, CoPt will exhibit fcc crystal structure with low anisotropy. Only when post annealing or high temperature deposition is done at around 600-700 ^{o}C that such ordering transformation may occur and $L1_0$ phase started to form. The fabrication at such an elevated temperature may have some negative impact on the SN layer and thus affect the potential function of the layer. Even with the researches aiming for larger density of around 10 TB/inches^2, some challenges to obtain small grain size without degrading its magnetic properties still exist.

One aspect that distinguishes the CoPt or FePt based recording media from CoCr Pt-oxide media is the existence of its ordered structure. In the latter case, anisotropy is mainly governed by changing the composition of the material. On the contrary, the ordering of materials in CoPt or FePt based media is really important along with

the composition. Obtaining a highly ordered layer with long range parameter is obviously desired and is an absolute necessity to achieve high density recording.

1.5 Heat Assited Magnetic Recording

As mentioned before in this chapter, the storage capacity areal density of magnetic hard disk drives have been improved significantly since 1956. An intrinsic magnetic media limit, the superparamagnetic effects forced the hard disk drives to settle between a trade-off in the signal-to-noise ratio (SNR), stability of the magnetic bits against thermal energy, and the ease of writability. These problems have prevented the magnetic storage industry from being able to scale its storage capacity areal density at the historical benchmark of $\sim$40% per year [22, 23]. Heat Assisted Magnetic Recording (HAMR) is a new concept introduced in order to solve the "magnetic trilemma". The idea utilizes local heating of the magnetic recording media in order to break the necessary trade-off brought by the superparamagnetic effects [24]. Figure 1.5 shows the general idea of how the HAMR functions. Magnetic recording media in this system will be a hard magnetic material with large magnetic anisotropy and coercivity. Large magnetic anisotropy is necessary in order for the media to be thermally stable for an acceptable period of time because the grain sizes will be much smaller compared to today's PMR magnetic media grains. Small grains size are required to reduce the data bit area on the disk and a sufficiently large number of grains per bit to obtain a sufficient value of SNR. Generally the coercivity of the magnetic recording layer at room temperature is significantly larger than the head fields that is available in the current hard disk drives, making the magnetic medium unusable with a conventional magnetic head.

Each magnetic material has a intrinsic property called Curie temperature (T_c). When the magnetic medium is locally heated up to a temperature close to its T_c, the ferromagnetic material will start to turn into a paramagnet where all its magnetic moments start to weaken and be easily aligned by the external magnetic field. In order to prevent deterioration of the recording media by thermal agitation, the heating is confined in a tight area and is rapidly cooled down to room temperature. In a similar process of writing media, magneto-optical recording system uses heat at

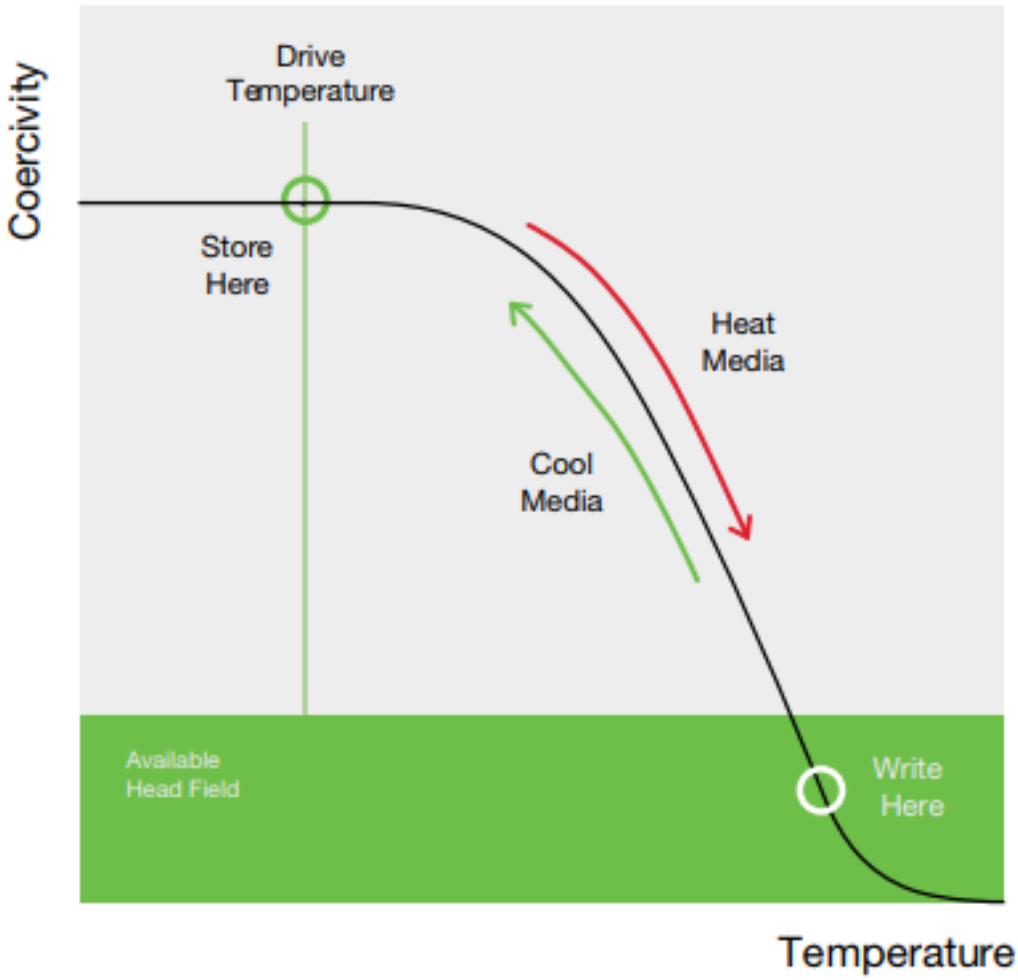

FIGURE 1.5: The coercivity versus temperature and the associated available effective head magnetic field illustrating the HAMR concept. Figure is adapted from [25].

a much larger area [26]. Another difference between HAMR and magneto-optical recording system is that HAMR utilizes a magnetic resistive sensor in order to read the data instead of the optical readout system based on Kerr rotation utilized in the conventional magneto-optical hard drives.

HAMR research began in the 1990s as a possible concept to expand the storage capacity areal density and overall performance of conventional magneto-optical hard disk drives, and also as a proposed solution to the scaling problem of longitudinal magnetic recording due to the superparamagnetic limits. Early pioneers such as Terastor and QUINTA Corporation [27, 28] experimented with putting magneto-optical recording system into the hard disk drives architecture. However, their performance were soon eclipsed by the conventional longitudinal magnetic recording which was successfully scaled to exceed 100 Gb/in^2 and subsequently the successor perpendicular magnetic recording which is scaled to over 1 Tb/in^2 [29].

During the early days of HAMR work, several technical challenges were asked [30]. Is it possible to confine the thermal energy to fit the size necessary for storage capacity of 1 Tb/in^2 and beyond? What material of high magnetic anisotropy could feasibly meet the requirements for modern hard disk drives, is scalable to the optimal grain size, and has good thermal properties? What would be the optimal source of said thermal energy, and is it possible to integrate the source into the conventional hard disk drives system? What materials are necessary to manufacture a robust head to disk interface (HDI) and recording subsystem (RSS) when the magnetic medium is locally heated up to a temperature close to its T_c? Up until now, HAMR focused researches have come up with answers to some of these challenges, while some are still being actively studied for the possible solutions. An illustration of an early HAMR based magnetic recording system with a free space light delivery is shown in Figure 1.6. The recording head consists of a magnetoresistive read sensor, an electromagnetic field source, a waveguide integrated light path, and a near field transducer (NFT). The source of light in this illustration is an external laser which is grating-coupled into the wavegide and is directed towards the NFT to generate surface plasmons. Then, the NFT will generate high-intensity field to heat the media locally as the media surface passes under the recording head. The coercivity of the media will be lowered as the temperature is increased, as illustrated in

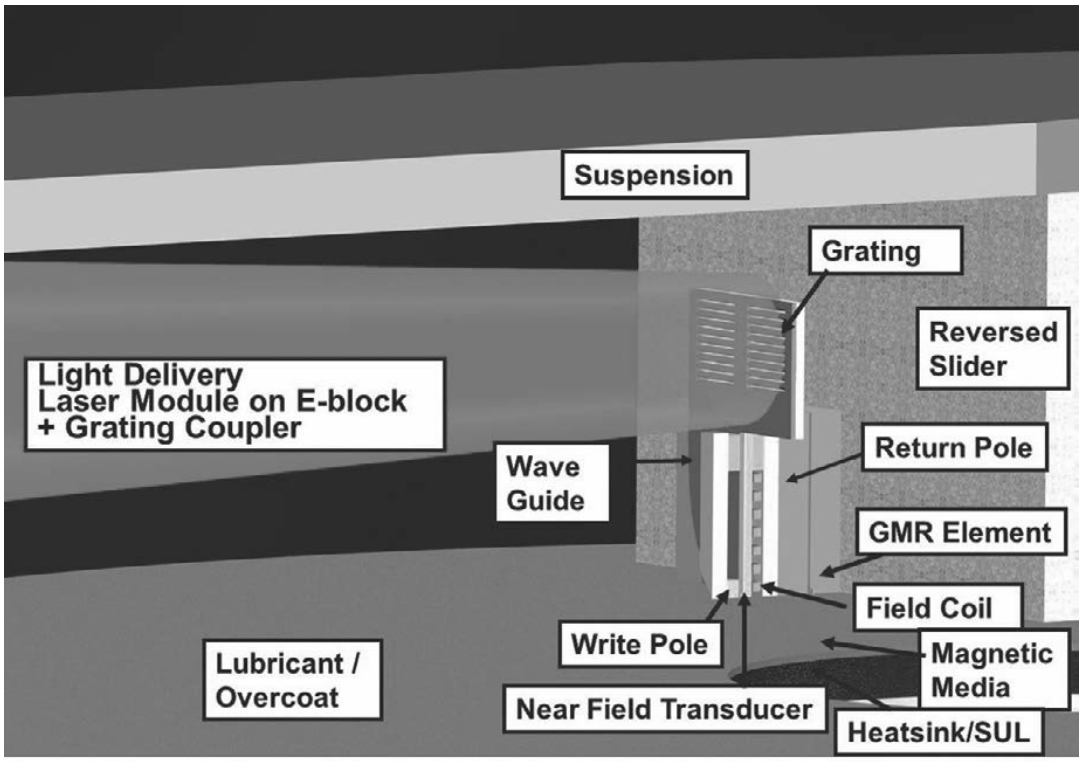

FIGURE 1.6: An illustration of the HAMR recording system showing a cutaway of the HAMR head. The HAMR head consists of a read and write element, a light path, and an NFT flying over the surface of HAMR media with a heat sink and a soft underlayer (SUL). Figure is adapted from [25].

Figure 1.5. Once the coercivity of the media is reduced below the magnetic field of the recording head, the magnetization then can be switched. To improve the performance of the HAMR hard disd drives, the media requires additional layers such a heat sink and a soft under layer (SUL) which can improve the thermal and magnetic properties during the process of magnetic recording.

1.6 Bit Patterned Media

Bit patterned media is an alternative new magnetic recording technology that focuses more on the volume V to solve the thermal stability issue. Before the bit patterned media technology, a single bit is defined by many magnetic grains grouped as one and the limit is governed by the grain boundary. On the other hand, bit patterned media utilizes artificially defined bits with boundaries that could consist of void or nonmagnetic materials. In this technology, a single domain bit could be formed by exchange coupling the grains in the magnetic material. This is impossible

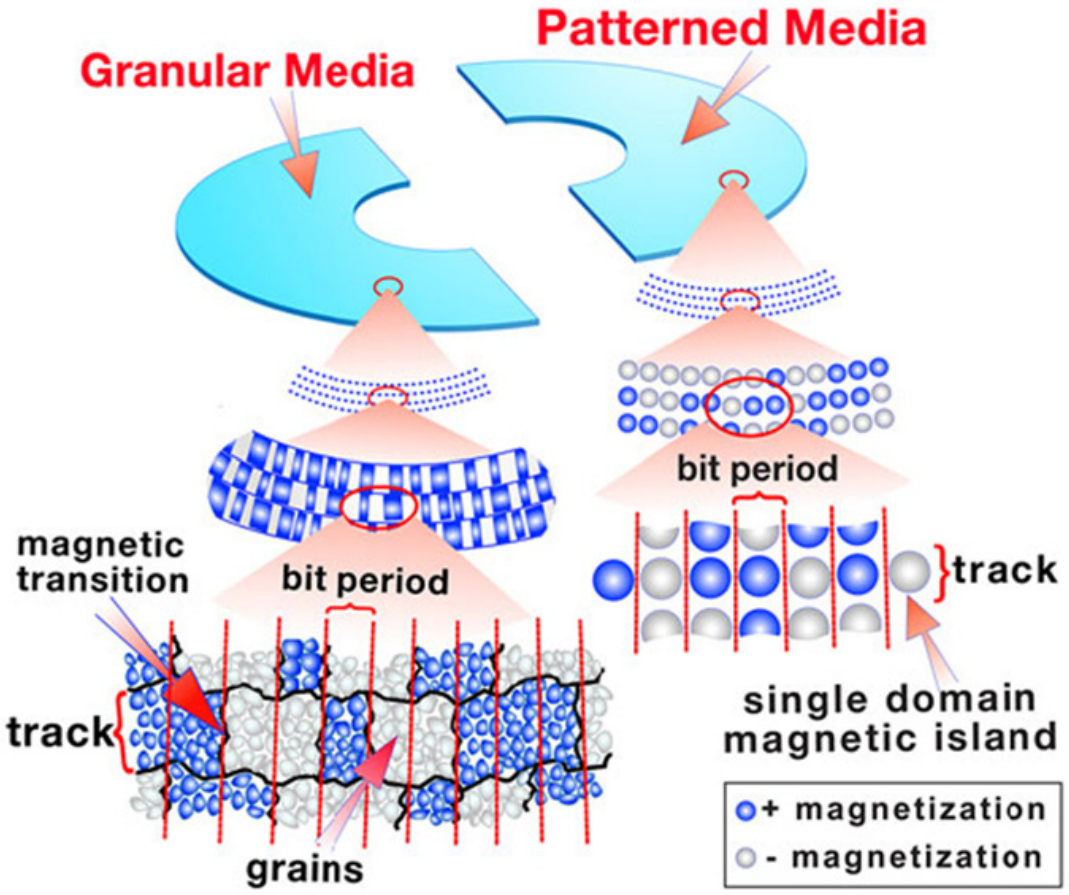

FIGURE 1.7: A comparison of the BPM concept vs. the current granular media. Figure is adapted from HGST.

to do in the old magnetic recording, mainly due to the fact that a strong exchange coupling between grains could lead to a rather large bit boundaries. In bit patterned media, however, increasing the exchange coupling would not affect the bit boundary as it is artificially defined using lithography process. As the magnetic body inside a patterned media is bigger than the volume of a single grain, no sacrifice of thermal stability nor the writability is necessary [31]. It is expected that patterned media technology will only start to be necessary to exceed the 1 TB/inches^2 limit.

In order to surpass that limit, a feature size lower than 12.5 nm is necessary. Considering a square bit, 12.5 nm would be sufficient. Nevertheless, using square bits may impose some issues on the head design. Thus, rectangular bits are usually preferred with a bit aspect ratio (BAR) larger than 2. However, a feature size smaller than 12.5 nm would be needed if the BAR is to be increased and this could prove to be an uphill task to ultimately overcome the 1 TB/inches^2 limit. The area of the magnetic unit in a bit patterned media is also found to be impactful to the signal

strength [32]. This area is dependent on the magnetic (lan) and the nonmagnetic (groove) region. The area of the magnetic unit will be larger as the feature size is getting smaller through modifying the lithography process. Therefore, one of the main task in producing this bit patterned media is to obtain small feature size. One potential solution to this issue is by using electron beam lithography to fabricate a master mold with small sized features and to duplicate this mold onto the media by utilizing the nano-imprint lithography (NIL). This method would be able to cut the cost and input needed to pattern a recording medium. Researches have also started to explore options other than lithography to pattern a media. A likely method combines some sort of self-assembly mechanism with lithography to store information at high density. One case uses di-block co-polymer alongside the NIL [33]. The NIL acts as the foundation to form the tracks and to confine the self-assembled dots to the tracks, enabling a long range order to be obtained. A dot with a size of around 40 nm could be manufactured using this method [34]. A method using anodize alumina nano-hole combined with NIL has also been proposed by Oshima et al [35]. By using lithographically fabricated tracks, the long range order in alumina nano-holes could be improved. The disk has also been proved to be able to be read and written during tests. Even though nano holes with the size of around 100 nm were used at the time, the research claimed that reducing the nano holes to around 13 nm is possible, making this technique a reasonable method to achieve 4 TB/inches^2. One problem remained in the self-assembly process is the size distribution of the nano-holes could be insufficient. The variations in the feature size may lead to noise problems [32].

1.7 Exchange-Coupled Composite

As discussed before, one of the alternatives to increase the capacity of magnetic recording is Exchange Coupled-Composite, which utilizes the basic application of a previously developed Exchange Spring Media. In ECC, a soft magnetic layer is added onto a hard magnetic layer. Then, by exploiting the exchange coupling between the hard and the soft magnetic layer, the switching field can be reduced while maintaining the thermal stability.

The exchange coupling only occurs at exchange length, which is an important length-scale parameter for a soft-hard magnetic structure. This is given by the following formula: lw =A*K_h where A is the exchange stiffness constant, describing the hard-soft layer coupling strength and K_h is the uniaxial anisotropy constant of the hard magnetic layer; lw is usually a few nanometers thick in the case of hard magnetic media (e.g., $L1_0$–CoPt, RE-TM hard magnetic alloys).

When the hard magnetic layer is in the perpendicular direction, the soft magnetic layer's magnetization should be in the longitudinal direction. Then, the hard-soft magnetic system will be divided into two regions, the first is where the whole system switches coherently (rigid magnet region), and the second one is where domain wall switching causes the system to switch incoherently (exchange spring system).

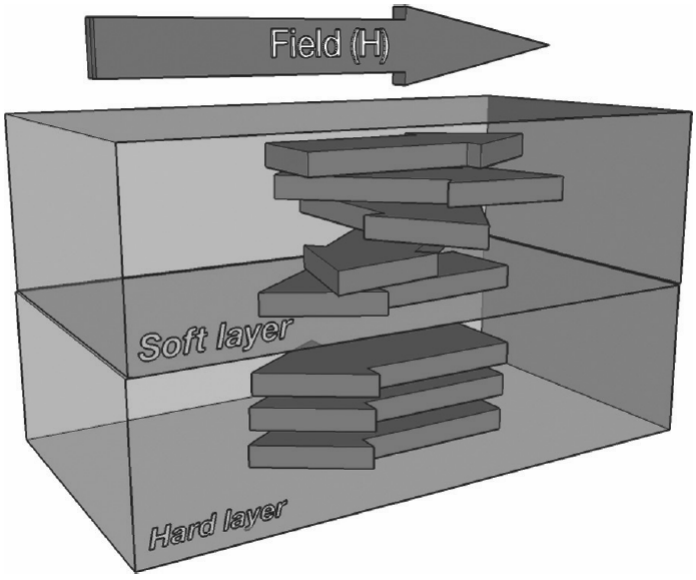

FIGURE 1.8: Schematic illustration of Exchange-coupled composite structure, where a soft magnetic layer is put on top of a hard magnetic layer. Figure is adapted from [1].

1.8 Background of this work

$L1_0$ FePt and CoPt based recording media has garnered much attention in recent years due to their applicability in perpendicular magnetic recording and the potential to be utilized in the future high density magnetic recording devices. Generally, CoPt has two crystal structures, the A1 and the $L1_0$. A1 phase is the disordered fcc phase with randomly positioned Co and Pt atoms. $L1_0$ phase is an ordered fct phase

with a high magnetocrystalline anisotropy energy K_u (10^7 erg/cc). It is notable that A1 phase can transform into $L1_0$ phase after undergoing heat treatment at temperature of around 800 °C.

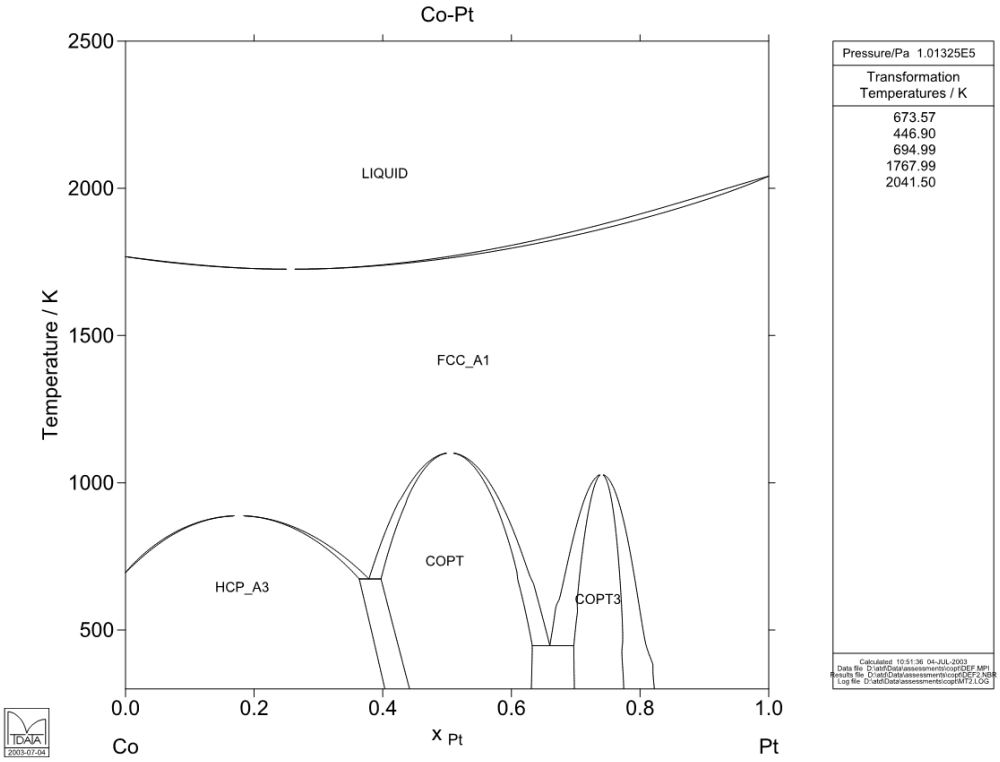

FIGURE 1.9: Phase diagram of CoPt alloy.

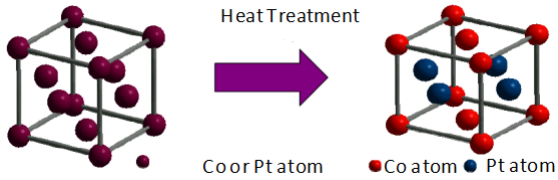

FIGURE 1.10: Ordering transformation in CoPt.

From this phenomenon, it is implied that the ordering transformation of CoPt from A1 to $L1_0$ phase has a significant role in the magnetocrystalline anisotropy, and ultimately promoting the diffusion of Co and Pt atoms proves to be significant. Various researches have been done in an attempt to promote the ordering transformation. Farrel reported that the deposition of CoPt at elevated temperature has a drastic impact on the ordering transformation.[36] It is believed that with elevated

temperature promotes diffusion of Co and Pt atoms such that the correct position for ordering transformation is achieved.[37]

Another way to promote ordering transformation by means of Co and Pt atoms diffusion is during the post-annealing process. Recently our group reported the increase of perpendicular coercivity in CoPt/TiN thin films with N partial pressure during the deposition.[38] The introduction of N plays a role in both the deposition and post-annealing process. During the deposition, N is incorporated in the CoPt film and increases its lattice parameter. The increase in lattice parameter relaxes the lattice mismatch between CoPt/TiN and stimulates epitaxial growth. On the other hand, during the post-annealing process, N diffuses out of the films, leaving behind vacancies that promotes diffusion of Co and Pt atoms. Although it has been speculated that the release of N is responsible for this occurrence, a more detailed investigation on the mechanism of N effects is needed.

On the other hand, the $L1_0$-CoPt also has an issue with its large switching field. One of the easiest way to decrease the switching field of a hard magnetic layer is by adding a soft magnetic layer to make a ECC structure. However, the addition of a soft magnetic layer migh complicates the fabrication process and thus the cost of production will increase in order to accommodate the extra materials or equipment needed in the production.

CoPt has the A1 structure which is also soft magnetically, therefore by coupling the $L1_0$-CoPt with the A1 CoPt a decrease in switching field could be realized experimentally without complicating the fabrication. Another advantage of using CoPt to form an ECC structure is that we can study the effect of soft layer deposition temperature in a same material ECC system without worrying about the change in anisotropy constant. This is due to the high ordering parameter of $L1_0$-CoPt such that even at 400 ^{o}C the ordering transformation will not occur, and A1 structure could be obtained at high temperature.

Finally, the nature of $L1_0$ ordering transformation is not fully understood. The reason is the existence of two symmetry breaking origins that may induce the perpendicular magnetic anisotropy. With high ordering transformation temperature, studying the $L1_0$ ordering transformation with CoPt has its advantage. This is due to the capability of separating the origins of broken symmetry that gives rise to the

perpendicular magnetic anisotropy itself, which are the alternating stacks of atoms and the face-centered tetragonal structure.

1.9 Objectives of This Work

With regards to the existing problems of $L1_0$ CoPt and its promising application in fundamental studies, this work focuses on:

- To uncover the mechanism of the ordering transformation improvement by means of nitrogen incorporation.
- To investigate the effect of broken symmetry caused by face-centered tetragonal transformation in CoPt and fabricate a CoPt film with high PMA at temperature lower than the usual fabrication temperature.
- To realize the exchange-coupled composite structure using CoPt as its only magnetic material.

1.10 Organization of This Thesis

- Chapter 1: Introduction

  This chapter is an introduction to magnetic recording technology, including its brief history, its development up to the current technology, and future magnetic recording technology. Additionally, the background of this study is included in order to shed light to the objectives of this study.

- Chapter 2: Fabrication and Characterization of CoPt/TiN bilayer films

  This chapter includes the details done in the experiments. First, the sputtering machine is described in detail. Then, several characterization techniques are elaborated and given examples of the results. For the experiment, TiN is grown on top of MgO (001) single crystal substrate and glass. On both substrates, TiN grows in the (001) direction, which makes it feasible for the underlayer of CoPt to promote the (001) oriented growth. Next, Nitrogen gas incorporation is found to affect the magnetic properties positively.

- Chapter 3: Effect of Nitrogen Incorporation on the Ordering Transformation of CoPt in CoPt/TiN Bilayer Films

  The growth of CoPt on top of TiN/MgO and MgO in the (001) direction obtained in the last chapter is studied more intensively in this chapter. On TiN/MgO a compressive strain is found inside the as-deposited film and the $L1_0$ ordering transformation is improved in the annealed film with the incorporation of Nitrogen during deposition. On the other hand, CoPt on MgO is deposited under a tensile strain condition, and the addition of Nitrogen degrades the ordering transformation after annealing. Next we reproduced the result of TiN/MgO samples by depositing CoPt on TiN/Glass where the (001) oriented growth is obtained. In this sample, the Nitrogen incorporation also improves the L10 ordering transformation after annealing with comparable result to the sample deposited on MgO.

- Chapter 4: Strong Perpendicular Magnetic Anisotropy Induced by Broken Symmetry of A1-CoPt

  In this chapter, the thickness of CoPt on TiN/MgO is changed in order to investigate the tetragonality effect on the magnetic anisotropy of the A1 structure of CoPt. It is found that at 2.5 nm, the CoPt grows in a lattice-matching epitaxial mode where the CoPt lattice is expanded to fit the larger TiN lattice (10% lattice mismatch). When the thickness is increased up to 10 nm, the strain inside the film becomes too large that strain-relaxation happens inside the film by introducing dislocation in the interface of CoPt/TiN. The c/a ratio of 2.5 nm CoPt is 0.974 which is similar to $L1_0$ and the PMA is roughly similar, while the 10 nm CoPt has a c/a ratio is 1 which is the same as an fcc-A1 with no PMA.

- Chapter 5: Control of Perpendicular Coercivity in A1-CoPt/L10-CoPt/TiN Trilayer films

  This chapter focuses on controlling the magnetic properties of the sample obtained in Chapter 3. It is found that by coupling the $L1_0$-CoPt film (hard magnet) with an A1-CoPt film (soft magnet), the switching field could be reduced while the saturation magnetization could be increased. This reduction could be

further optimized by changing the thickness, changing the deposition temperature of the soft layer and introducing a TiN intermediate layer in between the hard/soft layer. In this study, 2.5 nm thickness of CoPt soft layer is found to be the optimum thickness to reduce the switching field by half while maintaining a good Mr/Ms ratio. Moreover, by depositing the CoPt at higher temperature, density gradient is found inside the film where the Pt is concentrated at the surface while the Co is concentrated near the interface, improving the switching field reduction. Finally, the introduction of TiN is found to improve the switching field reduction when the thickness is at 1 nm. Beyond that thickness, the hard and soft layer is decoupled and the switching field starts to return to its original state.

- Chapter 6: Conclusion and future directions

Bibliography

[1]S. N. Piramanayagam, and K. Srinivasan, J. Magn. Magn. Mater. **321**, 485–494 (2009).

[2]P. Frank, and R. Wood, "A perspective on the future of hard disk drive (hdd) technology.", in Proc. asia pacific magn. rec. conf (2006), Paper FB–01.

[3]K. R. Coffey, M. A. Parker, and J. I. Howard, IEEE Trans. Magn. **31**, 2–4 (1995).

[4]B. R. Acharya, E. N. Abarra, and I. Okamoto, IEEE Trans. Magn. **37**, 1475–1477 (2001).

[5]S. Iwasaki, IEEE Trans. Magn. **16**, 71–76 (1980).

[6]J. R. Desserre, IEEE Trans. Magn. **20**, 663 –668 (1984).

[7]T. Ando, and T. Nishihara, IEEE Trans. Magn. **33**, 2983–2985 (1997).

[8]K. Tanahashi, R. Arai, and Y. Hosoe, IEEE Trans. Magn. **41**, 577–580 (2005).

[9]B. R. Acharya, J. N. Zhou, M. Zheng, G. Choe, E. N. Abarra, and K. E. Johnson, IEEE Trans. Magn. **40**, 2383 –2385 (2004).

[10]S. N. Piramanayagam, H. B. Zhao, J. Z. Shi, and C. S. Mah, Appl. Phys. Lett. **88**, 092506 (2014).

[11]S. N. Piramanayagam, and H. B. Zhao, J. Magn. Magn. Mater. **312**, 476–479 (2007).

[12]H. Yamane, S. Watanabe, J. Ariake, N. Honda, K. Ouchi, and S. Iwasaki, J. Magn. Magn. Mater. **287**, 153–158 (2005).

[13]Y. Inaba, T. Shimatsu, T. Oikawa, H. Sato, H. Aoi, H. Muraoka, and Y. Nakamura, IEEE Trans. Magn. **40**, 2486–2488 (2004).

[14]S. N. Piramanayagam, J. Z. Shi, H. B. Zhao, C. S. Mah, and J. Zhang, IEEE Trans. Magn. **41**, 3190–3192 (2005).

[15]D. Weller, H. Brändle, G. Gorman, C. J. Lin, and H. Notarys, Appl. Phys. Lett. **61**, 2726 (1992).

[16]N. Shukla, C. Liu, and A. G. Roy, Mater. Lett. **60**, 995–998 (2006).

[17]W. K. Shen, J. H. Judy, and J. Wang, J. Appl. Phys. **301**, 110–113 (2015).

[18]T. Kanbe, Y. Yahisa, H. Suzuki, H. Kataoka, Y. Takahashi, Y. Hirayama, T. Kanbe, Y. Yahisa, H. Suzuki, and H. Kataoka, J. Appl. Phys. **91**, 8611 (2002).

[19]A. Perumal, H. Ko, S. Shin, A. Perumal, H. Ko, and S. Shin, Appl. Phys. Lett. **83**, 3326 (2003).

[20]J. S. Chen, B. C. Lim, J. F. Hu, Y. K. Lim, B. Liu, and G. M. Chow, Appl. Phys. Lett. **90**, 042508 (2007).

[21]S. N. Piramanayagam, and K. Srinivasan, Appl. Phys. Lett. **91**, 142508 (2007).

[22]K. Z. Gao, O. Heinonen, and Y. Chen, J. Magn. Magn. Mater **321**, 495–507 (2009).

[23]S. H. Charap, P. Lu, and Y. He, IEEE Trans. Magn. **33**, 978–983 (1997).

[24]M. H. Kryder, E. C. Gage, T. W. McDaniel, W. A. Challener, R. E. Rottmayer, G. Ju, Y. T. Hsia, and M. F Erden, Proc. IEEE **96**, 810–1835 (2008).

[25]G. Vavaro, and F. Casoli, *Ultrahigh-density magnetic recording, Storage materials and media design* (Pan Stanford, 2016).

[26]T. W. McDaniel, and R. Victora, Handbook of Magneto-Optic Data Recording, Materials, Subsystems, Techniques (1996).

[27]G. Knight., Proceedings of the THIC Meeting (1998).

[28]J. F. Heanue, Proc. SPIE **3778**, 98–103 (1999).

[29]E. N. Abarra, B. R. Acharya, A. Inomata, and I. Okamoto, EEE Trans. Magn. **37**, 1426–1431 (2001).

[30]T. W. McDaniel, W. A. Challener, and K. Sendur, Digest of Joint NAPMRC (2003).

[31]B. D. Terris, and T. Thompson, J. Phys. D. Appl. Phys. **38**, R199–R222 (2005).

[32]H. J. Richter, A. Y. Dobin, R. T. Lynch, D. Weller, R. M. Brockie, O. Heinonen, K. Z. Gao, J. Xue, R. J. M, P. Asselin, and M. F. Erden, Appl. Phys. Lett. **88**, 222512 (2006).

[33]K. Naito, H. Hieda, Y. K. M. Sakurai, and K. Asakawa, IEEE Trans. Magn. **38**, 1949 –1951 (2002).

[34]A. Kikitsu, Y. Kamata, M. Sakurai, and K. Naito, IEEE Trans. Magn. **43**, 3685 –3688 (2007).

[35]H. Oshima, H. Kikuchi, H. Nakao, K. Itoh, T. Kamimura, T. Morikawa, T. Umada, H. Tamura, K. Nishio, and H. Masuda, Appl. Phys. Lett. **91**, 022508 (2007).

[36]R. F. C. Farrow, D. Weller, R. F. Marks, M. F. Toney, and H. M. College, Appl. Phys. Lett. **69**, 1166–1168 (1996).

[37]B. Laenens, F. M. Almeida, N. Planckaert, K. Temst, J. Meersschaut, A. Vantomme, C. Rentenberger, M. Rennhofer, and B. Sepiol, J. Appl. Phys. **105**, 073913 (2009).

[38]H. An, J. Wang, J. Szivos, T. Harumoto, T. Sannomiya, S. Muraishi, Y. N. G. Safran, and J. Shi, J. Appl. Phys. **118**, 203907 (2015).

Chapter 2

Fabrication and Characterization of CoPt/TiN bilayer films

This chapter covers the film fabrication method, microstructure analysis, and magnetic properties analysis. For CoPt and TiN films, dc magnetron sputtering was used to prepare the samples. More details on the sputtering machine and parameters during the deposition will be described in the first section of this chapter. The second section of the chapter will focus on the characterization of the films. This includes microstructure characterization such as XRD (both out-of-plane and in-plane), cross-section TEM, and AFM. The magnetic properties was analyzed using the vibrating sample magnetometer (VSM). Then, the basic theory of the machine will be discussed further in this chapter.

2.1 Material Selection

2.1.1 TiN underlayer

The idea of using $L1_0$ CoPt as a media for perpendicular magnetic recording can be described as the following. $L1_0$ CoPt has high magnetic anisotropy in the c-axis direction of its lattice, thus the growth of CoPt in the (001) direction is essential in achieving perpendicular magnetic anisotropy. Thus, material that can promote the (001) growth are typically used as an underlayer to induce the perpendicular magnetic recording in $L1_0$ CoPt media.

The typical underlayer used in experiments is the single crystal MgO (001). MgO also has a larger lattice constant compared to CoPt (10% difference) and will induce

lattice enlargement during the growth of the film. If the underlayer has larger lattice constant than the CoPt, the CoPt lattice will then be expanded in the in-plane direction. As the c/a ratio of A1 CoPt becomes similar to the ratio of $L1_0$ phase, the ordering transformation becomes easier and thus, the ordering transformation temperature could be reduced. Therefore, the choice of underlayer will be very important in order to control the lattice mismatch and *c/a* ratio of the A1 FePt or CoPt. Ding et al. reported a sharp increase in *c/a* ratio when the FePt is directly deposited on MgO(200) single-crystal substrate due to the existence of a critical lattice mismatch, beyond which misfit dislocations will be introduced between the interfaces and the strain energy will be relaxed.[1]

However, their work fails to consider the effects of growth mode of the FePt film when deposited directly on top of MgO substrate. Futamoto *et al.* recently reported that when FePt is deposited on MgO(001) underlayer, de-wetting of FePt may occur at high temperature and isolated crystal islands of FePt will form on the MgO surface.[2, 3] In these islands, the lattice close to the interface will remain strained but the lattice far from the interface will be relaxed, making the overall *c/a* ratio approaching unity.

In this work we used MgO(100) single-crystal substrate, which is the same as Ding *et al.*. For the underlayer, TiN is used due to the similarity of lattice constant with MgO (*a* of TiN = 0.4249 nm, *a* of MgO = 0.4213 nm) and the good wetting ability of CoPt on TiN.[4] TiN grew in the (001) direction with epitaxial relationship of MgO(001)[100]|| TiN(001)[100]

2.1.2 Growth of TiN on MgO

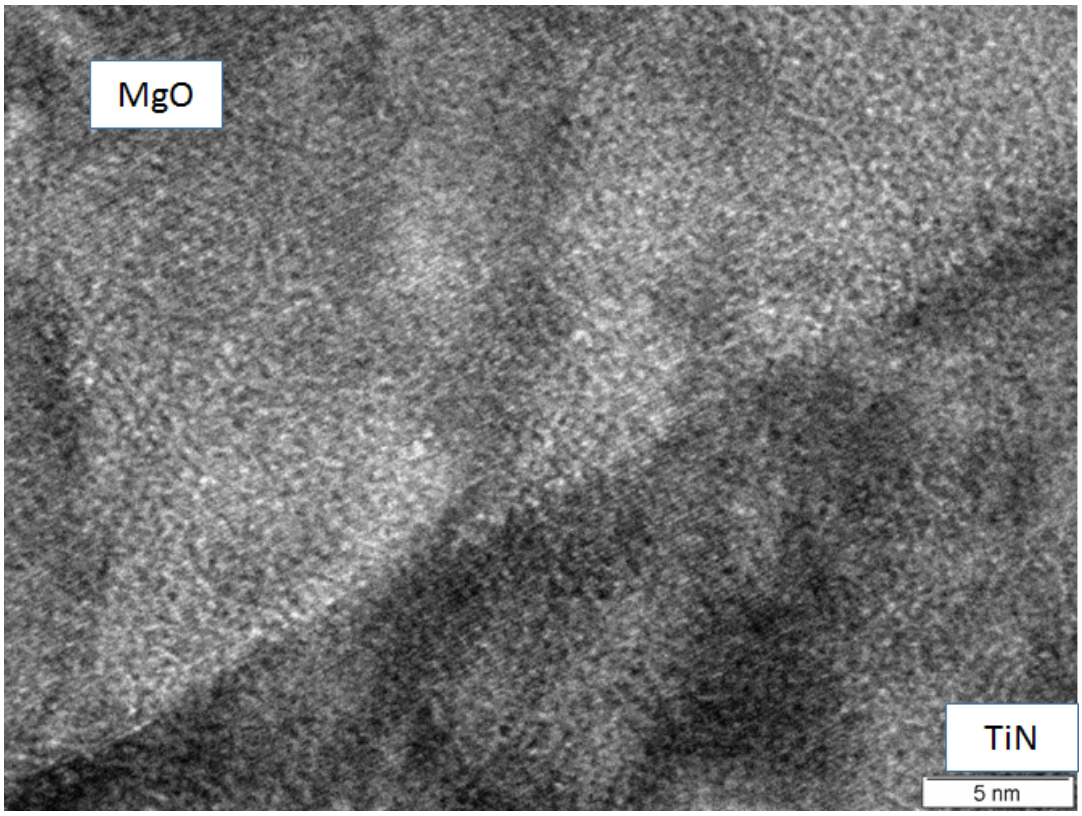

FIGURE 2.1: Cross-sectional TEM image. Taken from MgO/TiN(40 nm) sample.

TiN grown on MgO (001) single crystal substrate has been observed to grow in a lattice-matching epitaxial growth. This is due to the similarity of their lattice constant and crystal lattice. TiN is normally found as a fcc and the competition of (111) and (001) growth is important for this experiment. With the help of a single crystal substrate that can promote (001) growth, (001) preferred orientation growth has been achieved in this experiment.

2.1.3 Growth of CoPt on TiN/MgO

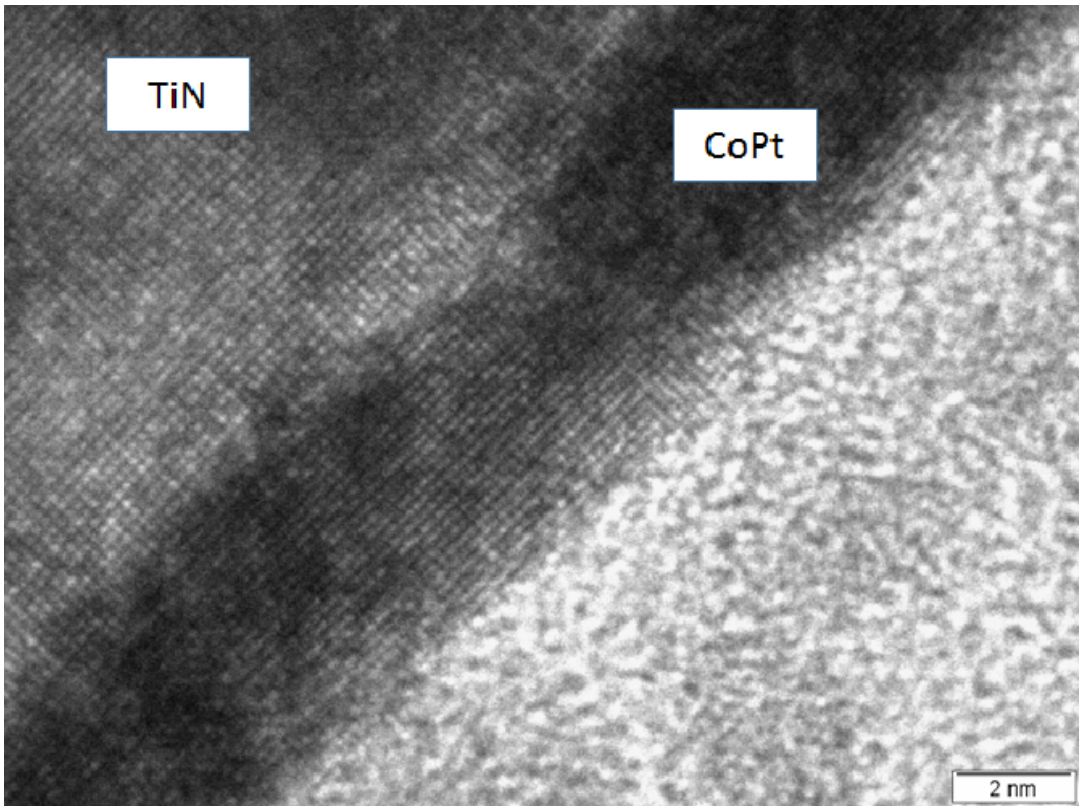

FIGURE 2.2: Cross-sectional TEM image. Taken from MgO/TiN(40 nm)/CoPt(2.5 nm) sample.

CoPt grown on MgO (001) single crystal substrate has a (001) preferred orientation growth that is good for $L1_0$ CoPt based perpendicular magnetic recording. However, due to the low surface energy of MgO (0.97 J/m^2), at low thickness the growth of CoPt tend to occur in the island growth mode which is disadvantageous as a recording media. TiN with higher surface energy (1.3 J/m^2) is theoretically better as an underlayer to reduce the contact angle between the underlayer and CoPt film. In this experiment, a smooth surface of CoPt (2.5 nm) film has been achieved on top of TiN, which meets the requirement for future magnetic recording media.

2.1.4 Growth of CoPt on TiN/Glass

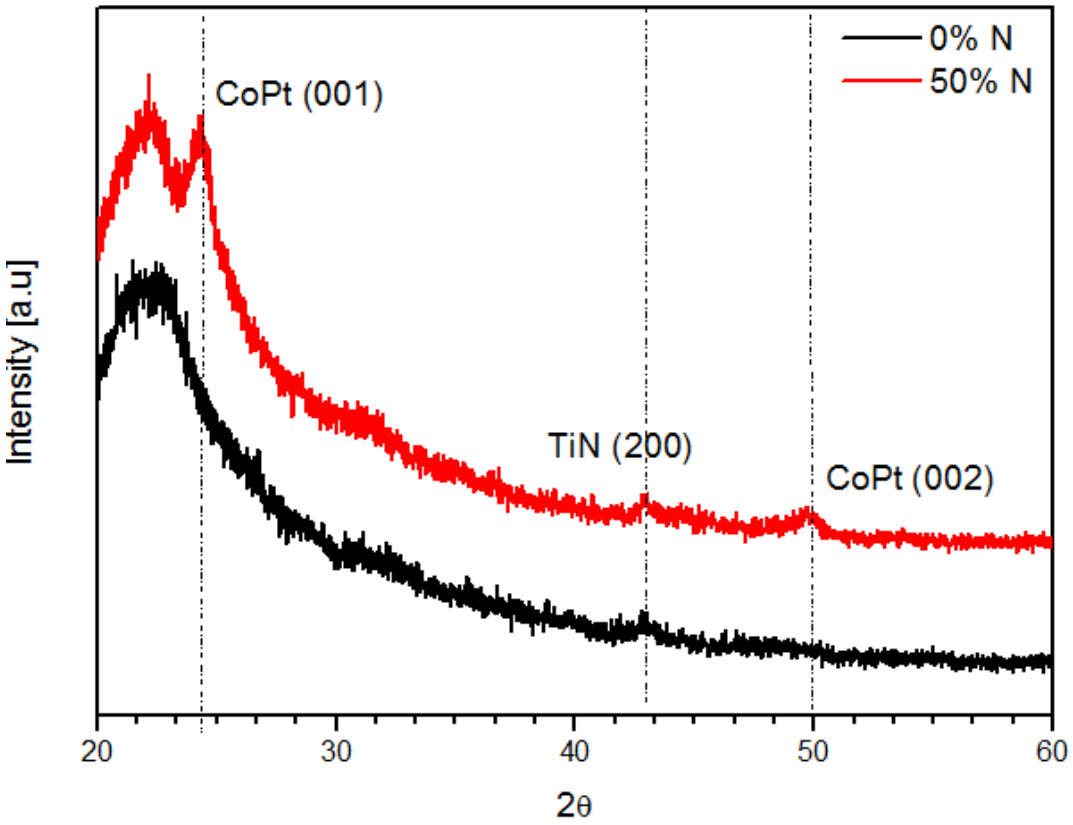

FIGURE 2.3: XRD result of Glass/TiN(40 nm)/CoPt(10 nm) annealed at 700 C sample.

TiN has a potential to replace MgO (001) single crystal as an underlayer to induce the (001) preferred orientation growth of CoPt due to their similarity in crystal structure and lattice parameter. Moreover, the cheap cost of fabrication TiN is another advantageous point over the high cost of MgO single crystal substrate. Hence, reproducing the (001) oriented growth of CoPt on TiN/Glass becomes important in this experiment.

Figure 2.3 shows the XRD peaks of Glass/TiN(40 nm)/CoPt(10 nm) annealed samples. At around 48 degree, the fundamental (002) peak has been observed in sample deposited under Nitrogen gas flow ratio, this proves that the (001) oriented growth of CoPt could be reproduced in TiN/Glass underlayer.

2.2 Fabrication of the film and post-deposition annealing

2.2.1 DC magnetron sputtering

DC magnetron sputtering was used in this experiment due to its versatility and advantages when ompared to normal DC sputtering machine. These advantages include: higher sputtering yield and better stability at lower pressure. This is due to the addition of magnetic field above the target surface which acts as a wall to constraint the movements of electrons and ions. Furthermore, DC magnetron has the ability to control the resulting films by adjusting the power, substrate temperature, sputtering gas, etc.

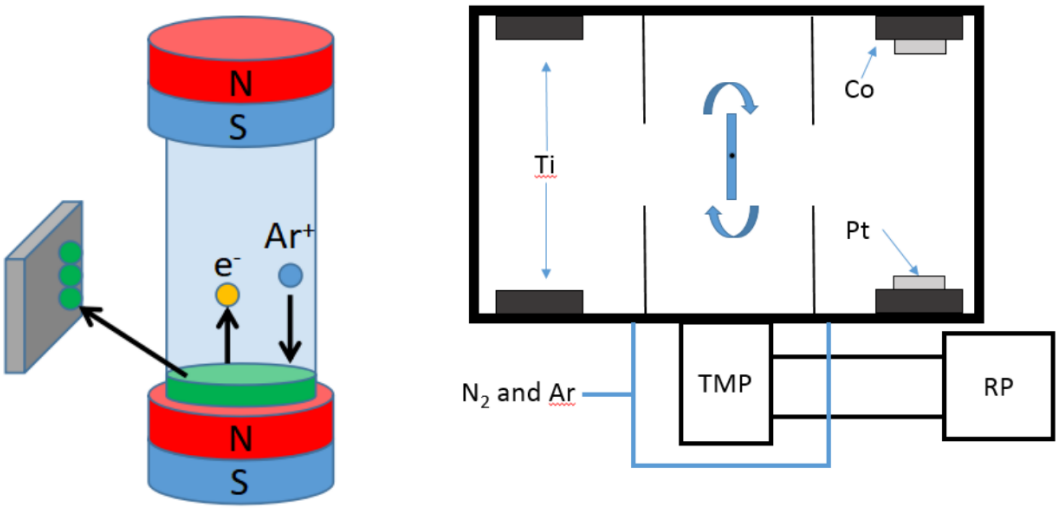

FIGURE 2.4: Schematic illustrations of the DC magnetron sputtering system used in the experiment.

The schematic of the machine used in this experiment is shown in Figure 2.1. The apparatus is a dual chamber with dual facing targets and a rotating stage. With the help of negative high voltage between target and the cover, Ar ions are forced to strike the target's substrate and subsequently electron and target atoms are released from the surface. The released electrons may collide with Ar atoms in the plasma and generate further Ar ions and electrons. Meanwhile, target atoms may hit the substrate placed on the stage and develop into thin film.[5] The base pressure used in the experiments were lower than 5 x 10^{-5} Pa. Then during the experiments, the working pressure was set to 0.2 Pa. As shown in Figure 2.1, the pumping equipment in this apparatus consist of a rotary pump that supports a turbo molecular pump.

During the pumping, first the rotary pump is used to lower the pressure up to 10^{-1} Pa. Then, the pump is switched to the turbo molecular pump to obtain the ultimate vacuum of lower than 5 x 10^{-5} Pa.

The sputtering gas used in the experiments were N2 and Ar. The gas flow ratio between the two is adjusted to 1:10 for TiN films fabrication. The target used for TiN fabrication is a pure Ti metal target. Meanwhile for CoPt the gas flow ratio of N2 is changed from 0% up to 50%. The target used int the fabrication of CoPt film is a composite target of Co and Pt with surface area ratio of (1.56:1).

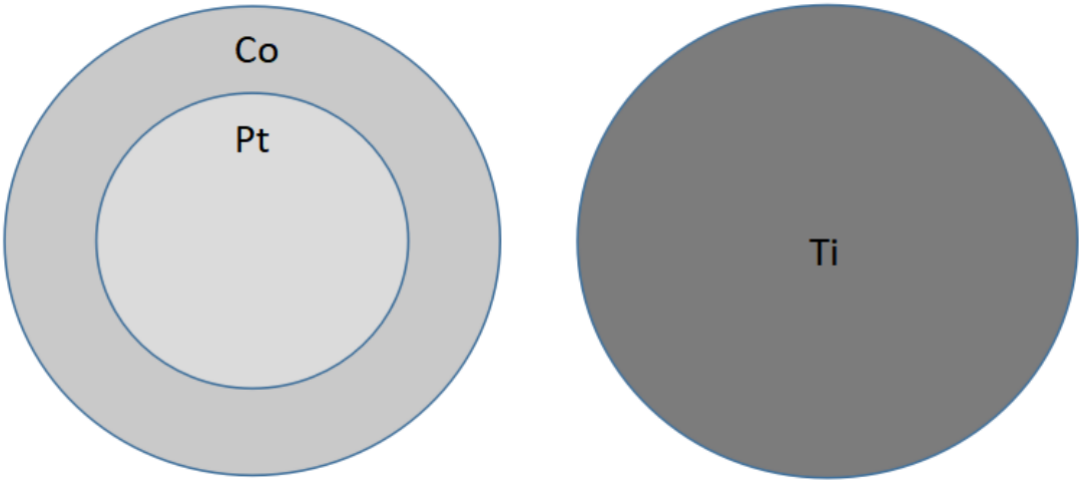

FIGURE 2.5: Schematic illustrations of the targets used in this experiment.

2.2.2 Post-deposition Annealing

In this experiment post-deposition annealing at temperature higher than 600 oC was used in order to stimulate L10 ordering of CoPt deposited on glass substrate with TiN intermediate layer. In this case, the sample is put inside a vacuum glass chamber. The vacuum before the deposition is around 1 x 10^{-5} Pa. The heat treatment involves increasing the temperature to the desired temperature within 20 minutes and then keeping it constant for 3 hours before finally cooling it down to room temperature.

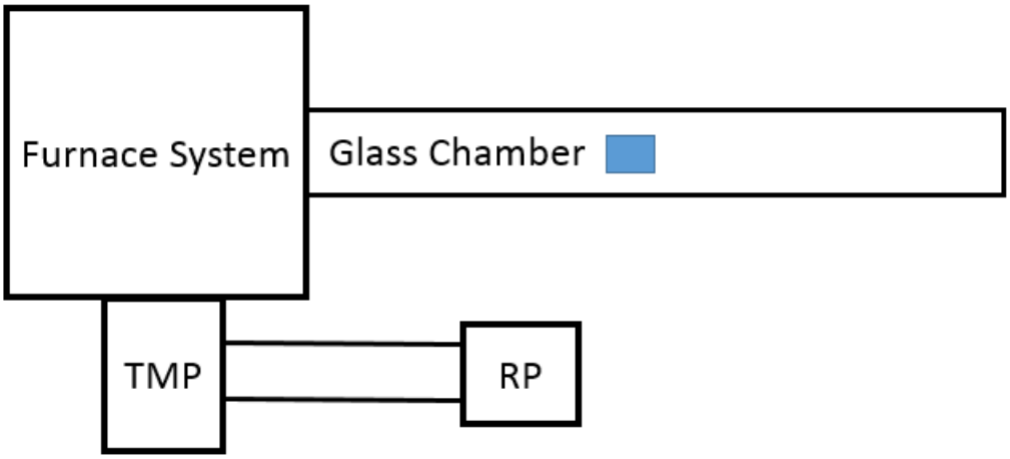

FIGURE 2.6: Schematic illustration of the annealing furnace used in this experiment.

2.3 Characterization of the Film

2.3.1 Structural Analysis

XRD

X-ray diffraction (XRD) is a method commonly employed in order to identify phases inside a crystalline material and additional information such as the dimension of its unit cells. In this work, a rotating stage is used in order to host a thin film samples. The thin film will then be analysed using x-ray in the out-of-plane and the in-plane direction.

A conventional X-ray diffraction instrument includes three simple elements: a tube of x-ray, a sample stage, and a detector.

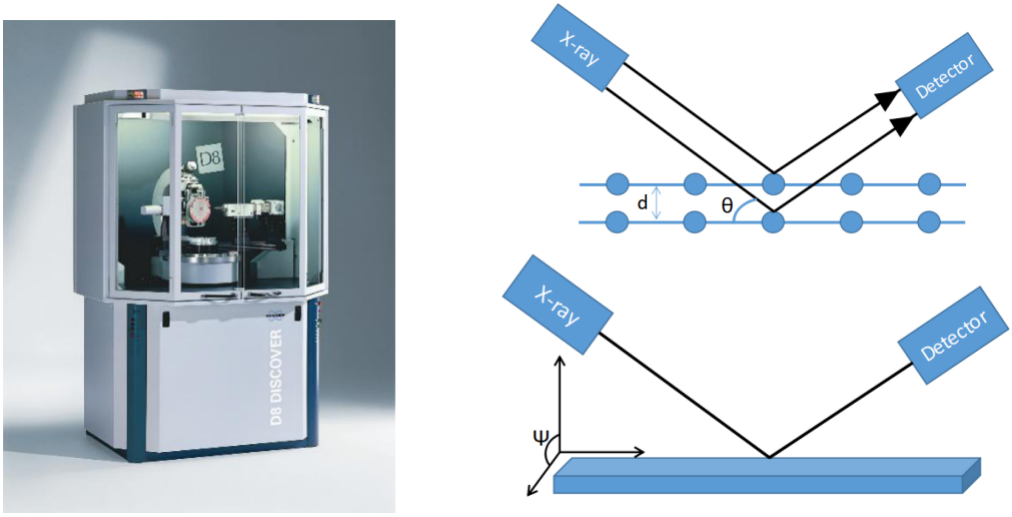

FIGURE 2.7: (left)Bruker's X-ray Diffraction D8-Discover instrument. Figure is adapted from [6], (right)Schematic illustration of the mechanism of X-Ray Diffraction Technique.

When a filament inside a tube of cathode ray is heated, electrons will be produced and accelerated due to applied voltage and will hit a target material. If such electrons have energy large enough to displace the inner shell electrons inside the target material, X-rays are generated. The target material used in this work is copper with a λ of around 1.5418Å.

These X-rays will then be used in a XRD instrument through the use of Bragg's Law: $2d\sin\theta=n\lambda$ [7]. The X-rays produced inside the tube will be directed toward the sample and then will be scattered on several planes. The incoming angle of beam is called θ while the interplanar distance is termed d. When the Bragg's law is satisfied, there will be a constructive interference and peak will form in the result.

In a thin film XRD measurement, the simplest method is using the out-of-plane XRD where the $\psi = 0^o$. The measurement is conducted on a Bruker D8 Discover Diffractometer made by Bruker AXS. The operation condition is at 35 kV and 300 mA. This method is used in this work to obtain the order parameter, out-of-plane grain size, c-lattice constant, and to prove the existence of ordering transformation.

Nevertheless, a thin film sample might have a different grain size in the in-plane direction mainly due to its thin nature. Thus an in-plane XRD measurement is conducted by changing the ψ to around 89^o. The main reason to choose the degree is because if an absolute 90^o is used, XRD peaks would not be able to be detected because the thickness of the sample is in the nanometre scale.

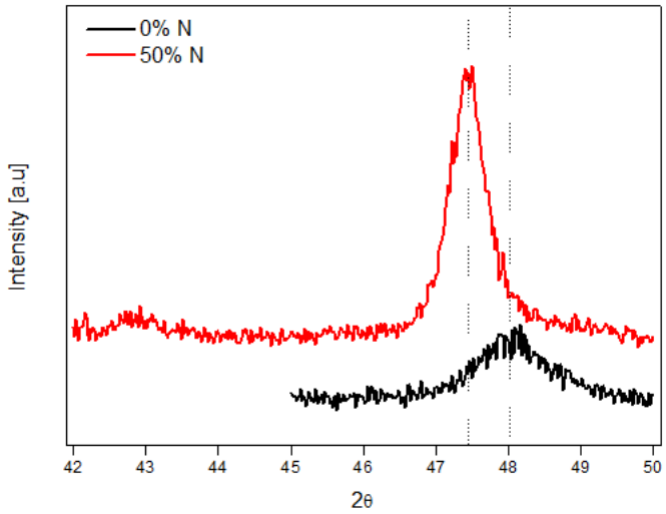

FIGURE 2.8: Typical graph for XRD of CoPt/TiN bilayer films

XRR

X-ray reflectometry (XRR) is a useful technique to analyze and investigate thin films' structures, interfaces, and surfaces by utilizing the total external reflection effect of X-rays. This technique has several advantages as it is non destructive, and can be applied in a lot of materials whether it is a single or multi-layer films, a magnetic or semiconducting materials, and optical materials.

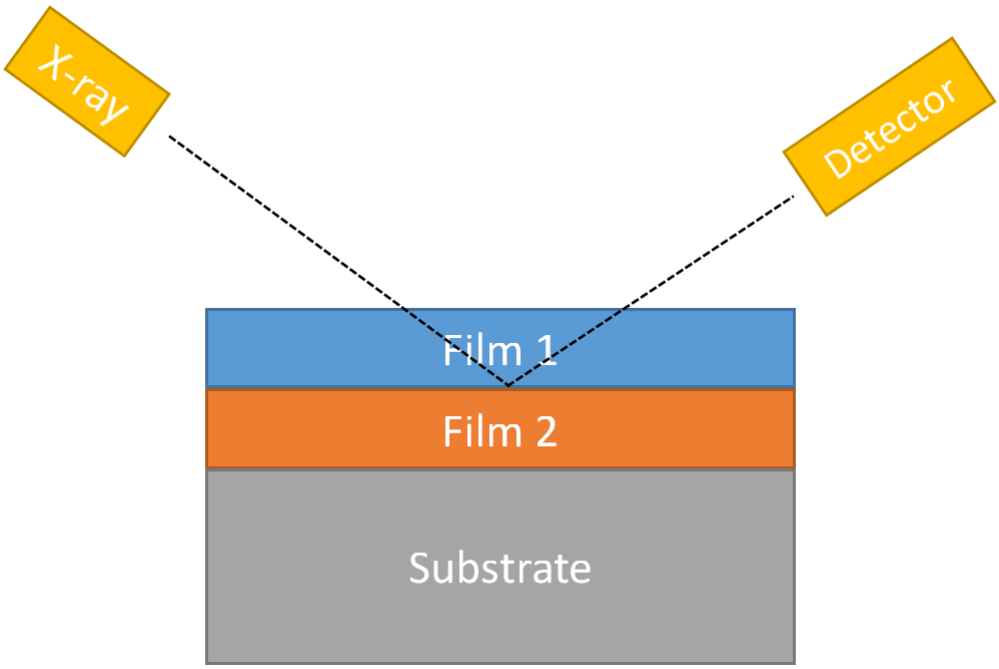

FIGURE 2.9: Schematic illustration of the mechanism of X-Ray Reflectivity Technique.

In XRR, the x-ray beam is aligned around the critical angle, which is around the grazing incidence angles. Below said critical angle of total external reflection, the x-ray beam can only go into several nanometer deep into the samples. However, if the critical angle is exceeded, the penetration depth of x-ray beam will increase significantly. When the electron density changes, or around every interface, the x-ray beam will be reflected and creates oscillation patterns to be observed by the detector and plotted into a reflectivity curves. From said curves, the parameters of the structures including thickness, surface roughness, and density can be determined regardless of the crystallinity of the structure.

TEM

Transmission electron microscopy (TEM) is one of the most powerful tool used to observe the microstructure of the sample up to the atomic level. Electrons of very high energy is passed through an ultra-thin sample, then the electrons that interacted with the atoms are focused and magnified through a series of lenses. Finally, the image is then projected onto a screen. The interactions between the electrons and the atoms are really useful to analyze microstructures such as grain boundaries and dislocations.

- In the diffraction mode, as the electrons are passed through the ultra-thin sample, electrostatic potential set up by elements in the specimen act as a scattering center of the electrons. The transmitted electrons that have passed the sample are then focused by the electromagnetic objective lens from the specimen into one point in the image plane. The image plane in this case is often the back focal plane of the objective lens.hat the image plane is where the image will be formed. (Figure 2.7 (left))

- In image mode, intermediate lens is adjusted such that the image plane is where the image will be formed. (Figure 2.7 (right)) This mode includes the bright-field, dark-field, and high resolution TEM.

  a) Bright-field and Dark-field The back focal plane contains the diffraction pattern that includes the direct beam electrons and diffracted beam electrons. These electrons can be blocked by an objective aperture and thus one or the

other can produce different images. If the objective aperture is used to block the diffracted beam electrons, only the direct beam electrons will pass through and create the image. This is called the bright-field image and the contrast is dependent on the mass and thickness of the sample. On the other hand, if the direct beam electrons are blocked by the objective aperture, only the diffracted beam electrons will pass through and dark-field image will form.

b) HRTEM The high resolution mode is achieved by combining the direct beam electrons and the diffracted beam electrons together to form an image. In order to achieve this, a huge objective aperture is necessary to allow both direct and diffracted electron beams to pass through. Then, by adjusting the focus, tilt angle of the beam and position of the specimen, the high resolution image could be formed.

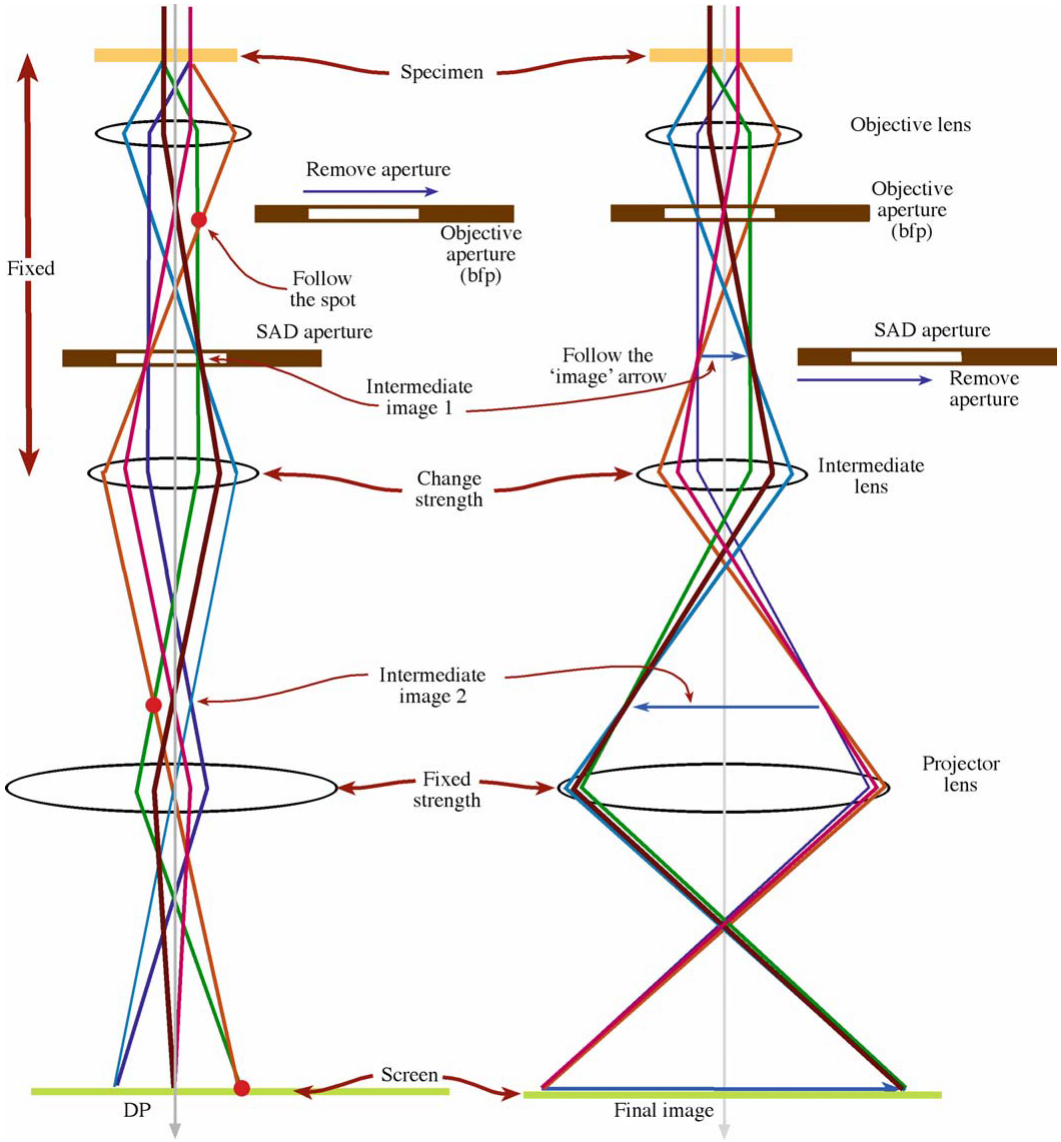

FIGURE 2.10: Schematic illustration of the mechanism of Transmission Electron Microscopy Technique. (left) diffraction mode, (right) image mode. Figure adapted from [8].

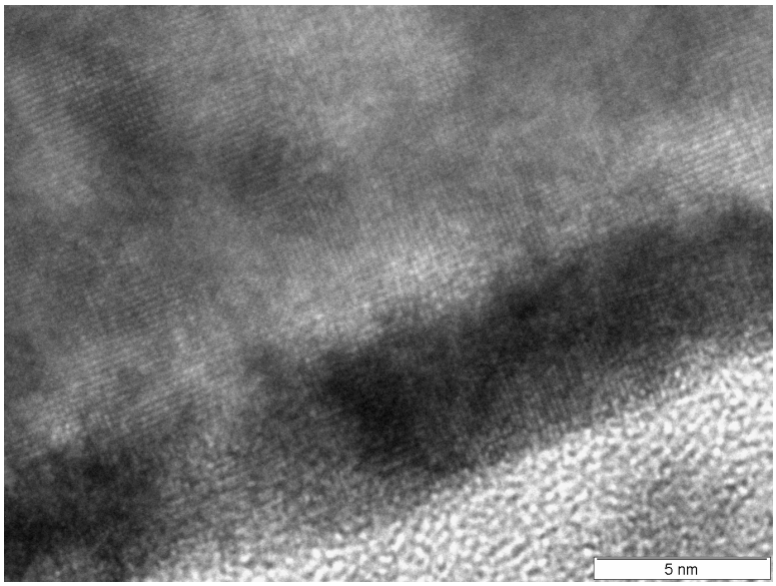

FIGURE 2.11: Typical cross-sectional TEM image. Taken from TiN(40 nm)/CoPt(2.5 nm) sample.

AFM

One of the most conventional way to analyse the surface of a sample is by using an Atomic Force Microscopy (AFM). A typical AFM instrument consists of a sharp tipped cantilever, signal producer, and a detector. As the tip of the AFM gets closer towards the surface of a sample, the force between the surface and the tip allows the tip to contour the surface by bending and changing the degree of signal. The difference in the degree of the signal is received by the detector and processed into an image.

The main use of AFM in this work is to get a sharp look at the contour of the surface and to calculate the roughness of the surface. The AFM used is Hitachi AFM 5000N.

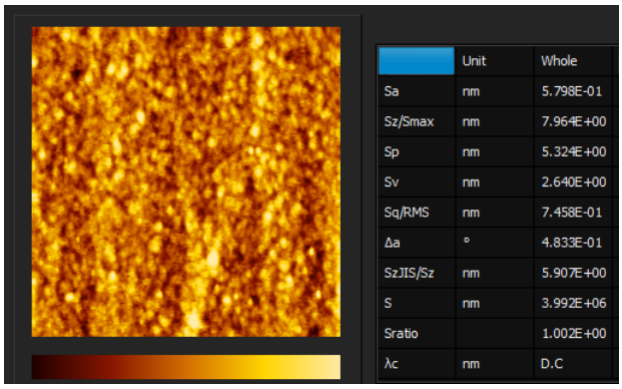

FIGURE 2.12: Typical AFM image of CoPt/TiN bilayer films

2.3.2 Magnetic properties analysis

VSM

Figure 2.6 depicts a typical magnetic hysteresis loops obtained by using vibrating sample magnetometer (VSM). The y-axis is the magnetization, while the x-axis is the applied magnetic field. As the magnetic field is increased, so does the magnetization until a saturated state is achieved (saturated magnetization, M_s). Reducing the H to zero would not be enough to completely erase the magnetization as some magnetization remains as the remnant magnetization, M_r. Further decrease in H in the opposite direction will finally reduce the M to zero, and such point is called the coercive field or H_c.

In thin film samples, magnetization could easily lie on the in-plane direction or the out-of-plane direction. Such direction is commonly termed easy magnetization axis. In the figure, the red line represents the out-of-plane magnetization. This is measured by flowing magnetic field across the thin film sample in the out-of-plane direction. On the contrary, the in-plane magnetization (black line) is measured by fielding magnetic field parallel to the thin film sample. The shaded area is the difference between out-of-plane and in-plane magnetization curves and it represents the effective anisotropy energy K_{eff}. The anisotropy energy is defined by: $H_k M_s/2$. When the easy magnetization axis of a material lies in the in-plane direction, the effective anisotropy energy will be negative, on the contrary, easy magnetization axis lying on the out-of-plane direction means that perpendicular magnetic anisotropy (PMA) is achieved.

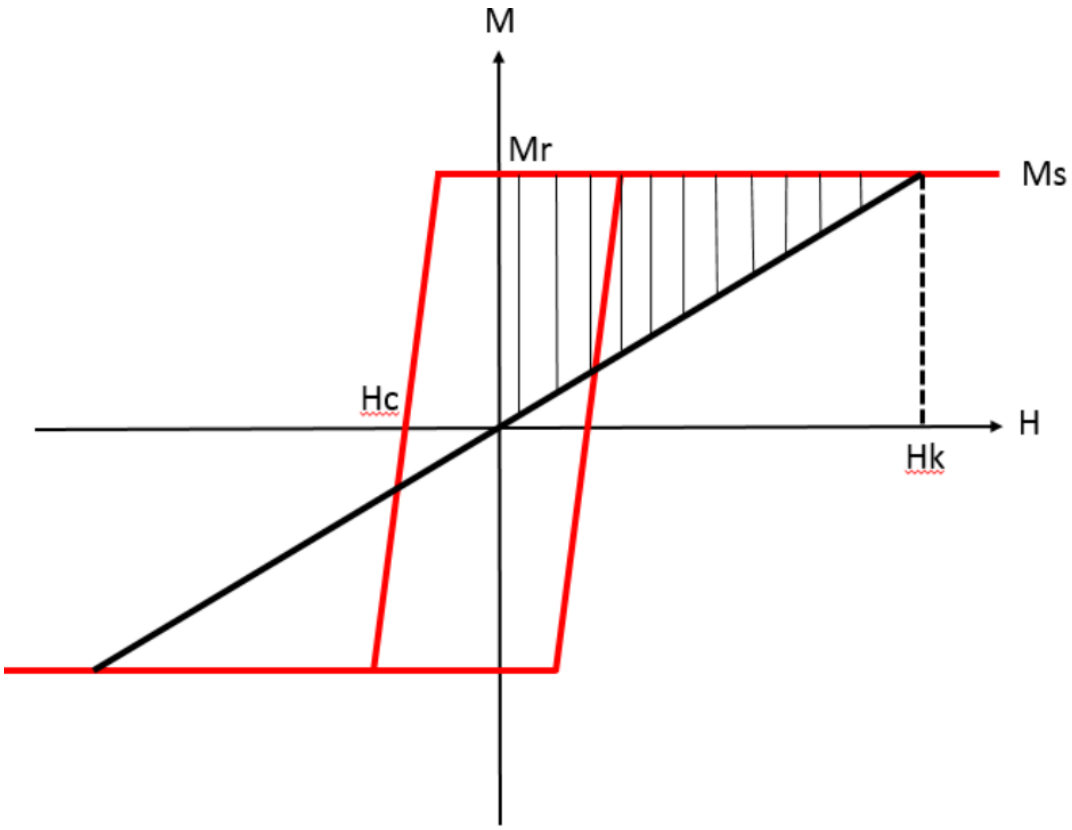

FIGURE 2.13: Ideal M-H curve of a magnetic material.

Magnetic properties of CoPt/TiN bilayer films

In this study, most of the samples are deposited under N_2 gas flow ratio and then annealed at a certain temperature for several hours. In order to get the best magnetic properties, these parameters will be studied. The first parameter to be set is the N_2 gas flow ratio. The figures below shows the M-H curves of TiN(40 nm)/CoPt(10 nm) bilayer films. The N_2 gas flow ratio was varied, and the samples are post-annealed at 700°C.

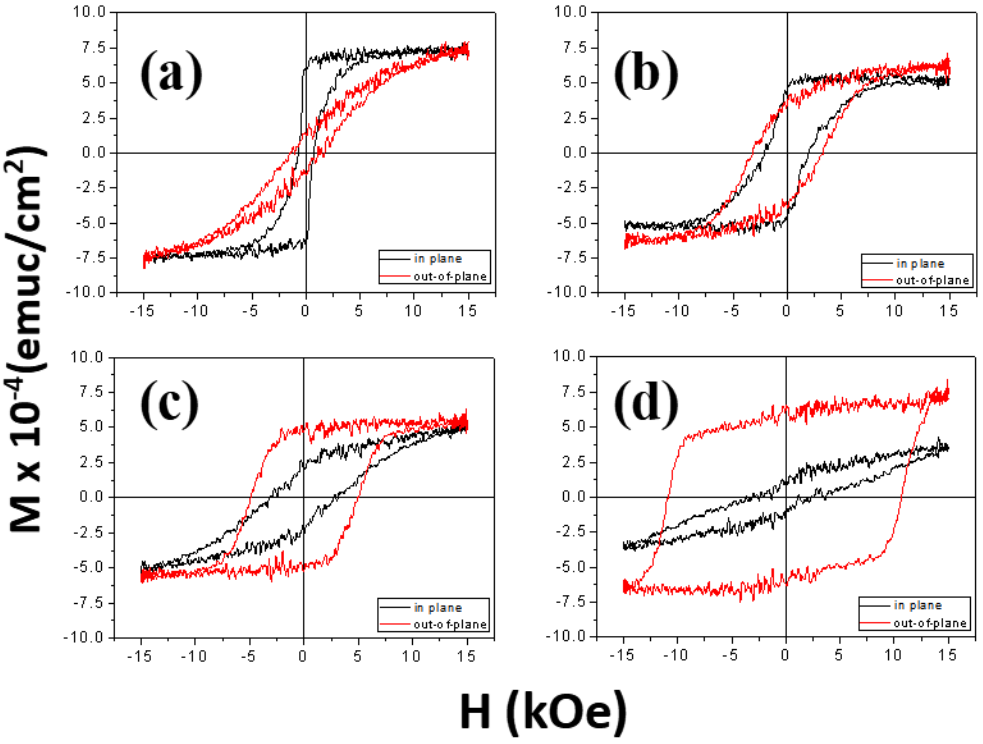

FIGURE 2.14: M-H curves of Glass/TiN(40 nm)/CoPt(10 nm) deposited under x% of N_2 gas flow ratio. Gas flow ratio is varied at (a) 0%, (b) 20%, (c) 40%, (d) and 50%.

From the figure above, it could be observed that not all samples have developed the $L1_0$ phase. This is apparent from the black and red lines of the VSM graph that displays the in-plane and out-of-plane hysteresis loops respectively. At 0% N_2 gas flow ratio, the sample still show the in-plane easy axis of magnetization even after annealing at 700°C. The usual ordering temperature of CoPt alloy is around 800°C so this result is still acceptable. After introducing N_2 gas during the deposition, the magnetization become isotropic without any easy axis of magnetization. This could be called as the point where the $L1_0$ phase starts to form inside the film. However, the transformation is not complete which is why the in-plane component still exist inside the film. When the N_2 gas flow ratio is increased to 40%, the out-of-plane component becomes dominant and the easy axis of magnetization switches to direction normal to the plane. This indicates further $L1_0$ phase transformation inside the film. The easy axis of magnetization become even more oriented towards the out-of-plane direction when the N_2 gas flow ratio is increased to 50%, which could be observed from the dominant out-of-plane hysteresis loop compared to the in-plane

counterpart.

Now that we have established the best N_2 gas flow ratio for the deposition, the next step is to study the effect of post-deposition annealing temperature. The next figures display the hysteresis loops of sample deposited under 50% N_2 gas flow ratio. The post-deposition annealing temperature is varied at 600, 700, and 800 °C for three hours.

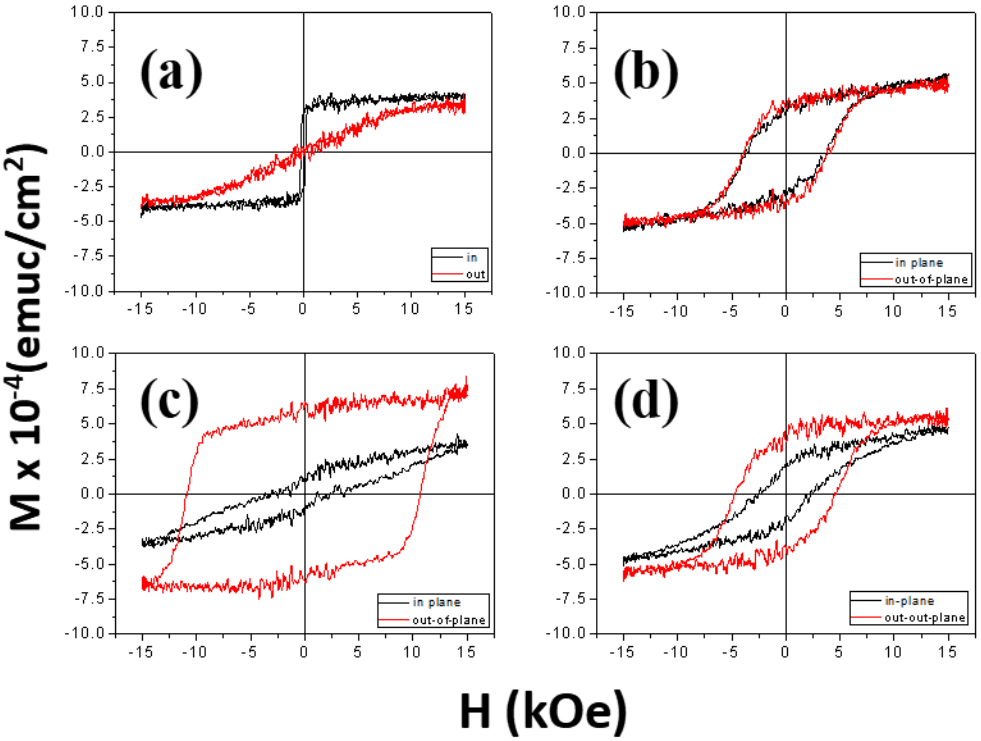

FIGURE 2.15: M-H curves of Glass/TiN(40 nm)/CoPt(10 nm) deposited under 50% of N_2 gas flow ratio. Post-annealed at (a) RT, (b) 600 °C, (c) 700 °C, (d) and 800 °C.

Figure 2.12 (a) shows the as-deposited sample which has in-plane easy axis of magnetization. This could be explained from the lack of $L1_0$ ordering transformation and the domination of the disordered A1 structure that has in-plane easy axis of magnetization. As the sample is annealed at 600 °C, the $L1_0$ starts to order inside the film. This is evident from the magnetic property change from anisotropic into isotropic magnetization, which indicates that a phase with out-of-plane easy axis of magnetization exists inside the film. It is beneficial to note that the point at which $L1_0$ starts to order in the 50% sample is lower compared to the 20% sample. The best magnetic property in terms of out-of-plane magnetization could be found when the

sample is annealed at 700 °C. This could be observed from the large difference in terms of area covered by the out-of-plane and in-plane hysteresis loops. Another interesting point to note is the worsening of out-of-plane magnetization when the annealing temperature is increased to 800 °C. This does not necessarily mean that the $L1_0$ ordering is worse compared to the sample annealed at 700 °C. One possible reason is perhaps due to re-crystallization inside the film that will increase the average grain size. The increase in average grain size will lead to a reduction in domain wall pinning sites and effectively reducing the out-of-plane coercivity.

From this study, we have determined the best condition for depositing TiN(40 nm)/CoPt(10 nm) on top of glass substrate. The N_2 gas flow ratio is fixed at 50% while the post-deposition annealing temperature is set at 700 °C for three hours.

Bibliography

[1]E. L.C.J. S. Y. F. Ding, J. S. Chen and G. M. Chow, J. Appl. Phys. **97** (2005).

[2]M. O.N. I. M. Futamoto, M. Nakamura and T. Shimotsu, AIP Advances **6** (2016).

[3]M. F.F. K. T. Shimizu, M. Ohtake and N. Inaba, IEEE Trans. Magn. **53** (2017).

[4]H. An, J. Wang, J. Szivos, T. Harumoto, T. Sannomiya, S. Muraishi, Y. N. G. Safran, and J. Shi, J. Appl. Phys. **118**, 203907 (2015).

[5]*Sputter deposition techniques.* http://www.uccs.edu/~tchriste/courses/PHYS549/549lectures/sputtertech.html.

[6]*Structure and transport characterization.* https://nanooxides.kaust.edu.sa/Pages/Characterization1.aspx.

[7]B. D. Cullity, *Elements of x-ray diffraction* (1978), p. 139.

[8]D. B. Williams, and C. B. Carter, *Transmission electron microscopy* (2009), pp. 153, 183.

Chapter 3

Effect of Nitrogen Incorporation on the Ordering Transformation of CoPt in CoPt/TiN Bilayer Films

As described in Chapter 1, $L1_0$ FePt and CoPt has piqued interests from researchers around the world for their application as the magnetic recording media based on perpendicular magnetic recording technology and their potential to be further applied in future technologies of magnetic recording. The $L1_0$ phase is usually formed from the disordered A1 structure at high temperatures (>500 ^{o}C). Two of the most promising magnetic storage technologies that can utilize this structure are exchange coupled composite and anisotropy graded media, mostly due to their potential to exploit the different ordering kinetics of the $L1_0$ phase.[1] By tuning the ordering kinetics, different magnetic anisotropy constant can be realized across a multi-layer magnetic thin film, and through the hard-soft layer exchange coupling, the switching field of the system can be reduced. The ordering kinetic can be varied by ways of changing the deposition temperature,[2] inserting under layers to induce strain inside the films,[3] and by adding third elements into the alloy (Sn, Pb, etc.).[4] Unfortunately, these techniques require longer fabrication time or more complicated equipments due to the extra targets, which may increase the total cost of production. Thus, finding an optimum fabrication method that can manufacture a multilayer film structure with different magnetic anisotropy constant is an important step to the future of magnetic recording technology.

One way to tune the ordering transformation kinetics is by flowing gas during

the fabrication and post-annealing. Several researchers have reported their work which focused focused on incorporating gas atoms (hydrogen and nitrogen) during the fabrication or annealing.[5, 6] Forming gas (5% H2 and 95% Ar) flowed durint the post-deposition annealing has the potential to improve the coercivity of nanoparticles of FePt, this could be explained by the reductive effect of the forming gas.[6] Lai et al. proposed a secondary explanation that includes the possibility of hydrogen atoms dissolving inside the FePt lattice.[7] A1 structure of FePt and CoPt is similar in structure as the Pd atoms, in which hydrogen atoms have been found in the octahedral interstitial sites.[8] These interstitial atoms of hydrogen are trapped by vacancies inside the film with a relatively high binding energies. The phenomenon of hydrogen atoms trapping implied that the total energy needed to form a vacancy-hydrogen complex should be reduced by the total amount of binding energy.[9–12]

Improvement in perpendicular coercivity in CoPt and FePt has also been observed through means of nitrogen incorporation. In FePt, the formation of iron nitride and improved long-range ordering is proposed by Wang et al. as the main reasons behind the increased coercivity.[13] However, in CoPt films, formation of cobalt nitride is not detected inside the films, an alternative explanation is given by An et al., which state that dissolving nitrogen atoms will increase the lattice parameter and help to offset the difference in lattice constant between the CoPt and the under layer, which promotes epitaxial growth and thus, a better ordering transformation.[14] Furthermore, nitrogen atoms have been found to escape the lattice of CoPt during post-annealing.[13]

with regards to this, the work in this chapter aim to uncover the mechanism of the ordering transformation improvement by means of nitrogen incorporation. The effect of nitrogen incorporation is confirmed by depositing CoPt thin films on MgO, TiN/MgO, and TiN/Glass substrates.

3.1 Deposition of CoPt/TiN bilayer films

CoPt films were deposited on MgO single crystal (001) substrate and fused quartz with TiN seed layer to promote the epitaxial growth using dc magnetron sputtering at 400 °C. A base pressure of 5×10^{-5} Pa and deposition pressure of 0.2 Pa were

conditioned for the experiment. The target used was a 2 inch Co and Pt composite target (surface area ratio of the Co and Pt inside the target is 1.56:1). CoPt films were deposited in a N_2 and Ar mixture with N_2 gas flow ratio of x% (x = 0, 20, 40, 50) while the TiN layers were sputtered with a fixed ratio of 10% N_2 gas flow ratio. The thickness of CoPt films were fixed at 10 nm and the TiN layers were 0, 5, and 40 nm for the samples deposited on MgO and 40 nm for the samples deposited on fused quartz. Thickness of the films was carefully controlled by controlling the deposition time with pre-known deposition rate. Post-deposition annealing was done at 600, 700, and 800 °C for 3 h in vacuum (better than 1×10^{-5} Pa). The magnetic properties were measured by using a vibrating sample magnetometer (VSM) Riken Denshi BHV-50V with an applied field of $\pm$ 10 kOe. The crystal structures were characterized by x-ray diffractometer (Bruker D8 Discover diffractometer) by applying Cu Kλ radiation. Co and Pt ratio inside the film is 44:56 which was measured by inductively coupled plasma-optical emission spectrometer. In the ICP-OES, the sample is heated at high temperature until it is converted into excited ions. When the ions return to their ground state, they will emit a radiation(s) which will be detected and measured by detectors.

3.2 CoPt thin film deposited on MgO

3.2.1 Magnetic properties measurement

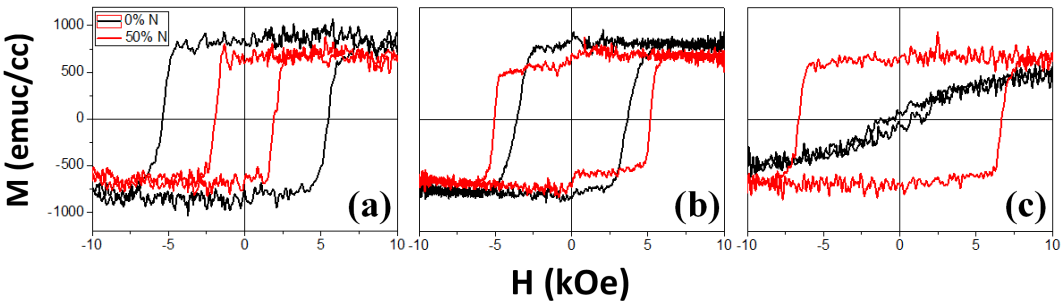

FIGURE 3.1: Perpendicular M-H curves of CoPt thin films deposited on (a) MgO single crystal substrate, (b) TiN (5 nm)/MgO substrate, (c) TiN (40 nm)/MgO substrate.

Figure 3.1 exhibits the typical M-H curves of the CoPt/MgO and CoPt/TiN/MgO samples. The red lines and black lines represent samples deposited under a partial

N_2 gas flow and no N2 gas flow, respectively. It can be seen from Figure 3.1 (a) that, on MgO (001) substrate, the incorporation of N_2 gas deteriorates the perpendicular coercivity. On the other hand, on the MgO substrate with TiN under layer, the incorporation of N_2 gas improves the perpendicular coercivity as shown in Figure 3.1 (b). The effect of incorporating N_2 gas is most striking when the TiN thickness is increased to 40 nm as shown in Figure 3.1 (c). In such a case, the M-H loops suggest that incorporation of N_2 gas greatly improves the ordering transformation and perpendicular coercivity, while no ordering transformation occurred after annealing at 700 ^oC for the sample without the partial N_2 gas flow.

3.2.2 Structure characterization

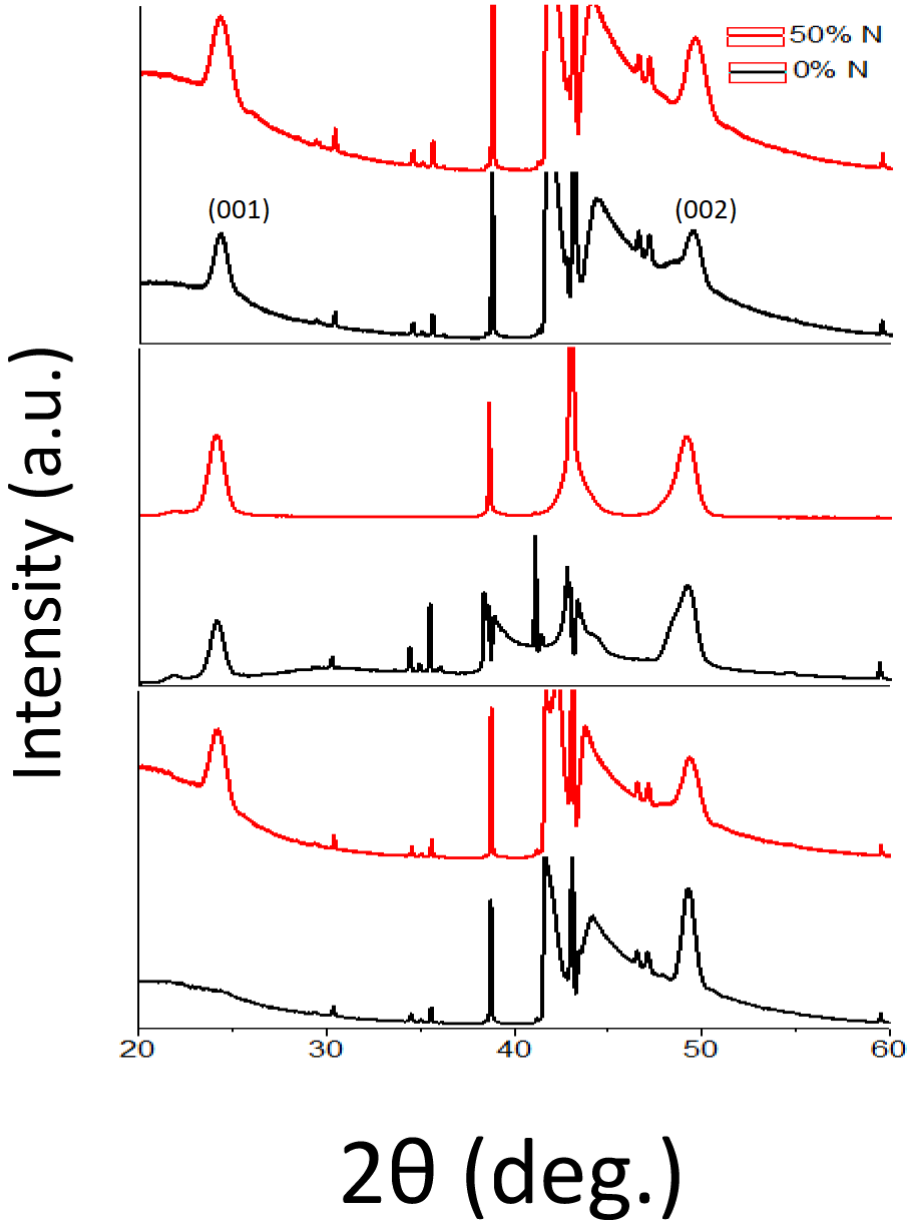

FIGURE 3.2: Out-of-plane XRD of (a) CoPt/MgO, (b) CoPt/TiN(5 nm)/MgO, and (c) CoPt/TiN(40 nm)/MgO annealed samples.

In order to confirm the main cause of the difference in coercivity, the out-of-plane XRD results of the samples were displayed in Figure 3.2. Chemical ordering parameter S is considered a reliable feature to describe the degree of ordering and thus, the magnetic anisotropy inside a $L1_0$ based material. Ordering parameter is defined as the following:

$$S^2 = (I_{001}/I_{002})_{\text{measured}}/(I_{001}/I_{002})_{\text{calculated}}$$

Where the I_{001}, and I_{002} are the integrated intensity of superlattice peak (001) and the fundamental peak (002). $(I_{001}/I_{002})_{measured}$ means the measured intensity ratio of the peaks and the $(I_{001}/I_{002})_{calculated}$ represents the calculated intensity ration which is defined as:

$I_{calculated} = |F|^2 p(LP)e^{-2M}$, $LP = (1 + \cos^2 2\theta)/(\sin^2 \cos\theta)$

F represents the structure factor, p defines the multiplicity factor, LP is the abbreviation of Lorents-polarization factor, and e^{-2M} is the temperature factor. Previous work in our research group has done the calculation and calculated the to be around 1.893, which is similar to the value of other research group.[15] The largest ordering parameter could be found in CoPt/MgO (0% N_2) and CoPt/TiN(40 nm)/MgO (50% N_2) which are around 0.845 and 0.826 respectively. This result coincides with the fact that both the samples also have the largest perpendicular coercivity. This proves that the coercivity in this experiment is largely influenced by ordering parameter and therefore, the ordering transformation. It can also be observed that when deposited on MgO, CoPt has better ordering parameter without nitrogen (S = 0.845) compared to when nitrogen is incorporated (S = 0.744). On the contrary, CoPt deposited on TiN has better ordering parameter when nitrogen is incorporated during the deposition. At 5 nm, the ordering parameter improved from 0.614 to 0.73. At 40 nm, the ordering parameter improvement is more significant as without nitrogen there is no ordering transformation and with nitrogen it increases to 0.826.

The previous results suggest that the difference in nitrogen effects in CoPt/MgO and CoPt/TiN/MgO samples could be attributed to the difference in the strain conditions of the films during the deposition. In order to understand the relation between partial N2 gas flow and strain energy, XRD measurements were done to get the lattice parameter in the out-of-plane and in-plane direction of the as-deposited CoPt/MgO and CoPt/TiN/MgO samples. The results of the *c/a* lattice parameter measurement are illustrated in Figure 3.3 (a). The ratio between c and a lattice parameters could help explain the strain conditions of the films. When the in-plane lattice constant a is larger than the out-of-plane lattice constant c, it means that the sample is deposited under a tensile stress, on the contrary, if the out-of-plane lattice constant c is larger than the in-plane lattice constant a, it means that the sample is

deposited under a compressive stress. In addition, the introduction of nitrogen generally promotes compressive stress (observed by the increased *c/a* ratio) during the deposition as shown in Figure 3.3 (a) in which the red dotted line (N2 incorporated samples) is higher than black dotted line (no N2 samples). CoPt/MgO sample deposited under no N2 flow shows tensile stress ($c/a < 1$) and a decrease in perpendicular coercivity as the strain changes from tensile to the compressive direction. On the other hand, CoPt/TiN/MgO samples are subjected to a compressive stress ($c/a > 1$), and display an increasing perpendicular coercivity with compressive stress. This indicates that samples deposited under no N2 flow benefit from the tensile stress to improve the $L1_0$ ordering and achieve perpendicular magnetic anisotropy. This finding is in agreement with the reports of other researchers.[15]

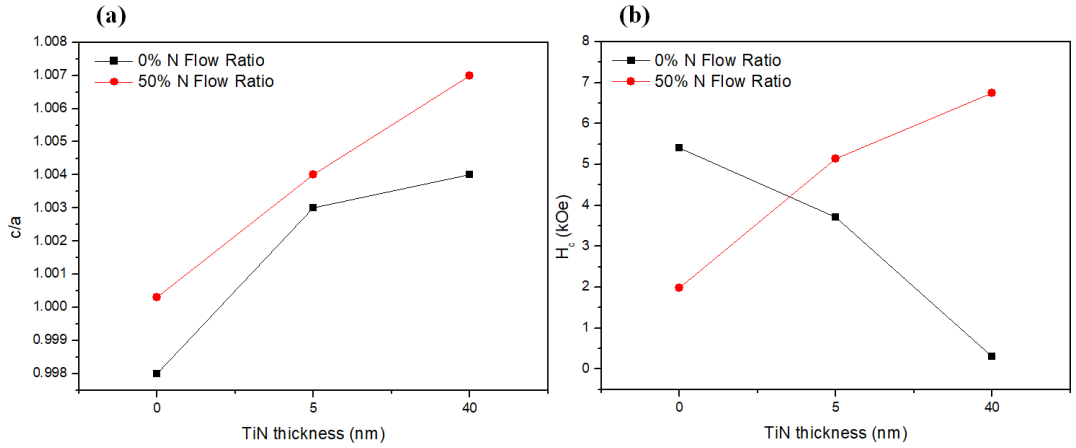

FIGURE 3.3: (a) TiN thickness vs c/a constant of as-deposited CoPt samples and (b) TiN thickness vs out-of-plane coercivity H_c of annealed CoPt samples.

For the thin 5 nm TiN under layer samples, the compressive strain is smaller compared to the 40 nm TiN under layer, and the samples still exhibit PMA even without the incorporation of nitrogen gas. It could be assumed that the strain from the MgO substrate still could induce ordering transformation in CoPt due to the thinness of the TiN under layer. However, by incorporating nitrogen gas, the coercivity and ordering parameter of CoPt/TiN(5 nm)/MgO increases. This signifies that there is another mechanism that improves ordering other than the strain inside the film. For the 40 nm TiN under layer sample, the sample only show $L1_0$ ordering under compressive stress, which is contradictive to the common belief that tensile stress is

better for ordering. Moreover, the ordering only happens when nitrogen is incorporated during deposition. This unique finding displays an undeniable evidence of a new mechanism brought forth by the nitrogen atoms during the deposition and annealing which will be discussed later.

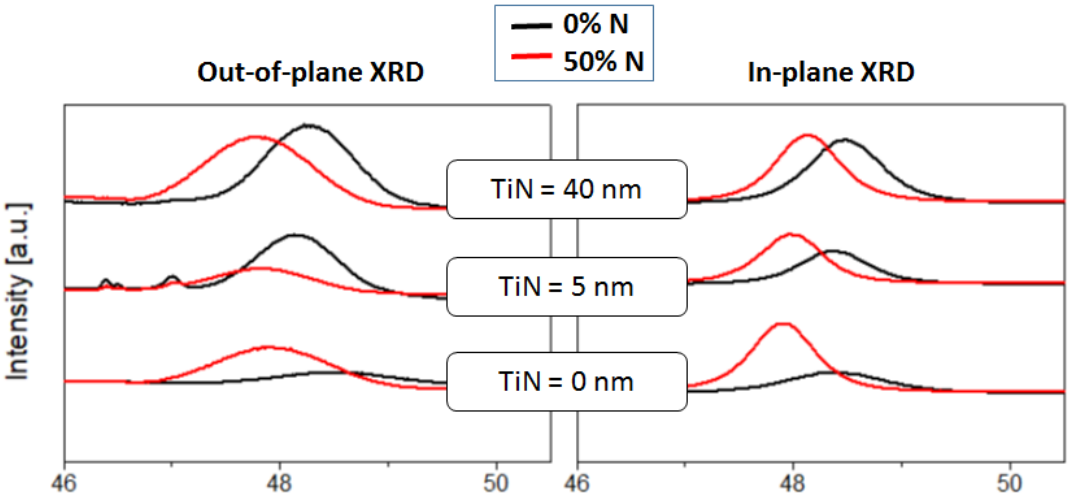

FIGURE 3.4: XRD profiles of as-deposited CoPt samples taken in (a) out-of-plane orientation and (b) in-plane orientation.

The XRD profiles of as-deposited samples are illustrated in Figure 3.4. XRD profiles of samples both with and without TiN intermediate layer show a left-hand shift of CoPt (002) peak after the introduction of nitrogen during the deposition. The shift of CoPt (002) peak to the left indicates that both the a and c lattice parameters were increased during the deposition. The increase in lattice parameter can be attributed to the dissolution of nitrogen atoms into the CoPt lattice during the deposition. Previous research stated that the introduction of nitrogen atoms inside the film relaxes the lattice mismatch, promotes epitaxial growth and increases the crystallinity of CoPt (002).[16] This is true in the in plane direction, but in the perpendicular direction, such fact can only be observed on CoPt/MgO samples but not on the CoPt/TiN/MgO samples. This makes us believe that the CoPt thin films grown on MgO and TiN have different growth process.

3.2.3 Discussion

On MgO single crystal substrate, the CoPt grows epitaxially and the enlargement of lattice parameter does relax the lattice mismatch resulting in a better epitaxial

growth and a higher crystallinity. On TiN, the CoPt film grows incoherently and the incorporation of nitrogen atmosphere degrades the crystallinity. This is perhaps due to the dissolution of nitrogen atoms inside the thin film, which introduced compressive stress which was relieved by dislocations. The increased number of defects is the main reason of the deteriorated crystallinity.

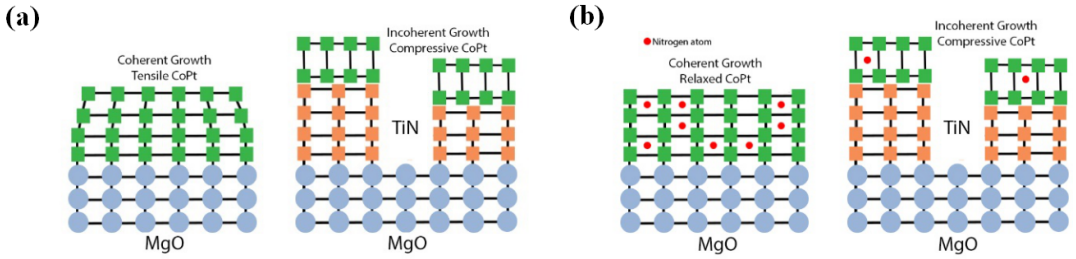

FIGURE 3.5: Schematic growth processes of CoPt films with (a) 0% nitrogen gas flow ratio and (b) 50% nitrogen gas flow ratio, on MgO substrates.

For samples deposited on MgO substrate, a higher crystallinity is related to a lower tensile stress during the deposition. The dissolution of nitrogen atoms inside the thin film during sputtering resulted in the enhancement of lattice parameter in all direction. The enlargement of CoPt lattice parameter reduces the lattice mismatch between CoPt and MgO. The lattice mismatch between CoPt and MgO is responsible for the tensile stress during the deposition (evident from the fact that a lattice parameter is larger than c lattice parameter during deposition). It has been reported that tensile stress is beneficial for the rotation of $L1_0$ c-axis towards the perpendicular direction during the post-annealing process. Moreover, tensile stress increases the a lattice parameter while reducing the c lattice parameter, creating a good condition for a face centred tetragonal ($L1_0$) ordering.[17] That is to say, the strain energy stored in the lattice is one of the driving force for $L1_0$ transformation. For the sake of explanation, we call this phenomenon the strain-induced ordering. Therefore, the reduction of tensile stress due to the N_2 gas incorporation will result in the reduction of strain energy of CoPt film and thus, its degree of order. This leads to the degradation of its perpendicular magnetic anisotropy and the perpendicular coercivity.

For samples deposited on MgO substrate with TiN intermediate layer, larger compressive stress results in larger perpendicular coercivity, which indicates a better ordering transformation. This result contradicts the previous research that stated

tensile stress is beneficial towards the ordering of $L1_0$ phase. In order to explain this, the average grain size in the TiN layer was measured from XRD peaks. Due to the similarity of TiN and MgO peak positions, it is difficult to get TiN peak from TiN/MgO samples, thus, TiN/Glass sample was deposited under the same condition and measured with XRD. From the peak that was obtained, a Gaussian function peak was fitted and the FWHM was calculated in radian. Then, using Scherrer equation: $L = K\lambda/(FWHM \times cos\theta)$, the average grain size of TiN film can be obtained.

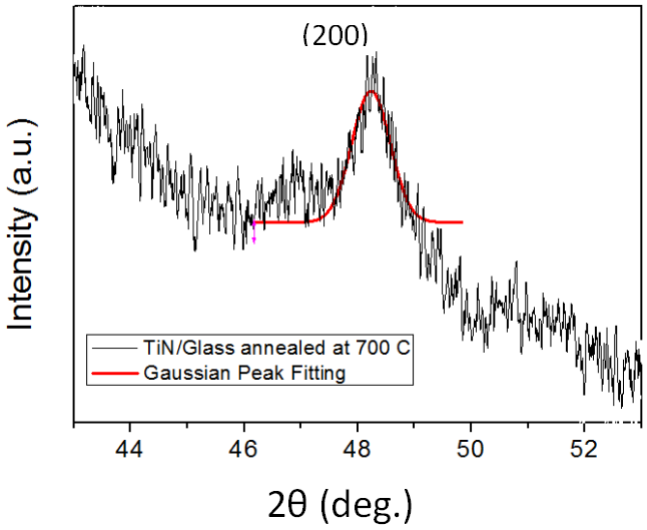

FIGURE 3.6: XRD profiles of TiN layer on glass substrate.

In our research, the average grain size of TiN was measured to be around 11.5 nm, which comparable to the grain size of as-deposited CoPt with and without N_2 gas incorporation (12.3 and 10.82 nm respectively). This indicates that the growth of CoPt on TiN does not happen in a long-range scale but rather short-ranged inside each grains of TiN. This explains why the strain induced ordering is not dominant in this case and indicates that a new mechanism is responsible for the improved ordering transformation of samples deposited on TiN layer. In fusion reactor research, it is widely known that ion implantation will induce vacancies that will trap the implanted ions.[18, 19] Therefore, in the presence of interstitial gas atoms, vacancies should exist in the form of vacancy-gas atoms clusters. Therefore, their formation energy should be decreased by about the sum of the vacancy-gas atoms binding energies.[20] This can be illustrated by the term the e_f^c, formation energy of vacancy-gas atom complex, which is equal to the formation of vacancy energy, e_f^v, minus the

total amount of e_b, vacancy-gas atom binding energies; viz.

$e_f{}^c = e_f{}^v - e_b$.

For hydrogen atoms, the binding energy of vacancy-hydrogen is substantially high that the reduction in formation energy is noticeable, and this enhanced the equilibrium concentration of the vacancies (vacancy-hydrogen clusters). For most metals, the diffusion functions by the vacancy mechanism. The metal atoms diffusivity, D, is expressed as:

$D = x_v\, D_v$

Where the diffusivity of vacancy, D_v, diminishes with increasing trapped gas atoms, but a significant increase in vacancy concentration, x_v, is more than enough to offset the reduction of D_v.[12] The diffusion of metal atoms should be improved with the increase number of vacancies inside the thin film.

Similar to hydrogen, nitrogen gas has also been reported to increase the lattice parameter of TiN by dissolving interstitially in the octahedral sites of the TiN lattice.[21] CoPt, like FePt and TiN in previously stated researches, has a face centered cubic structure thus it is highly possible that nitrogen atoms dissolve interstitially in the octahedral sites of fcc CoPt. Furthermore, a superabundant vacancies-like state induced by nitrogen was found in an experiment by Kikuchi et al.[22] Therefore, we suggest a mechanism called diffusion-driven ordering for our results.

One way to track the existence of superabundant vacancies inside the thin film is by confirming the existence of volume shrinkage in the samples when nitrogen is incorporated during the deposition. In order to restrict the external factors coming from the TiN under layer, CoPt/MgO samples were chosen to be measured and compared. Table 3.1 shows the a and c lattice parameters were all calculated from the XRD peaks from Figure 3.2, Figure 3.4 and Figure 3.7. In the as-deposited samples, it can be seen that with the incorporation of nitrogen, the atomic volume increases. This is due to the existence of interstitial nitrogen atoms inside the crystal lattice. However, when heated at high temperature, the sample with nitrogen incorporation is actually smaller compared to the sample without nitrogen. The reason could be that the interstitial atoms escaped the film and leave behind vacancies inside the lattice that will reduce the average atomic volume.

TABLE 3.1: Lattice Parameters of CoPt/MgO samples.

As-deposited samples	**Annealed samples**
CoPt/MgO - 0% N_2	**CoPt/MgO - 0% N_2**
c = 3.751 Å	c = 3.697 Å
a = 3.758 Å	a = 3.784 Å
V = 52.9737 Å^3	V = 52.936 Å^3
CoPt/MgO - 50% N_2	**CoPt/MgO - 50% N_2**
c = 3.794 Å	c = 3.682 Å
a = 3.793 Å	a = 3.782 Å
V = 54.5837 Å^3	V = 52.6656 Å^3

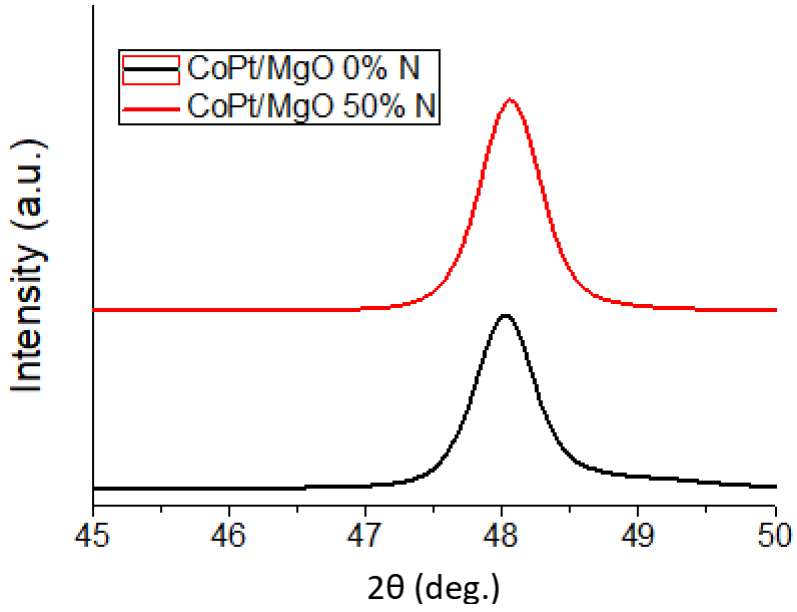

FIGURE 3.7: In-plane XRD of CoPt/MgO annealed samples.

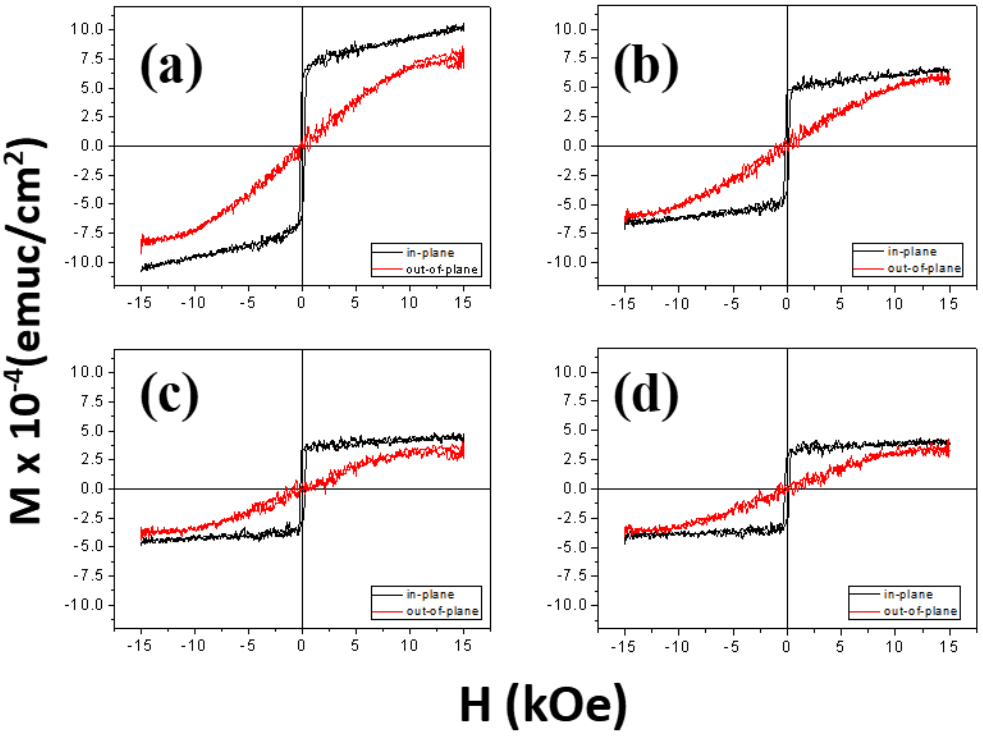

FIGURE 3.8: M-H curves of as-deposited CoPt films with (a) 0% N_2, (b) 20% N_2, (c) 40% N_2, and (d) 50% N_2.

3.3 CoPt thin film deposited on glass

The effect of nitrogen gas incorporation is further studied by depositing CoPt with TiN intermediate layer on glass substrate. Depositing on an amorphous substrate eliminates the possibility of a strain-induced ordering due to tensile stress and further emphasizes the diffusion-driven ordering.

Figure 3.12 displays the out-of-plane coercivity H_c of the CoPt (0% N_2) and CoPt (50% N_2) as deposited samples and post-annealed samples as a function of annealing temperature. In the as deposited state, both samples exhibit a low H_c of several hundred Oe. This result shows that the current magnetic state is of the soft magnetic state and thus no ordering has occurred. The trend of increasing H_c with respect to annealing temperature is also observed in our results which is in agreement with those reported by Luo et al.[23]

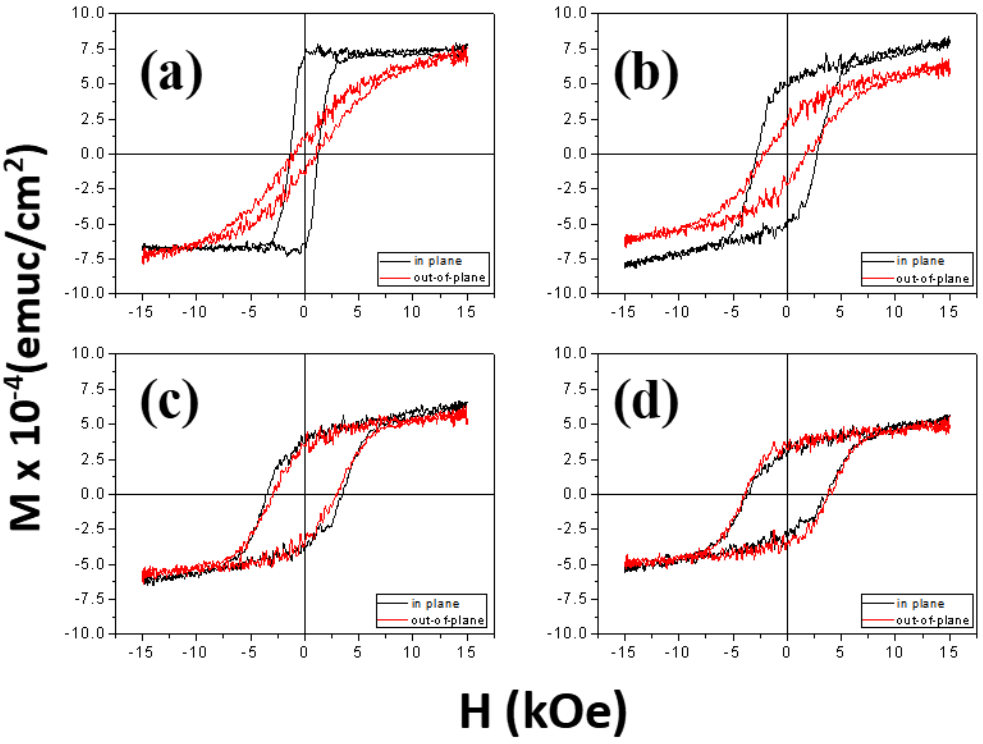

FIGURE 3.9: M-H curves of CoPt films post-annealed at 600 °C with (a) 0% N_2, (b) 20% N_2, (c) 40% N_2, and (d) 50% N_2.

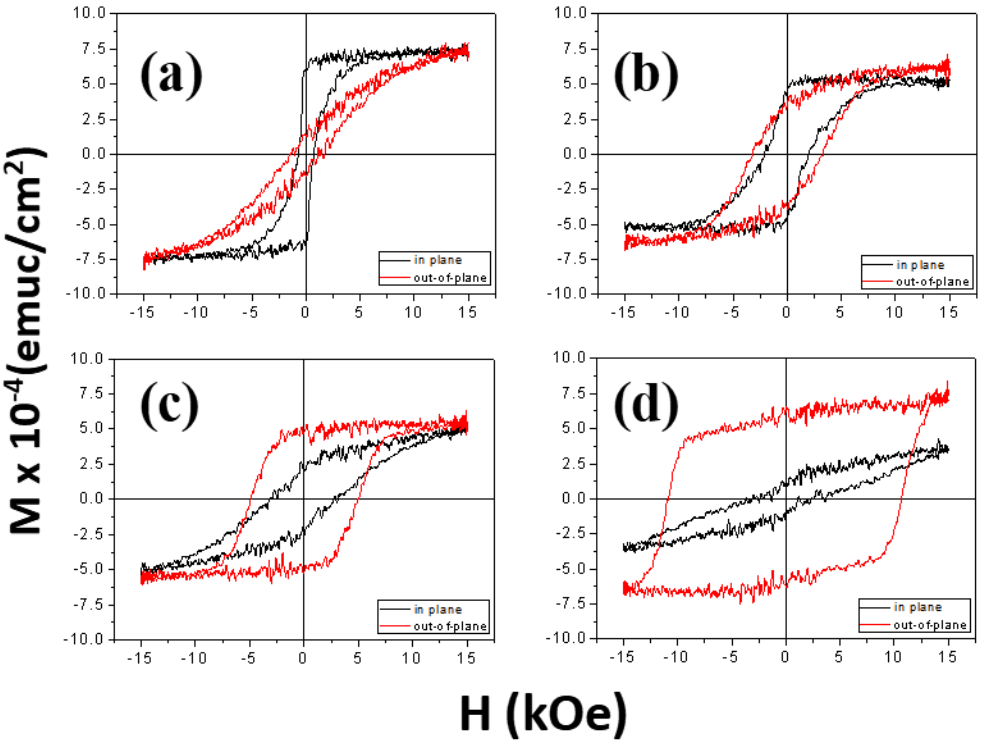

FIGURE 3.10: M-H curves of CoPt films post-annealed at 700 °C with (a) 0% N_2, (b) 20% N_2, (c) 40% N_2, and (d) 50% N_2.

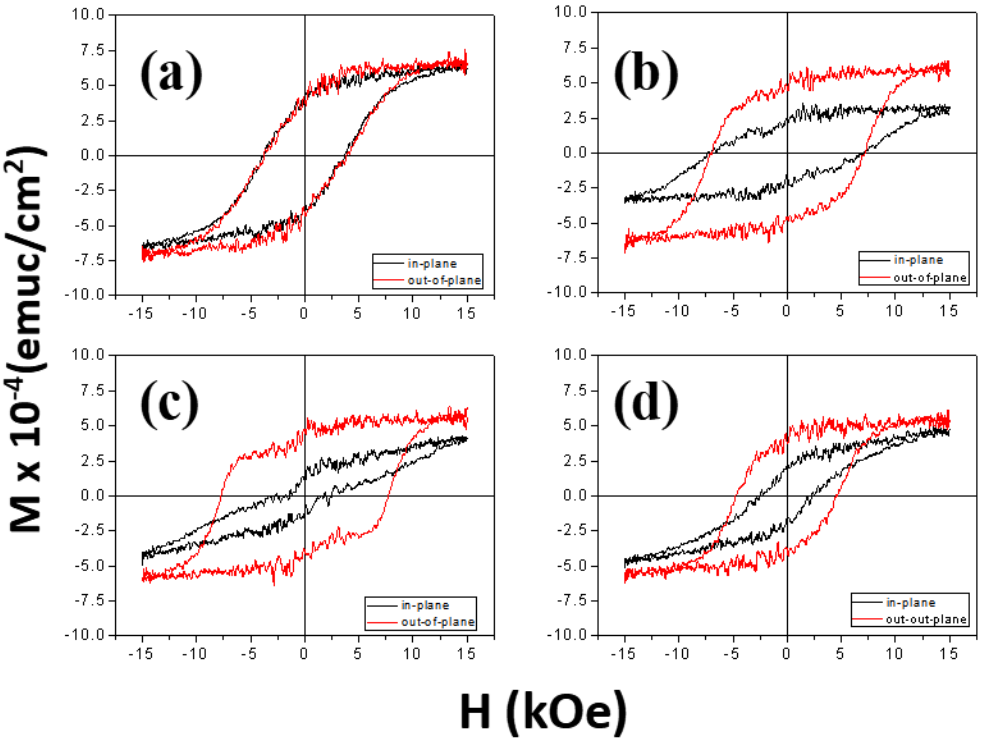

FIGURE 3.11: M-H curves of CoPt films post-annealed at 800 °C with (a) 0% N_2, (b) 20% N_2, (c) 40% N_2, and (d) 50% N_2.

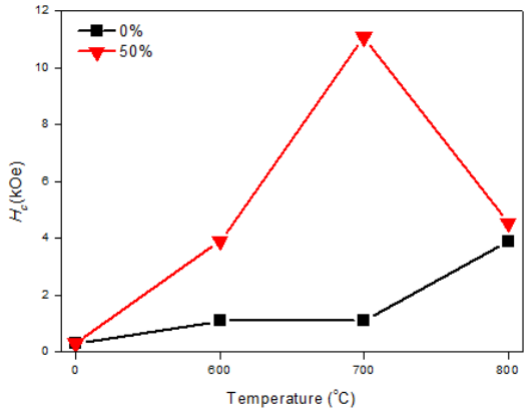

FIGURE 3.12: Out-of-plane coercivity of CoPt (0% N_2) and CoPt (50% N_2) versus annealing temperature.

The effect of the incorporation of nitrogen gas during the deposition starts to show at the post-annealed samples. With the partial N_2 gas flow, a large coercive field of around 4 kOe can be achieved at 600 °C for 10 nm CoPt thin film. On the contrary, samples without the partial N_2 gas flow can only achieve H_c of such magnitude at 800 °C, or 200 °C higher than sample with the nitrogen gas flow. This result points out that the ordering transformation of sample with 50% nitrogen gas

ratio starts at around 600 °C or lower temperature and is lower than that of the 0% nitrogen gas ratio sample. This means that by flowing nitrogen gas during deposition and annealing the thin film, a 200 °C reduction in ordering temperature can be obtained.

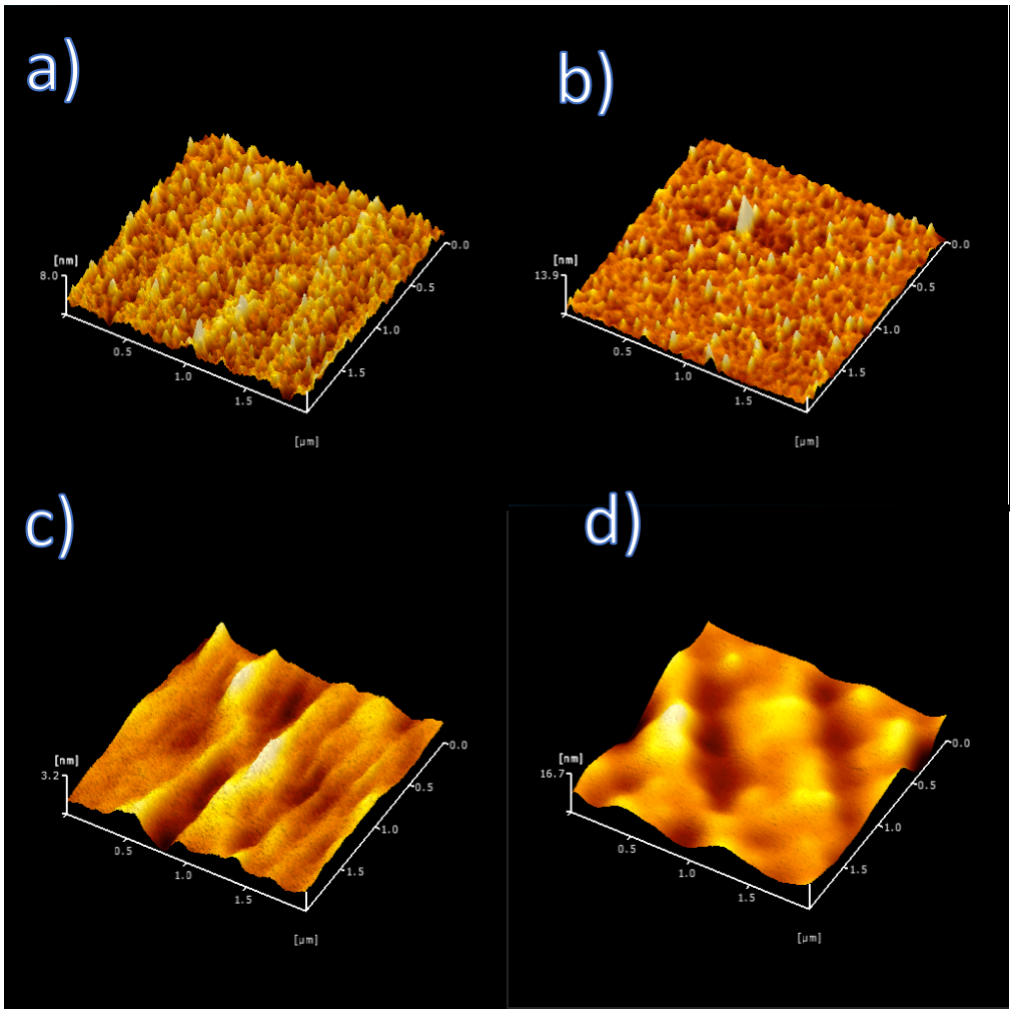

FIGURE 3.13: Surface morphology of CoPt/TiN (40 nm)/Glass samples with a.) 50% nitrogen gas flow ratio and b.) 0% nitrogen gas flow ratio.

It is also observed that the H_c of CoPt film with 50% nitrogen gas flow ratio drops when the annealing temperature increases to 800 °C. This could be due to the increase in grain size due to annealing at high temperature. Figure 8 illustrates the morphology of CoPt/TiN/Glass with 50% nitrogen gas flow ratio that was taken with AFM. When the sample was annealed at 800 °C, the morphology changes from a quite rough surface to a smooth surface, this indicates that recrystallization occurred at this temperature and increases the grain size of the CoPt film. The increase

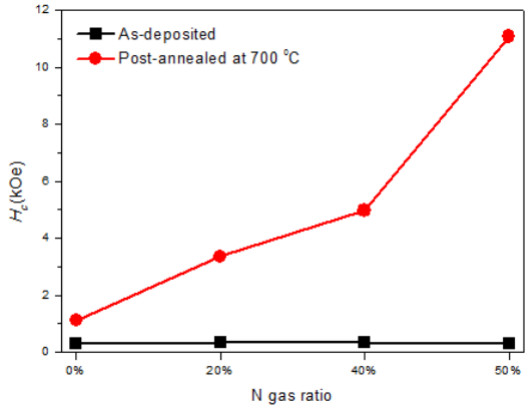

FIGURE 3.14: Out-of-plane coercivity of CoPt thin film as a function of N concentration.

in average grain size will decrease the number of domain wall pinning sites and thus the coercivity.[24] In comparison, the sample without nitrogen incorporation might not experience large increase in grain size which is evident from the larger surface roughness. This is due to the lack of Co and Pt atoms mobility compared to the sample with nitrogen incorporation. However, the CoPt/TiN/Glass (0% N_2) has a better ordering transformation at 800 °C compared to 700 °C due to the higher energy.

The largest H_c was achieved at 700 °C of around 11 kOe which is more than 10 times larger than the H_c of samples without nitrogen incorporation could achieve at the temperature. Therefore, in order to study the relation between nitrogen gas ratio and H_c, a graph of out-of-plane H_c as a function of nitrogen flow ratio was plotted as shown in Figure 10. It is revealed that nitrogen gas ratio strongly influences the H_c. All the as-deposited samples showed no substantial change in the H_c. On the other hand, all post-annealed samples showed a significant increase in H_c with nitrogen gas flow ratio, indicating that the improvement of Co and Pt atoms diffusion rate is more dominant during the post-annealing process rather than during the sputtering.

3.4 Magnetic Anisotropy Calculation

For a media to be suitable in magnetic recording technology, a certain formula has to be satisfied. The formula is as the following: $K_u V/k_B T > 60$.

The term $K_u$refers to the magnetic anisotropy of the media, which can be estimated from the difference in area below the perpendicular and in-plane M-H loops,

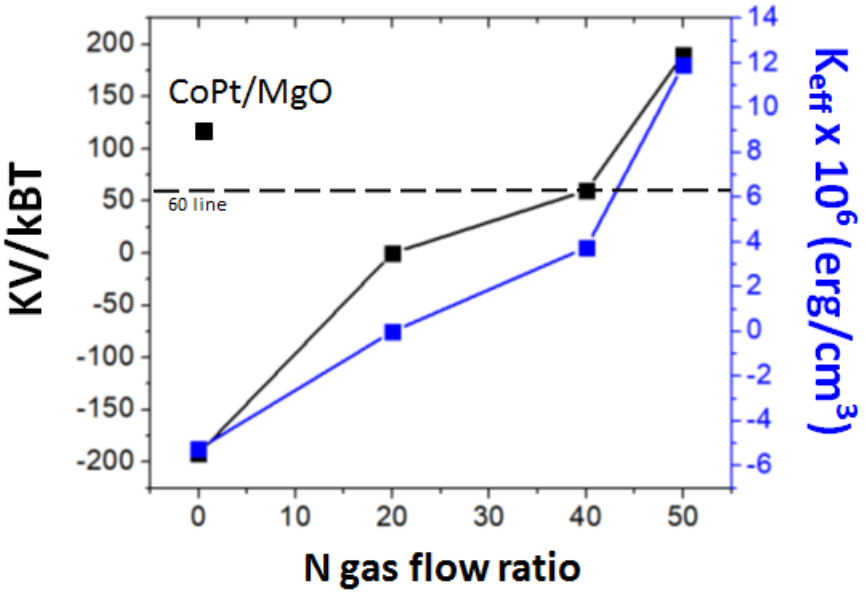

FIGURE 3.15: Magnetic anisotropy constant of CoPt/TiN/Glass annealed samples as a function of Nitrogen gas flow ratio.

V is the volume of the grain, which will be based on the ideal future magnetic recording technology grains, k_B is the Boltzmann constant, while T is the temperature. In order for the media to sustain the information at room temperature for more than 10 years, the result should be larger than 60.

In the figure, we could see that as the Nitrogen gas flow ratio is increased, the magnetic anisotropy constant also increases. Ultimately, at 50% N gas flow ratio, the requirement to sustain information for more than 10 years is satisfied. A reference point from CoPt deposited on MgO is also included as a comparison, it could be observed that our sample of CoPt deposited on the cheaper TiN and glass substrate is more stable compared to the single crystal sample.

3.5 Nitrogen Concentration Estimation

In order to better visualize the magnitude of the effect of Nitrogen gas flow ratio on the real concentration of Nitrogen inside the lattice, an estimation obtained from calculating the lattice expansion has been done from the data of the CoPt/TiN/Glass samples.

Nitrogen atoms are assumed to be filling the voids in the octahedral position of the CoPt lattice. As the Nitrogen gas flow ratio during the deposition is increased,

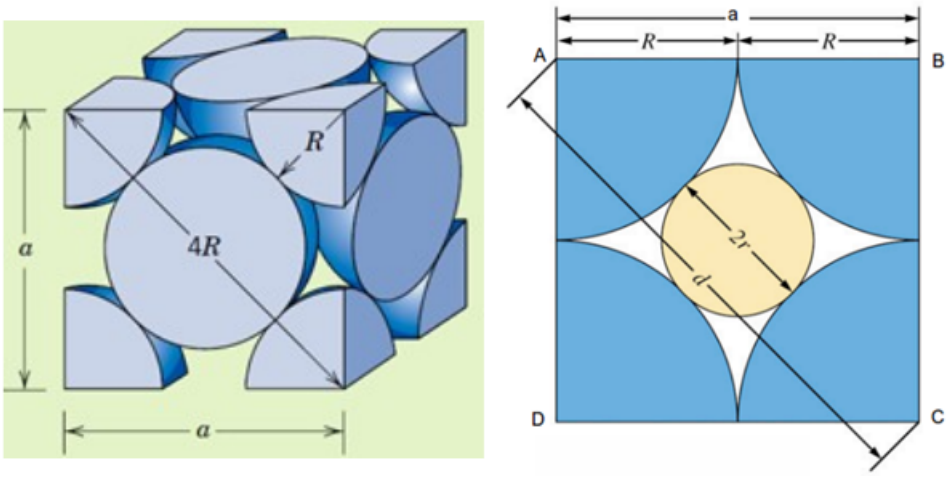

FIGURE 3.16: Schematic images of the atom configuration of fcc CoPt.

the number of Nitrogen inside the lattice is assumed to be increased, which is evident from the increased lattice constant during the as-deposition state. Without the Nitrogen atoms, the octahedral void size in our samples are 5.513 nm in size, while the atomic radius of Nitrogen atoms is roughly 6.5 nm in size. Hence, by calculating the ratio of difference between our sample octahedral size expansion and the pure Nitrogen atom filled octahedral size expansion, we could estimate the real concentration of Nitrogen in our samples.

TABLE 3.2: Lattice of CoPt/TiN/Glass samples. a represents the lattice constant, R represents the estimated atomic radius, r represents the estimated octahedral void radius

Flow Ratio	a, Å	R, Å	r, Å	Nitrogen at. %
0%	3.767	1.330	0.5513	0
20%	3.769	1.332	0.5516	0.3
40%	3.771	1.333	0.5519	0.6
50%	3.774	1.334	0.5522	0.91

From the above table, it could be observed that as the Nitrogen gas flow ratio is increased, the real atomic concentration of Nitrogen in the CoPt lattice also increase at the same rate. However, when the Nitrogen gas flow ratio is increased from 40% to 50%, the real atomic percentage is increased at a higher rate than the gas flow ratio. This is also evident from the abrupt increase in perpendicular coercivity of the

annealed samples when the Nitrogen gas flow ratio is increased from 40% to 50%.

3.6 Summary

In summary, the mechanism of how the nitrogen atoms affect the $L1_0$ CoPt ordering transformation has been investigated. Improvement in the ordering transformation has been achieved by incorporating nitrogen into CoPt films deposited on TiN intermediate layers. However, the incorporation of nitrogen degrades the coercivity in samples deposited directly on MgO substrates. The following are the explanations:

1. For CoPt grown on MgO single crystal substrate, the nitrogen incorporation increases the lattice parameter, relaxing the lattice mismatch and promotes the crystallinity of CoPt. However, the reduction of lattice mismatch decreases the tensile stress, which is essential in rotating the $L1_0$ c-axis towards the perpendicular direction in the post-annealing process.

2. For CoPt grown on TiN intermediate layer, the nitrogen atoms introduced during the deposition dissolves interstitially into the CoPt thin film and reduce the energy formation of vacancy, leading to an increase in the number of vacancies. The vacancies become path where the Co and Pt atoms can diffuse through during the post-annealing process. The increase in diffusion rate of the Co and Pt atoms promotes the ordering of $L1_0$ CoPt, resulting in an increase in the perpendicular coercivity and a reduction in ordering temperature.

Improvement of magnetic properties and reduction in ordering temperature through the incorporation of nitrogen gas enhances the feasibility and potential of $L1_0$ CoPt in future applications.

Bibliography

[1]D. Suess, J. Lee, J. Fidler, and T. Schrefl, J. Magn. Magn. Mater. **321**, 545–554 (2009).

[2]R. F. C. Farrow, D. Weller, R. F. Marks, M. F. Toney, and H. M. College, Appl. Phys. Lett. **69**, 1166–1168 (1996).

[3]Y. Zhu, and J. Cai, Appl. Phys. Lett. **87**, 2003–2006 (2005).

[4]O. Kitakami, Y. Shimada, K. Oikawa, H. Daimon, and K. Fukamichi, Appl. Phys. Lett. **78**, 1104–1106 (2001).

[5]K. R. Coffey, M. A. Parker, and J. I. Howard, IEEE Trans. Magn. **31**, 2–4 (1995).

[6]K. Elkins, T. Vedantam, J. Liu, H. Zeng, S. Sun, Y. Ding, and Z. Wang, Nano Lett. **3**, 1647–1649 (2003).

[7]C. Lai, Y. Wu, and C. Chiang, J. Appl. Phys. **97**, 95–98 (2005).

[8]A. Zuttel, C. Nutzenadel, G. Schmid, C. Emmenegger, P. Sudan, and L. Schlapbach, Appl. Surf. Sci. **162**, 571–575 (2000).

[9]H. Osono, T. Kino, Y. Kurokawa, and Y. Fukai, J. Alloys Compd. **231**, 41–45 (1995).

[10]Y. Fukai, Y. Ishii, Y. Goto, and K. Watanabe, J. Alloys Compd. **313**, 121–132 (2000).

[11]M. Iwamoto, and Y. Fukai, Materials Transactions **40**, 606–611 (1999).

[12]Y. Fukai, Phys. Scr. **T103**, 11–14 (2003).

[13]H. Wang, W. Mao, X. Ma, H. Zhang, Y. Chen, Y. He, and E. Jiang, J. Appl. Phys. **95**, 2564–2568 (2004).

[14]H. An, J. Wang, J. Szivos, T. Harumoto, T. Sannomiya, S. Muraishi, Y. N. G. Safran, and J. Shi, J. Appl. Phys. **118**, 203907 (2015).

[15]J. Mei, F. Yuan, W. Liao, Y. Yao, H. Lin, H. Lee, and J. Hsu, J. Appl. Phys. **109**, 10–13 (2011).

[16]H. An, J. Wang, T. Sannomiya, S. Muraishi, Y. Nakamura, and J. Shi, J. Phys. D. Appl. Phys. **48**, 155001 (2015).

[17]K. Hono, and Y. Takahashi, *Ultra-high-density magnetic recording* (), pp. 245–277.

[18]W. Moller, J. Nucl. Mater. **111-112**, 669–673 (1982).

[19]S. Myers, P. Richards, W. Wampler, and F. Besenbacher, J. Nucl. Mater. **165**, 9–64 (1989).

[20]Y. Fukai, J. Alloys Compd. **356–357**, 263–269 (2003).

[21]D. Williams, F. Baiocchi, R. Beairsto, J. Brown, and R. V Knoeli, J. Vac. Sci. Technol. B Microelectron. Nanom. Struct. **5**, 1723–1729 (1987).

[22]M. Kikuchi, T. Tanaka, and R. Tanaka, Metall. Trans. **5**, 1520–1521 (1974).

[23]C. Luo, and D. Sellmeyer, IEEE Trans. Magn. **31**, 2764–2766 (1995).

[24]R. Yu, S. Basu, Y. Zhang, A. Parvizi-Majidi, and J. Xiao, J. Appl. Phys. **85**, 6655 (1999).

Chapter 4

Strong Perpendicular Magnetic Anisotropy Induced by Broken Symmetry of A1-CoPt

The exponential growth of data generation demands even larger storage in the future.[1, 2] In light of this, hard disk drives as the current dominant storage media must continue to expand the storage capacity and reduce the cost. One of the most promising media for future high density magnetic recording is the $L1_0$ phase based media which could be found in several materials including CoPt and FePt. These materials are of the face centered tetragonal structure and consist of alternating stacks of Co/Fe and Pt atoms with high magnetocrystalline anisotropy, high Curie temperature and chemical stability.[3–5] The $L1_0$ phase of FePt and CoPt is stable at room temperature, but due to the slow diffusion speed of the atoms, generally high temperature treatment is necessary to facilitate the ordering transformation.[6] This high temperature may result in grain growth and coupling of adjacent grains which is detrimental to practical usage.[7, 8]

In order to avoid such problems, lower temperature formation is needed, and several researchers have reported ways to deposit FePt or CoPt films at lower temperatures.[9–13] One interesting idea comes from Y.F. Ding *et al.*,[14] where they utilize the difference in lattice mismatch between FePt film and several intermediate layers in order to reduce the ordering transformation temperature. They explain that by using intermediate layers with different lattice constant compared to FePt,

it would be possible to induce a strained epitaxial growth of FePt. For intermediate layers with larger lattice constant than FePt, the lattice constant will be strained horizontally and compressed perpendicularly. With the lattice of the FePt expanded horizontally, the *c/a* ratio will be more similar to the $L1_0$ phase and thus lower ordering temperature could be obtained. However, this idea is still based on the ordering transformation of $L1_0$, thus the reduction of temperature is still limited by the diffusion of Fe and Pt atoms.

Theoretically, the magnetocrystalline anisotropy of the $L1_0$ phase results from two different ways of breaking the symmetry.[15] The first one is by stacking the atoms in an alternating stacks where Co/Fe atoms lie on one plane and Pt atoms lie on the other plane along the *c*-axis direction. The second one comes naturally with the ordering, which is the transformation of the cubic structure into a tetragonal structure where the *a* lattice constant is expanded while the *c* lattice constant is shrunk. The broken symmetry coming from the lattice distortion could be more advantageous than the ordering transformation due to the absence of diffusion, making it possible to deposit at a lower temperature. Unfortunately, in $L1_0$ phase it is really hard to separate the contribution of these two symmetry breaking methods beside using first-principle theoretical calculations.[15] Therefore, it is currently unknown whether is it possible for the broken symmetry to induce magnetocrystalline anisotropy without the ordering experimentally. With regards to this gap in knowledge, we designed an experiment where large lattice mismatch is used to induce tetragonal lattice distortion of CoPt film deposited at a temperature relatively lower than the ordering transformation temperature. The objective of this study is to clarify the effect of the broken symmetry of A1-CoPt on the magnetic properties.

4.1 Substrate and underlayer selection

The idea of lowering the ordering transformation by Ding *et al.* could be explained as the following. Underlayer with (200) textured growth is used as a seed layer for the FePt film to grow in the (001) with epitaxial relationship of Underlayer(200)$\langle 110 \rangle$ || FePt(001)$\langle 100 \rangle$. If the underlayer has larger lattice constant than the FePt, the FePt lattice will then be expanded in the in-plane direction. As the *c/a* ratio of A1

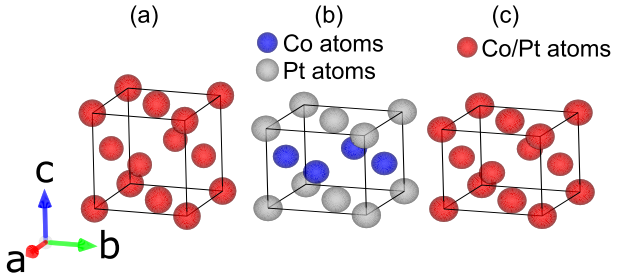

FIGURE 4.1: Structures of (a) A1 and (b) $L1_0$ ordered Co-Pt alloy. The strained A1 structure is shown in (c) for comparison.

FePt becomes similar to the ratio of $L1_0$ phase, the ordering transformation becomes easier and thus, the ordering transformation temperature could be reduced.

Therefore, the choice of underlayer will be very important in order to control the lattice mismatch and *c/a* ratio of the A1 FePt or CoPt. They reported a sharp increase in *c/a* ratio when the FePt is directly deposited on MgO(200) single-crystal substrate due to the existence of a critical lattice mismatch, beyond which misfit dislocations will be introduced between the interfaces and the strain energy will be relaxed.[14]

However, their work fails to consider the effects of growth mode of the FePt film when deposited directly on top of MgO substrate. Futamoto *et al.* recently reported that when FePt is deposited on MgO(001) underlayer, de-wetting of FePt may occur at high temperature and isolated crystal islands of FePt will form on the MgO surface.[16, 17] In these islands, the lattice close to the interface will remain strained but the lattice far from the interface will be relaxed, making the overall *c/a* ratio approaching unity.

In this work we used MgO(100) single-crystal substrate, which is the same as Ding *et al.*. For the underlayer, TiN is used due to the similarity of lattice constant with MgO (*a* of TiN = 0.4249 nm, *a* of MgO = 0.4213 nm) and the good wetting ability of CoPt on TiN.[18] TiN grew in the (001) direction with epitaxial relationship of MgO(001)[100]|| TiN(001)[100]

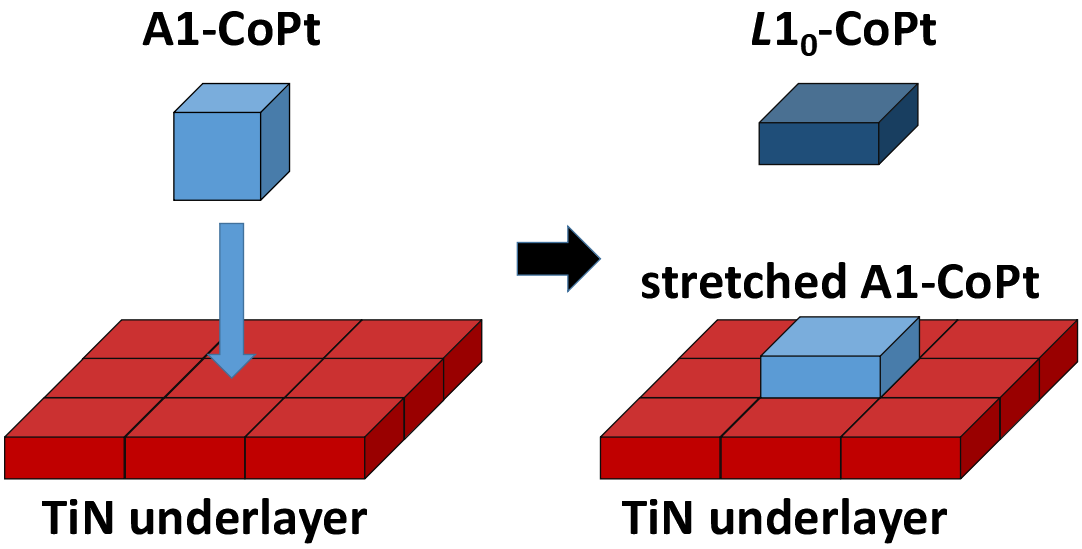

FIGURE 4.2: Schematic of the experimental design in order to get A1-CoPt with dimensions similar to the $L1_0$-CoPt

4.2 Fabrication of CoPt/TiN bilayer films on MgO and characterization techniques

CoPt (x nm), where x = 2.5, 5, and 10 nm films were deposited on MgO(100) single-crystal substrates with 40 nm thick TiN intermediate layer at 400 °C. The CoPt films and the underlayers were sputter-deposited by DC magnetron sputtering. The base pressure was lower than 5×10^{-5} Pa and the deposition pressure was 0.2 Pa. A 2 inch Co and Pt composite target was used as the target (ratio of the surface area of Co and Pt is 1.56:1). The CoPt films were deposited under a mixture of Ar and N_2 with a ratio of 50 : 50, and for TiN, the N_2 ratio was fixed at 10%. Prior to deposition, the MgO substrates were heated at 400 °C for 2 hours to ensure the surface cleanness. After the deposition of CoPt films, 30 minutes of in situ annealing was done at the same temperature as the deposition.

Vibrating sample magnetometer (VSM) Riken Denshi BHV-50V with an applied field of $\pm$ 10 kOe was used to measure the magnetic properties. X-ray diffractometer (Bruker D8 Discover diffractometer) with Cu K radiation was used to characterize the microstructures. The ratio of Co and Pt inside the film is 44:56 which was confirmed by using inductively coupled plasma-optical emission spectrometer.

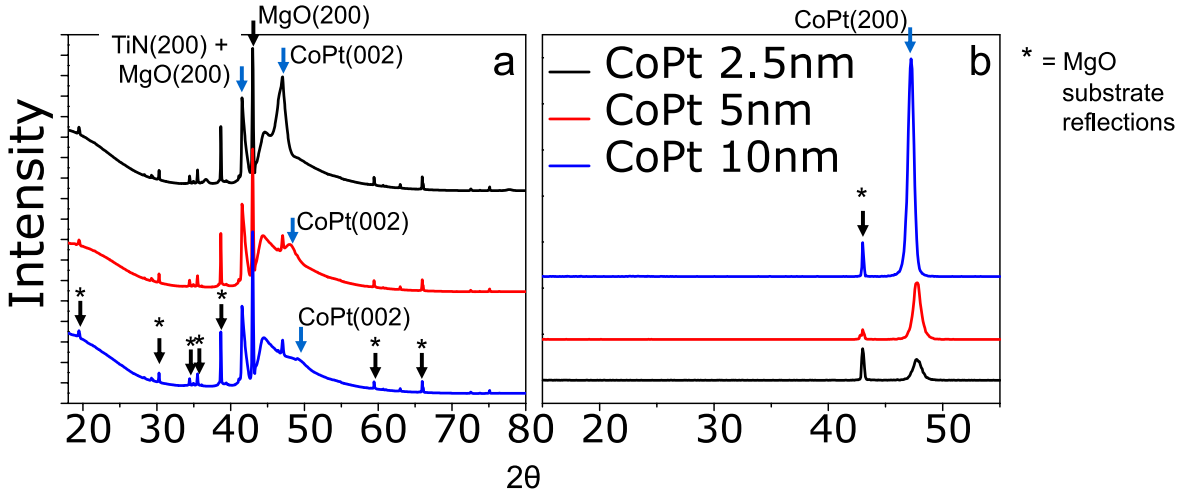

FIGURE 4.3: XRD scan of as-deposited CoPt(x nm)/TiN/MgO in the (a) out-of-plane direction, and (b) in-plane direction.

4.3 Structure characterization

Figure 4.3 shows the out-of-plane XRD results of the samples. The superlattice $L1_0$ phase was not detected in any of the samples. This could be confirmed from the absence of (001) peak that is usually found in the range of 23 - 24°. The reason behind the lack of $L1_0$ phase ordering transformation is the low deposition temperature (400 °C) which is way below the usual temperature needed to induce the ordering transformation of CoPt (∼800°C). (002) peak could be observed in all samples, revealing a good (001) oriented epitaxial growth of the CoPt on the TiN.

To illustrate the strain energy condition inside each films, the c and a lattice constant, as well as the *c/a* lattice ratio were calculated using Bragg's Law from the (002) peaks of the out-of-plane and (200) peaks of the in-plane XRD results. Then the relationship between the the c and a lattice constant, as well as the *c/a* lattice ratio and CoPt thickness was plotted in Figure 4.4. Lattice volume expansion could be observed from the evolution of c and a lattice parameters as the CoPt sample thickness increases. As the thickness was increased from 2.5 nm to 5 nm, the *c*-lattice constant increased while the *a*-lattice constant remained stable. When the thickness was increased further to 10 nm, both the *c* and *a*-lattice constant increased. The lattice volume expansion could be attributed to the N atoms inside the lattice. Previous report from our group discovered that N atoms would be incorporated inside the

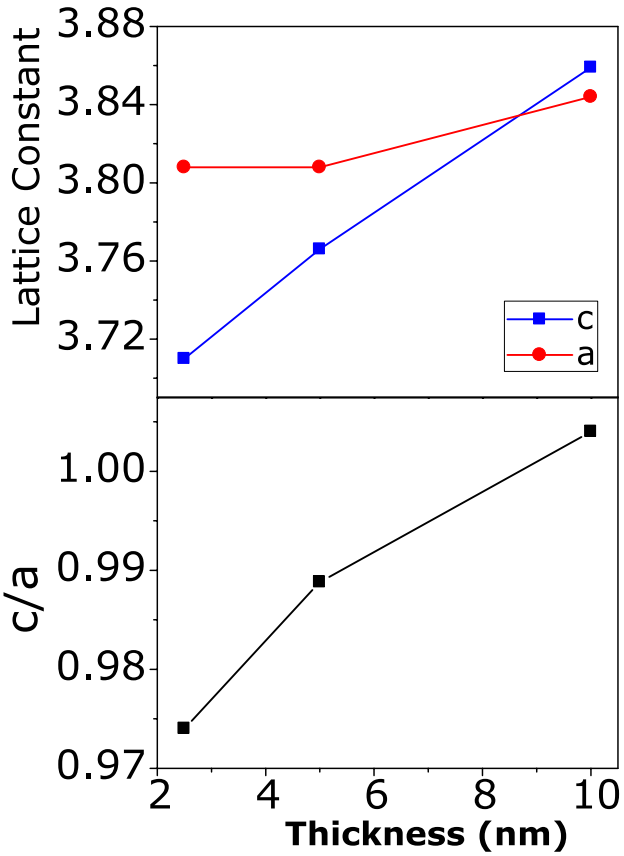

FIGURE 4.4: CoPt thickness vs. c and a lattice constant as well as the *c/a* lattice constant ratio of as-deposited CoPt/TiN/MgO samples.

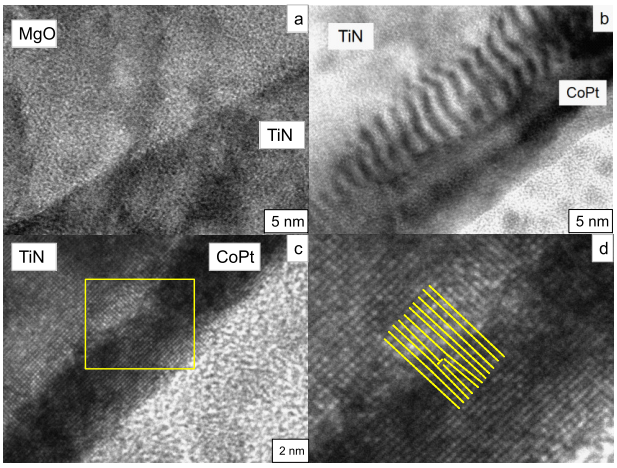

FIGURE 4.5: Cross-section TEM images of (a) TiN/MgO, (b) CoPt(10 nm)/TiN, (c) CoPt(2.5 nm)/TiN, and (d) Magnified region of CoPt(2.5 nm)/TiN.

lattice during deposition, effectively expanding the lattice parameter.[19, 20] At the 2.5 nm sample, this lattice expansion facilitated the lattice-matching epitaxial growth due to the strain energy induced by lattice mismatch. Hence, the lattice shows a *c/a* ratio of around 0.974, which is really similar in dimensions when compared to the $L1_0$ lattice. This means that in the 2.5 nm sample, even though the Co and Pt atoms are disordered inside the lattice, the lattice dimensions are closer to a tetragonal compared to a cubic. During the in situ annealing, the incorporated N atoms would escape the film, and the lattice would shrink.[19] However, the 10 nm CoPt film shows a *c/a* ratio of around 1.004, which is near the value of a normal cubic lattice. The disappearance of the broken symmetry at 10 nm could be attributed to the strain relaxation inside the film. The increased strain energy from extra thickness plus the lattice mismatch would be too large and it is more favorable to induce self-energy dislocations such as misfit dislocations in the interface to relieve the strain.[21] During the in situ annealing, some incorporated N atoms could escape but due to the large thickness, some of the N atoms would be trapped inside the lattice of the upper region of the film and increase the overall lattice volume.[19]

The lattice mismatch between CoPt and TiN is around 10.4%, which fall in the borderline between perfect epitaxial and heteroepitaxial growth.[22] In heteroepitaxial growth, the lattice mismatch is relieved by strained crystal lattice and dislocations at the interface.

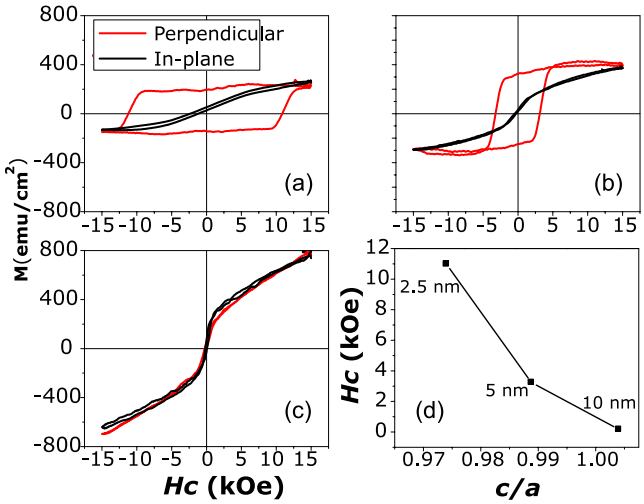

FIGURE 4.6: M-H curves of as-deposited CoPt/TiN/MgO samples with the thickness of (a) 2.5 nm, (b) 5 nm, and (c) 10 nm. The relationship between the *c/a* ratio and perpendicular coercivity is plotted in (d).

Cross-section TEM images are shown in Figure 4.5 in order to further understand the strain condition inside each films. In Figure 4.5(a) a clear epitaxial growth could be observed between the TiN intermediate layer and MgO substrate, which is consistent with our consideration. In Figure 4.5(c), the 2.5 nm sample shows a good lattice-matching epitaxial growth between the CoPt and the TiN layer and just a number of misfit dislocations. This means that the CoPt film grows heteroepitaxially on top of TiN. However, the density of misfit dislocations in this film could be assumed to be small and the strained crystal lattice is the dominant mechanism to relieve the strain due to lattice mismatch. This results in the expanded lattice along the plane. In comparison, at 10 nm the density of misfit dislocations is higher compared to the 2.5 nm sample, which is evident from the lattice bending inside the film. In heteroepitaxial growth, the strain energy increases proportionally to the film thickness. Subsequently, the number of misfit dislocations and extra half planes also increases, resulting in large strain field at the interface and bending of the lattice.

4.4 Magnetic properties measurement

In order to investigate the magnetic properties, M-H curves of the samples have been illustrated in Figure 4.6. At 2.5 nm (Figure 4.6(a)), the CoPt film shows a perpendicular coercivity of around 11 kOe. The perpendicular coercivity value was decreased by more than half at 5 nm, and disappears completely at 10 nm. For $L1_0$ based media, the increase of perpendicular magnetic anisotropy would usually be attributed to the increase in ordering parameter S.[23–25] However, in our samples, XRD results show that only A1 disordered phase exists inside the film. Further investigation was done by plotting the relationship between the c/a ratio and perpendicular coercivity in Figure 4.6(d). In our experiment, magnetoelastic contribution on perpendicular magnetic anisotropy is negative because of the positive λ_{001}.[26] Thus, a strong relationship can be assumed between the H_c and the broken symmetry of the A1 structure. At 2.5 nm, the lattice constant ratio shows that the film is expanded along the plane. This is due to the epitaxial growth of CoPt on top of the TiN intermediate layer, where the lattice mismatch between the two layers induce a strain inside the film. The resulting CoPt lattice is a disordered tetragonal lattice with dimensions comparable to that of the $L1_0$ phase lattice (c/a ratio = 0.974). Distortion of the disordered cubic lattice into a tetragonal results in a broken symmetry of A1-CoPt lattice and increase the magnetocrystalline anisotropy, leading to a large perpendicular coercivity.[27] On the other hand, when the CoPt thickness is increased to 10 nm, the strain energy inside the film is relaxed by means of misfit dislocations. Inside the partially relaxed layer, the CoPt lattice will not be distorted and a normal cubic lattice could be found inside the film. Without the ordering and the lattice distortion, the A1-CoPt would have no contribution towards the magnetocrystalline anisotropy and hence, no perpendicular coercivity could be observed. Hence, from this result we can strongly consider that the magnetic properties are positively affected by the broken symmetry of the A1-CoPt lattice.

4.5 Summary

2.5 nm thick CoPt with perpendicular coercivity of 11 kOe has been successfully deposited at 400 °C which is much lower than the usual fabrication temperature of $L1_0$ CoPt (∼800°C). The film grows epitaxially in the (001) direction on top of TiN intermediate layer and MgO substrate. The lattice mismatch between TiN and CoPt introduces strain inside the CoPt film and distorts the crystal lattice. The resulting crystal lattice have dimensions that are comparable to the $L1_0$ lattice and possess magnetocrystalline anisotropy due to the broken symmetry. Moreover, in our results there is no $L1_0$ ordering transformation in all samples, which led us to consider that in our case, broken symmetry of the A1-CoPt lattice is the main reason behind the perpendicular magnetic anisotropy. Therefore, we believe that our ultra-thin CoPt films fabrication would not be hindered by limited diffusion speed of Co and Pt atoms and with further optimization, lower deposition temperature could be achieved.

Bibliography

[1]R. Wood, J. Magn. Magn. Mater. **321**, 555–561 (2009).

[2]E. Grochowski, and R. D. Halem, IBM Sys. J. **42**, 338–346 (2003).

[3]M. Watanabe, and T. Masumoto, J. Appl. Phys. **76**, 3971–3973 (2000).

[4]Y. Hsu, S. Jeong, D. E. Laughlin, and D. N. Lambeth, J. Appl. Phys. **89**, 7068–7070 (2001).

[5]Y. Takahashi, T. Ohkubo, M. Ohnuma, and K. Hono, J. Appl. Phys. **93**, 2690–2696 (2003).

[6]T. Maeda, T. Kai, A. Kikitsu, T. Nagase, and J. Akiyama, Appl. Phys. Lett. **80**, 2147–2149 (2002).

[7]C. Platt, K. Wierman, E. Svedberg, R. van de Veerdonk, and J. Howard, Appl. Phys. Lett. **92**, 6104–6109 (2002).

[8]Y. S. Yu, H. B. Li, W. Li, M. Liu, and W. Fei, J. Magn. Magn. Mater. **320**, L125–L128 (2008).

[9]O. Kitakami, Y. Shimada, K. Oikawa, H. Daimon, and K. Fukamichi, Appl. Phys. Lett. **78**, 1104–1106 (2001).

[10]T. Shima, T. Moriguchi, S. Mitani, and K. Takanashi, Appl. Phys. Lett. **80**, 288–290 (2002).

[11]C. H. Lai, C. H. Yang, C. C. Chiang, T. Balaji, and T. K. Tseng, Appl. Phys. Lett. **85**, 4430–4432 (2004).

[12]C. C. Chiang, C. H. Lai, and Y. C. Wu, Appl. Phys. Lett. **88**, 152508 (2006).

[13]Y. C. Wu, L. W. Wang, and C. H. Lai, Appl. Phys. Lett. **91**, 072502 (2007).

[14]E. L.C.J. S. Y. F. Ding, J. S. Chen and G. M. Chow, J. Appl. Phys. **97** (2005).

[15]T. J. Klemmer, N. Shukla, C. Liu, X. W. Wu, E. B. Svedberg, O. Mryasov, R. W. Chantrell, D. Weller, M. Tanase, and D. E. Laughlin, Appl. Phys. Lett. **81**, 2220–2222 (2002).

[16]M. O.N. I. M. Futamoto, M. Nakamura and T. Shimotsu, AIP Advances **6** (2016).

[17]M. F.F. K. T. Shimizu, M. Ohtake and N. Inaba, IEEE Trans. Magn. **53** (2017).

[18]H. An, J. Wang, J. Szivos, T. Harumoto, T. Sannomiya, S. Muraishi, Y. N. G. Safran, and J. Shi, J. Appl. Phys. **118**, 203907 (2015).

[19]H. An, J. Wang, J Szivos, T. Sannomiya, S. Muraishi, G. Safran, Y. Nakamura, and J. Shi, J. Appl. Phys. **118**, 203907 (2015).

[20]P. Caesario, T. Harumoto, Y. Nakamura, and J. Shi, J. Magn. Magn. Mater. **443**, 22–28 (2017).

[21]M. H. Hong, K. Hono, and M. Watanabe, J. Appl. Phys. **84**, 4403–4409 (1998).

[22]W. Wunderlich, Metals **4**, 410–427 (2014).

[23]Y. K. Takahashi, M. Ohnuma, and K. Hono, J. Magn. Magn. Mater. **246**, 1–2 (2002).

[24]C. Kim, J. J. Sapan, S. Moyerman, K. Lee, E. E. Fullerton, and M. H. Kryder, IEEE Trans. Magn. **46**, 023907 (2010).

[25]M. Ohtake, S. Ouchi, F. Kirino, and M. Futamoto, J. Appl. Phys. **111**, 07A708 (2012).

[26] H.Takahashi, S.Tsunashima, S.Iwata, and S.Uchiyama, J. Magn. Magn. Mater. **126**, 282–284 (1998).

[27]S. Ostanin, S. S. A. Razee, J. B. Staunton, B. Ginatempo, and E. Bruno, J. Appl. Phys. **93**, 453–457 (2003).

Chapter 5

Control of Perpendicular Coercivity in A1-CoPt/L10-CoPt/TiN Trilayer films

In the pursue of meeting the requirements of the always increasing data storage, researchers and companies that work in hard disk drive based recording industry have to get over the limitation of the so called magnetic recording trilemma.[1] This trilemma consists of long-term stability, ease of writability, and the decreasing size of the magnetic bits/particles. That is, to get a better storage density in the hard disk drive, the size of the magnetic bits inside the media must be reduced. At the density greater than 1 Tb/inches^2, typical magnetic storage media materials will be pushed past their superparamagnetic threshold at which thermal energy is able to cause random reversals in the media. In order to stabilize the thermal stability of magnetic bits of such small size, researchers turn to materials with high magnetic anisotropies, where generally these materials naturally come with large switching field that makes it difficult to write. Leading candidates for such materials that can solve both the small size and thermal stability issues are those that can form the $L1_0$ such as the FePt and CoPt. These materials have a very high magnetocrystalline anisotropy in the order of 10^{7} erg/cm^3 for bulk FePt and CoPt. With such a high magnetocrystalline anisotropy, it is possible to make magnetic bits with diameter of around 4 nm that can remain thermally stable for an acceptable time period. With

two out of the three problems solved, right now scientists are focusing on the third problem which is to ease the writability of such a stable media.

Several means of solutions have been proposed by researchers in order to ease the writability of such a hard magnetic media. One way is called Energy-Assisted Magnetic Recording, which uses energy from an outside source in order to reduce the switching field of the hard magnetic layer. The most famous is coined Heat Assisted Magnetic Recording, where heat is locally introduced in order to bring the hard magnetic bits closer towards its Curie temperature,T_c. As the temperature gets closer to its T_c, the hard magnetic layer starts to turn to a paramagnet and the switching field is reduced significantly. However, this concept introduces several other problems such as using heat in a electrical component that will surely decays its lifetime, and the necessity of an additional lubrication.

Another way to solve the problem consists of an easier setup that uses exchange coupling of a hard magnetic layer and a soft magnetic layer in order to help switch the hard phase. This was done by Hagedorn and it is proven to be able to reduce the coercivity of the system.[2] With regards to this concept, two identical ideas were proposed by Victoria and Suess as exchange coupled composite (ECC) and exchange spring media respectively.[3–5] Both ideas utilizes the early reversal in the soft magnetic layer in order to act as a lever to assist the switching of the hard magnetic layer. Moreover, the ease of writability is improved while the thermal stability is the same as the hard magnetic layer's thermal stability.[6]

Recently, researchers have been working on $L1_0$ media for ECC systems by coupling it with soft layers of Fe [7, 8] or fcc FePt [9–11], the latter is obtained by depositing the FePt at room temperature or using post-deposition treatment in order to disorder the ordered layer via a disordering process during the deposition of a cover layer. These works usually achieve the decoupling of lateral grains by means of deposition at high temperature in order to form nano particles on a bare substrate or matrix made of non-magnetic materials. In this study we examine the basic parameters for an ECC system of $L1_0$ CoPt and fcc CoPt. By studying the effect of hard magnetic layer thickness, soft magnetic layer thickness, soft layer deposition temperature, and intermediate thickness, the optimum condition for an ECC system will be used in order to finally manufacture an ECC system that is more suitable for

practical use.

5.1 Deposition of CoPt/TiN bilayer films

In this experiment, DC magnetron sputtering is used in order to manufacture all films using two composite targets of Co and Pt for the CoPt films, and pure Ti target for the TiN under layer and intermediate layer. The base layer for the ECC system is made by depositing 40 nm of TiN under layer on top of glass substrate in order to promote the (002) growth of the 10 or 5 nm hard CoPt layer. The base pressure is lower than 5 x 10^{-5} Pa, while the working pressure used is 0.2 Pa. The deposition of TiN layers is under 1:9 gas flow ratio of Nitrogen and Argon, while the hard CoPt layer is deposited under 1:1 Nitrogen to Argon gas flow ratio. For the base layer, the deposition temperature is set at 400 ^{o}C and post-deposition annealed at 700 ^{o}C for 3 hours in order to induce the ordering transformation.

In the first series we vary the thickness of the soft CoPt layer from 0-10 nm. In the second series the optimal soft layer thickness was picked and the deposition temperature is varied from room temperature up to 300 ^{o}C. For the third series an intermediate TiN layer (0-4 nm) is introduced in order to control the exchange coupling constant of the ECC systems.

All samples are then subjected to several characterization techniques including XRD and XRR using the Bruker series to investigate the microstructure of the films, while VSM is used to characterize the magnetic properties.

5.2 Soft layer thickness effect

5.2.1 Structural Characterization

Figure 5.1 shows the XRD peaks of CoPt(soft)/CoPt(hard)/TiN samples with varying soft layer thickness. All samples show a superlattice (001) peak at around 23^{o} which indicates ordering transformation of disordered CoPt into ordered phase. XRD peak for the base layer of CoPt(hard)/TiN could be found at the bottom of the figure. In this film, several fundamental CoPt peaks could be found such as (111) peak at around 41^{o}, (200) peak at 48^{o} and (002) peak at 49^{o}. The underlayer TiN

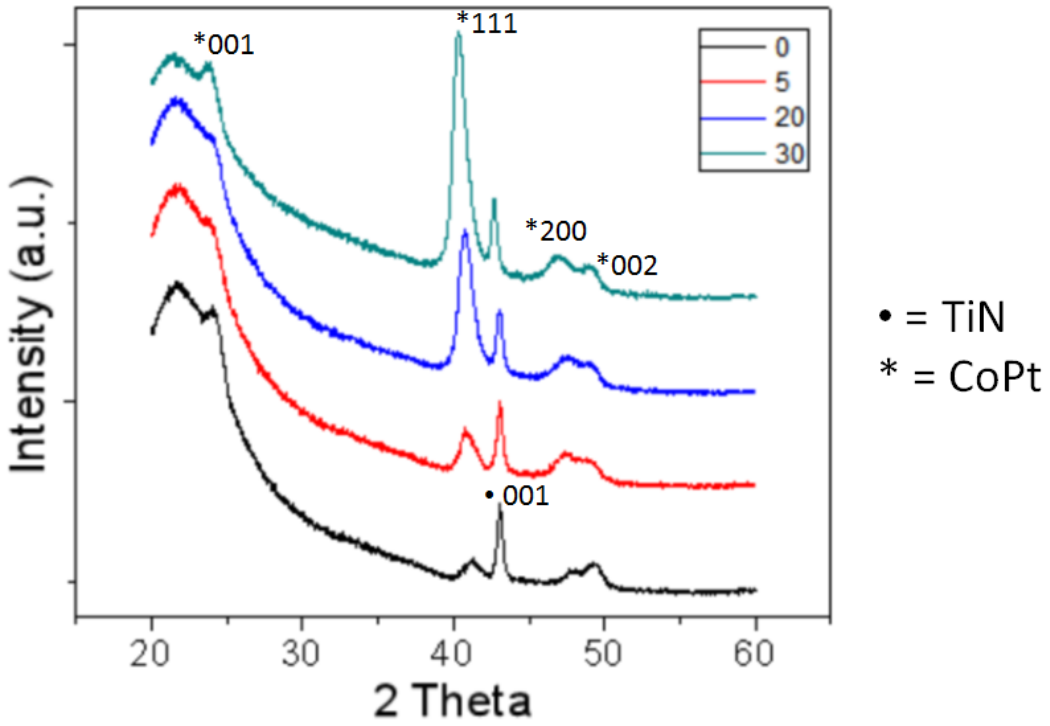

FIGURE 5.1: XRD peaks of CoPt(x nm)/CoPt(10 nm)/TiN/MgO samples with the thickness x = 0 - 30 nm.

peak could also be observed at 43° that indicates a good (001) preferred orientation. Thus the growth of the hard phase CoPt on (001) oriented TiN could be described by the following: Close to the interface, the CoPt grows epitaxially in the (002) direction and the crystal structure is a tetragonal instead of the cubic which is usually found in the bulk state. However, due to the increase of strain energy inside the film as the thickness increases, there is a self-relieving mechanism inside the film by growing on the plane with the lowest surface energy which is the (111) direction.

In the trilayer samples with soft layer CoPt on top of the base layer, the (111) peak grows as the soft layer thickness grows. This indicates a good epitaxial growth of soft CoPt on top of the bottom CoPt. It is noticeable that the (200) and (002) peaks are relatively unchanged with soft layer thickness which means that the bottom CoPt crystallinity is not affected by the soft layer deposition.

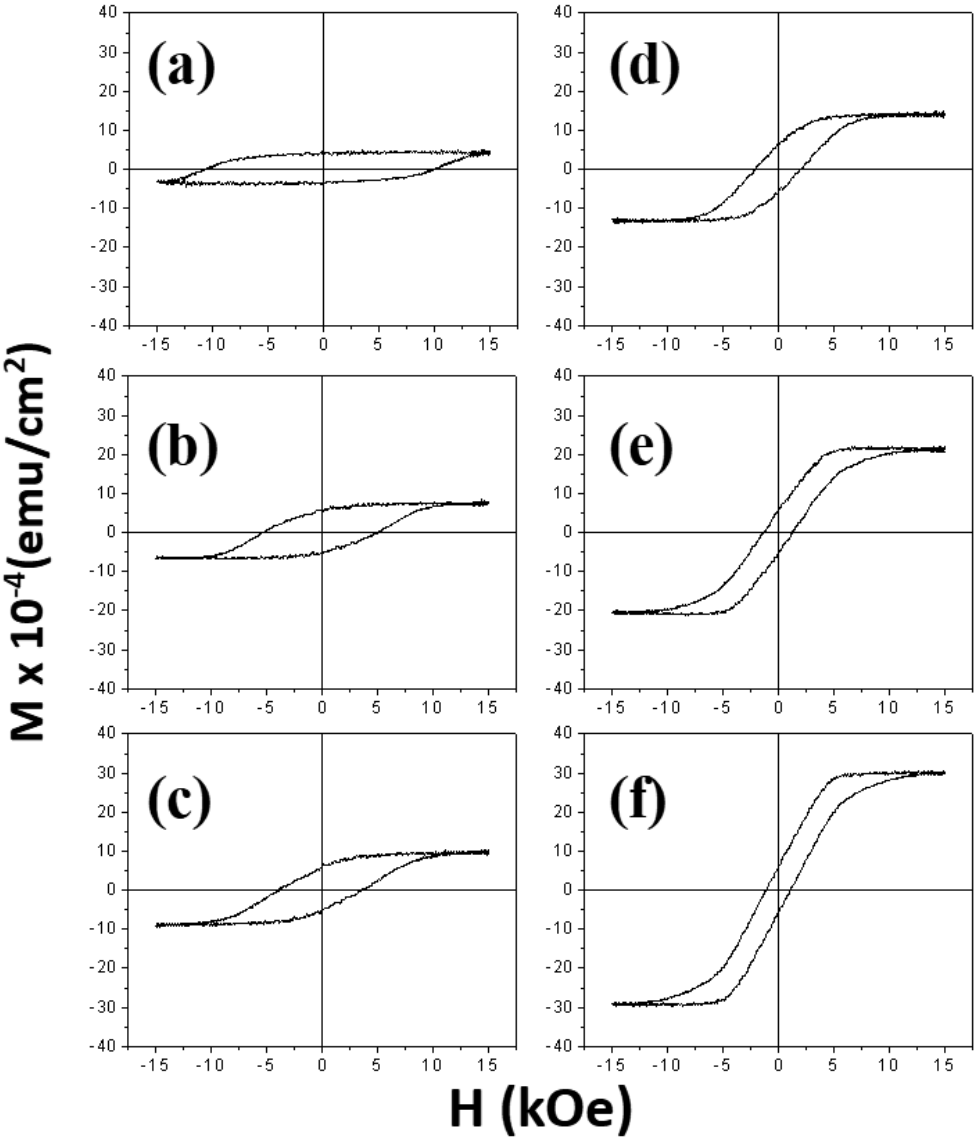

FIGURE 5.2: M-H curves of CoPt(x nm)/CoPt(10 nm)/TiN/MgO samples with the thickness x = 0 - 30 nm.

5.2.2 Magnetic Properties Measurement

Figure 5.2 shows the M-H curves of the base layer coupled with soft CoPt layer on top. The base layer shows a really large perpendicular H_c of around 10 kOe, indicating a good perpendicular magnetic anisotropy. When soft CoPt layer is coupled on top of the hard layer, the perpendicular H_c is reduced while the M_s is increased. This is due to the lower H_c and higher M_s in the soft layer. The reduction of H_c is affected by the soft layer thickness as shown in Figure 5.3. The exponential decrease of H_c is proof that the system is an exchange spring in nature. The critical soft layer thickness is assumed to be at 10 nm, over which the reduction of H_c could be considered negligible. It is also interesting to note that even when the soft layer thickness is 30 nm, there is no noticeable decoupling occuring inside the film, indicating a really good exchange coupling in the system. Up to 2.5 nm thickness of the soft layer, the nucleation field (H_n) is still in the second quadrant of the loops. However, as the soft layer thickness grows beyond 5 nm, the H_n starts to shift to the first quadrant, this is perhaps due to the demagnetizing field. As the soft layer thickness grows thicker, the demagnetizing field grows larger and thus finally will tilt the shape of the M-H curves. Figure 5.4 shows how the squareness of the M-H curve is affected by the soft layer thickness. In a similar fashion to the perpendicular H_c, the M_r/M_s ratio is decreasing in an exponential rate as the soft layer thickness is increased.

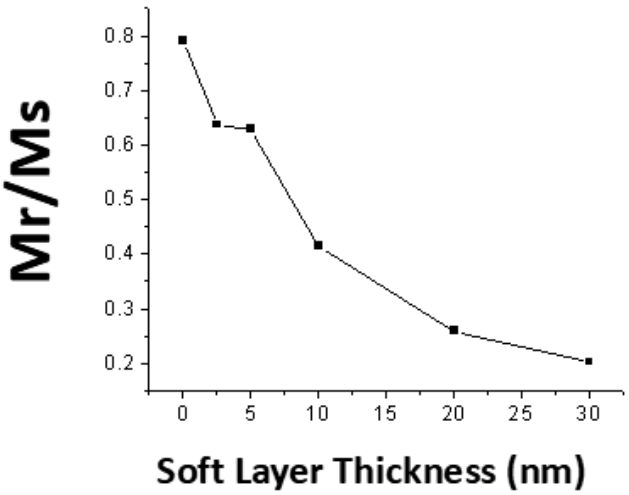

FIGURE 5.4: Mr/Ms ratio of CoPt(x nm)/CoPt(10 nm)/TiN/MgO samples with the thickness x = 0 - 30 nm, as a function of x.

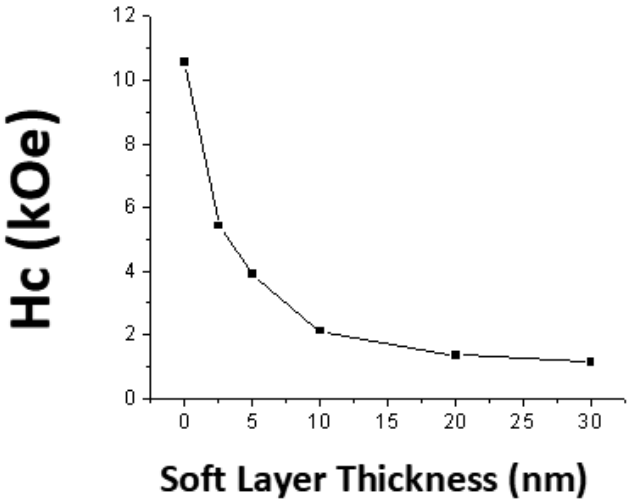

FIGURE 5.3: Perpendicular coercivity of CoPt(x nm)/CoPt(10 nm)/TiN/MgO samples with the thickness x = 0 - 30 nm, as a function of x.

5.2.3 Comparison to thinner hard layer

The base layer of CoPt(10 nm)/TiN(40 nm) resulted in a good perpendicular magnetic anisotropy with some component in the in-plane direction. This in-plane component mainly comes from the disordered A1 structure that grows in the (111) direction. The main reason for the change in growth orientation from (002) to (111) is due to the strain-relieving mechanism inside the film. Thus it would be interesting to compare the result of the 10 nm hard layer with the thinner 5 nm hard layer.

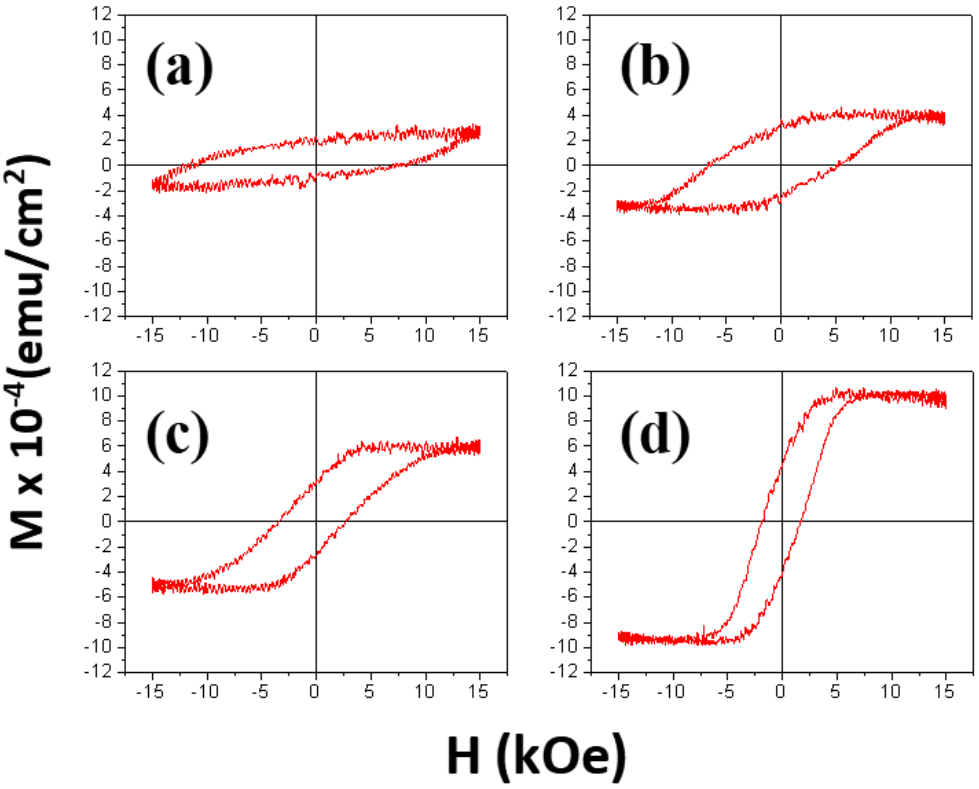

FIGURE 5.5: M-H curves of CoPt(x nm)/CoPt(5 nm)/TiN/MgO samples with the thickness x = 0 - 10 nm.

Figure 5.5 shows the M-H curves of the thin base layer of CoPt(5 nm)/TiN(40 nm). The pattern is similar to the thicker layer where the perpendicular H_c is reduced at an exponential rate as the soft layer thickness is increased. The squareness, which is taken from the ratio between the M_r/M_s is also showing a decrease with soft layer thickness, albeit with a slower rate compared to the thicker base layer. One interesting point to note is with the thinner base layer, we could get a higher percentage of ordered phase inside the hard layer and thus it is possible to predict the perpendicular H_c by using the formula

$$H_c = \frac{H_{r,hard} M_{s,hard} t_{hard} + H_{r,soft} M_{s,soft} t_{soft}}{M_{s,hard} t_{hard} + M_{s,soft} t_{soft}}$$

where H_r is the reversal field of hard and soft layer. However in this case, the $H_{r,soft}$ could be assumed to be zero because the layer has an easy axis of magnetization in the in-plane direction as seen in Chapter 3. Thus in this case the formula is revised

to:

$$H_c = \frac{H_{r,hard} M_{s,hard} t_{hard}}{M_{s,hard} t_{hard} + M_{s,soft} t_{soft}}$$

The comparison between the calculated perpendicular H_c and the experimental values of perpendicular H_c could be observed from Figure 5.6(middle). The calculated and experimental value are similar up to the soft layer thickness of 2.5 nm, beyond which the two values start to drift apart from one another. The result is perfectly acceptable as this weighted average approach is only applicable to thin soft layers (roughly below the exchange length of the materials). This indicates that the exchange length of the materials is around 2.5 nm.

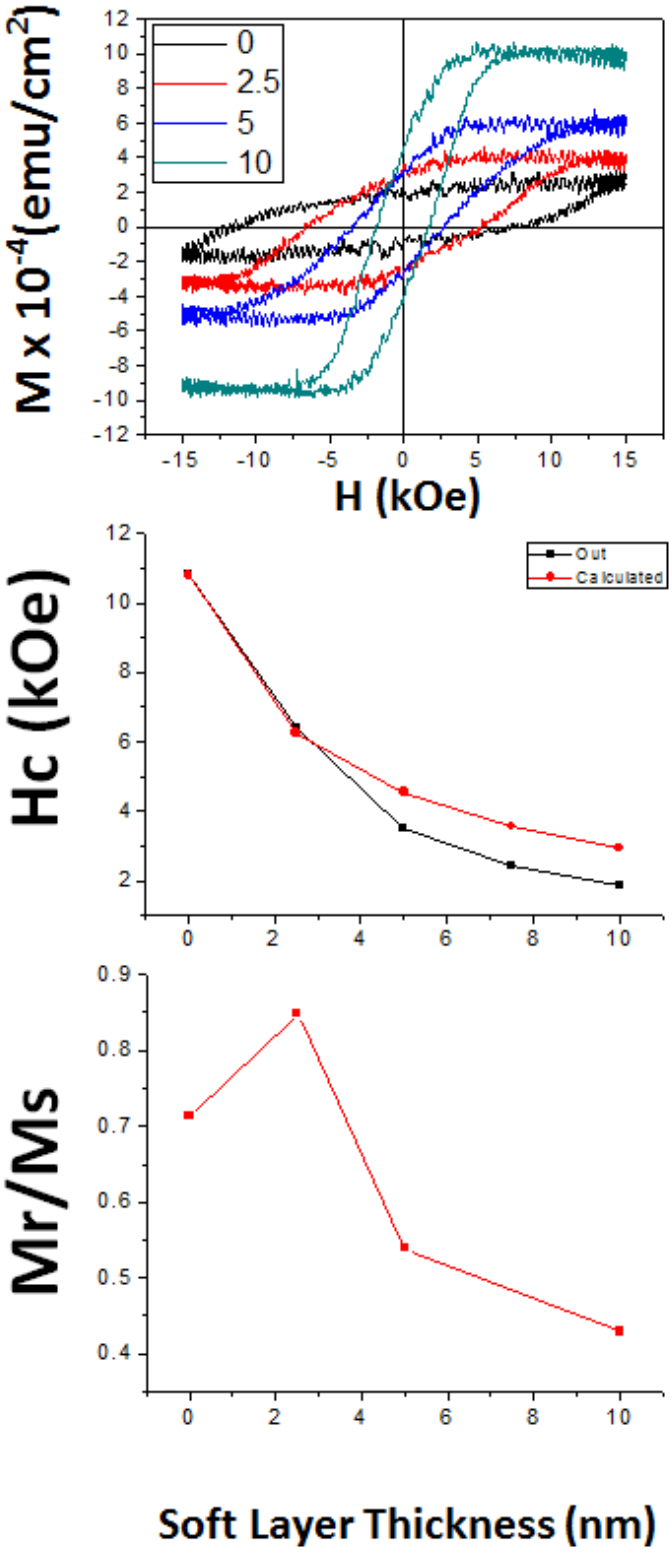

FIGURE 5.6: (Top) Overlapped M-H curves of Figure 5.5. (Middle)Perpendicular coercivity of CoPt(x nm)/CoPt(10 nm)/TiN/MgO samples with the thickness x = 0 - 30 nm, as a function of x. (Bottom)Mr/Ms ratio of CoPt(x nm)/CoPt(10 nm)/TiN/MgO samples with the thickness x = 0 - 30 nm, as a function of x.

5.3 Soft layer deposition temperature effect

5.3.1 Magnetic Properties Measurement

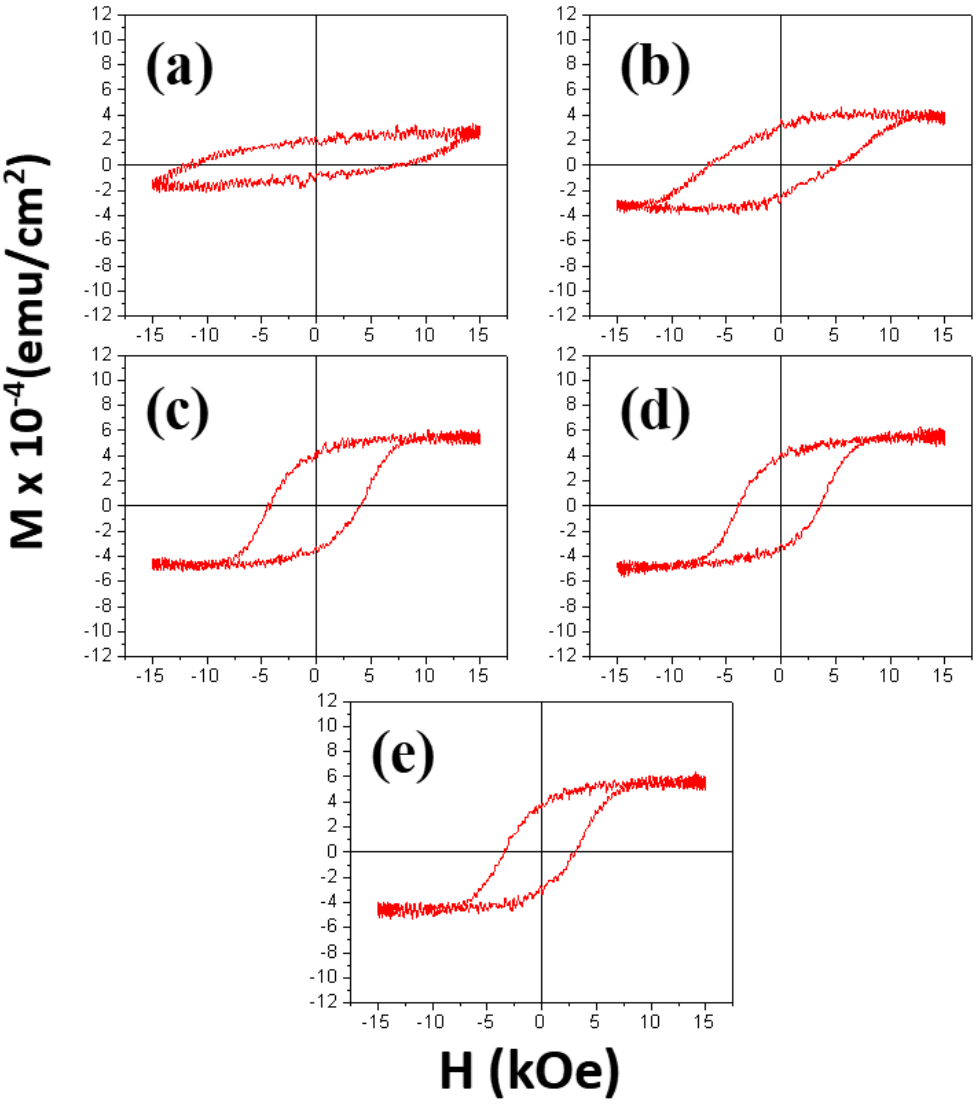

FIGURE 5.7: M-H curves in the perpendicular direction for 5 nm base layer deposited with 2.5 nm soft layer CoPt at (b) room temperature, (c) 100 ^{o}C, (d) 200 ^{o}C, and (e) 300 ^{o}C, the base 5 nm layer result is included as a reference in (a)

Figure 5.7 shows the M-H curves in the perpendicular direction for 5 nm base layer deposited with 2.5 nm soft layer CoPt at different deposition temperature. The graphs show a reduction of perpendicular H_c for all samples. When deposited at room temperature, 2.5 nm soft layer of CoPt could reduce the perpendicular H_c from

10,800 Oe to around 6,200 Oe. As the depostion temperature is increased to 100 °C, the perpendicular H_c is reduced further to 4,500.

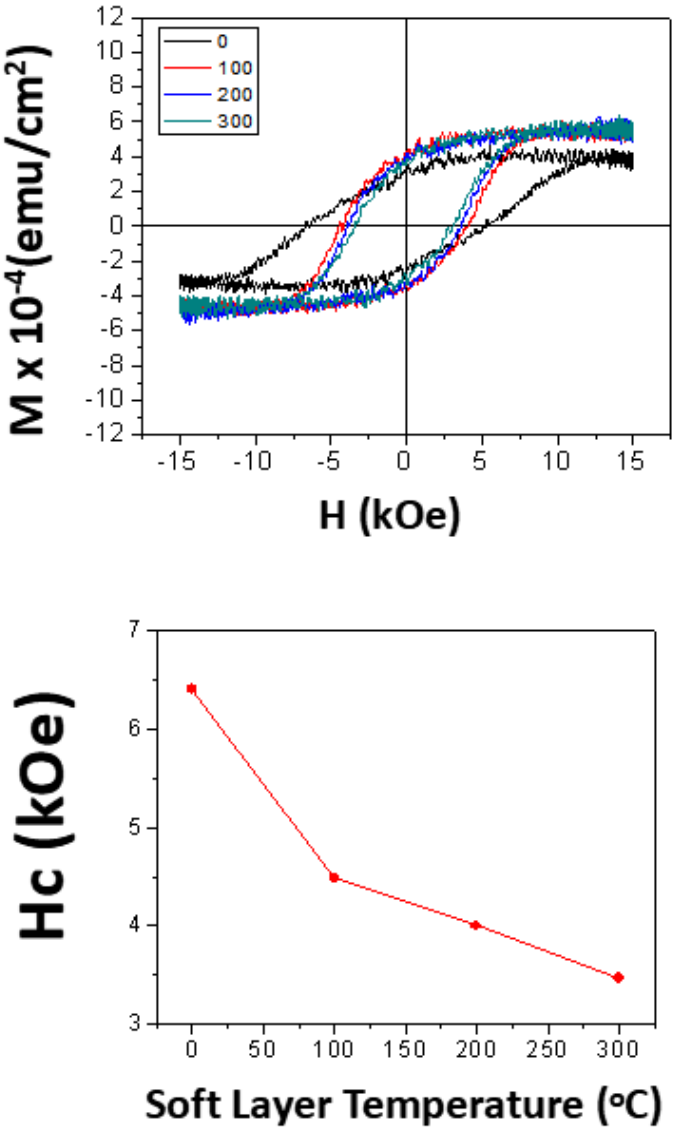

FIGURE 5.8: (Top) Overlapped M-H curves of Figure 5.7. (Bottom) Perpendicular coercivity of CoPt(2.5 nm)/CoPt(5 nm)/TiN/MgO samples deposited at varied temperature of 23-300 °C.

Previous researches on deposition temperature have an additional effect of changing the magnetic anisotropy of the soft layer, however in our case as the CoPt ordering temperature is too high (800 ^{0}C) compared to this experiment (∼300 °C) no change of magnetic anisotropy should be expected. This proves that deposition temperature innately have an effect on the exchange coupling of the CoPt(hard)/CoPt(soft)

bilayers. An interesting point to note here is that as the deposition temperature of the soft layer is increased up to 300 °C, the reduction of switching field is not significant compared to when the temperature is first increased to 100 °C.

5.3.2 Structural Characterization

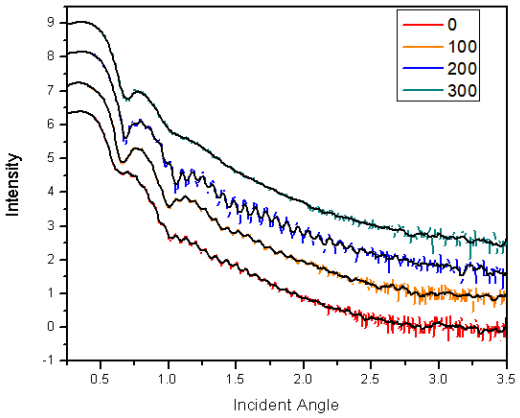

FIGURE 5.9: XRR curves of 5 nm base layer with 2.5 nm soft layer of CoPt on top deposited at several temperatures. Black lines represent the smoothing of the peaks in order to aid visual comparison.

In order to investigate how the deposition temperature affected the exchange coupling, we plotted the XRR peaks of samples of 5 nm base layer with 2.5 nm soft layer of CoPt on top in Figure 5.9. These graphs show the major peaks representing the thinner CoPt films and the minor peaks representing the thickner TiN films. From these graphs it is possible to differentiate between the sample deposited at room temperature and samples deposited at elevated temperatures. At room temperature, the second and third major peaks which represent the thinner layer are attenuated due to the roughness between the lower and upper CoPt layer. This interface roughness becomes smoother as the softer layer is deposited at higher temperature up to 200 °C. However, at 300 °C, the major peaks started to become deteriorated again and the interface roughness becomes similar to that of the sample deposited at the room temperature. This phenomenon could be explained by the annealing and interdiffusion effect. At room temperature, the surface of the hard CoPt layer is proven to be

rough by AFM calculation from Chapter 3 (Figure 3.13), this leads to a rough interface between the hard CoPt layer and the soft CoPt layer and a faster decay in the major peaks of the XRR. When deposited at 100 and 200 °C, the high temperature promotes diffusion on the surface and will result in a cleaner interface between the hard and soft layers, leading to a clearer major peaks in the XRR results. However, at 300 °C, the diffusion start to turn from surface diffusion into more of a bulk diffusion and the interface between the hard/soft magnetic layer becomes blurred which is evident from the deteriorated major peaks in the XRR results. An important point to note is that even though the interface roughness of the thinner films are changed at high temperature, the magnetic properties are barely changed between the samples. This proves that the roughness between the films do not play important roles in affecting the magnetic properties in this film.

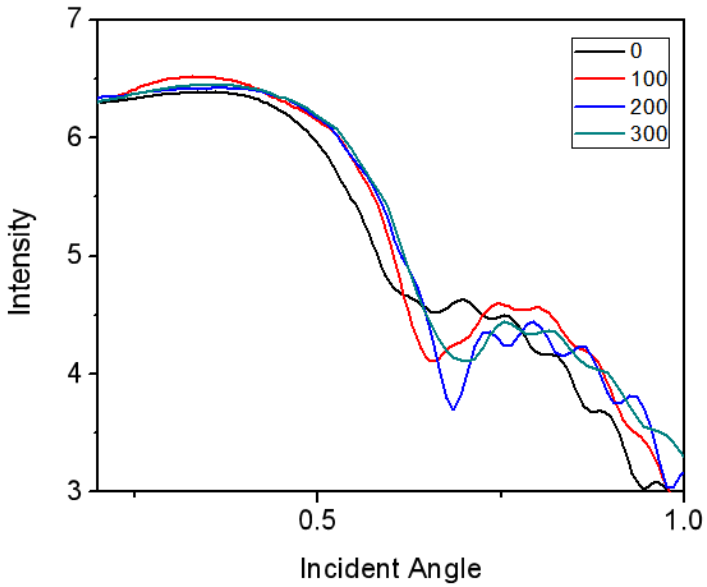

FIGURE 5.10: Overlapped critical angle of XRR curves from figure 5.9.

Another possible origin of the change in magnetic properties is the change in magnetic properties of the soft layer when deposited at higher temperature. A closer look at the critical angle of these samples (Figure 5.10) indicates that the density difference between the soft and hard CoPt layer in the sample deposited at room

temperature and elevated temperature is different. Due to the nature of their diffusion speed, both Co and Pt atoms are unlikely to be bulk diffused from the hard CoPt layer and it could be assumed that only the Co and Pt atoms in the soft layer would be affected the most by the change in soft layer deposition temperature due to the fact that atoms migration occur easier during the deposition than during post-deposition heat treatment. Therefore, most of the density difference is assumed to be coming from the soft layer. The difference in density of the soft layer will greatly affect the magnetic properties of the soft CoPt layer and thus, the switching field of the hard CoPt layer. A more in-depth investigation using Auger depth profiling reveals the profile of two samples deposited at room temperature and 100 ^{o}C (Figure 5.11). When we focus on the CoPt layer in the heterostructures, it could be seen that in both samples, the CoPt layer roughly starts from the 10^{th} cycle up to around the 40^{th} cycle. By calculating the thickness ratio of the soft/hard CoPt layer, the soft layer starts at around the 10^{th} cycle and ends at around the 20^{th} cycle, while the hard layer starts at around the 20^{th} cycle and ends at around the 40^{th} cycle. When the two figures are compared, it could be seen that at the interface of CoO/CoPt and CoPt/TiN (around the 10^{th} and 40^{th} cycle respectively) the Co intensity is similar. However, around the interface between the soft/hard layer (around the 20^{th} cycle) it could be clearly seen that in the soft layer deposited at elevated temperature, Co intensity is higher than in the soft layer deposited at room temperature. This indicates of different Co element profiles in the CoPt soft layer when deposited at different temperature, where when deposited at 100 ^{o}C, the cobalt atoms tend to be concentrated around the soft/hard layer interface, creating a gradient of density throughout the soft layer. On the other hand, when deposited at room temperature, the cobalt atoms tend to be distributed evenly throughout the layer. This difference in distribution of density of the soft CoPt layer might change the magnetic properties of the soft layer which could lead to a lower perpendicular coercivity of the harder layer.

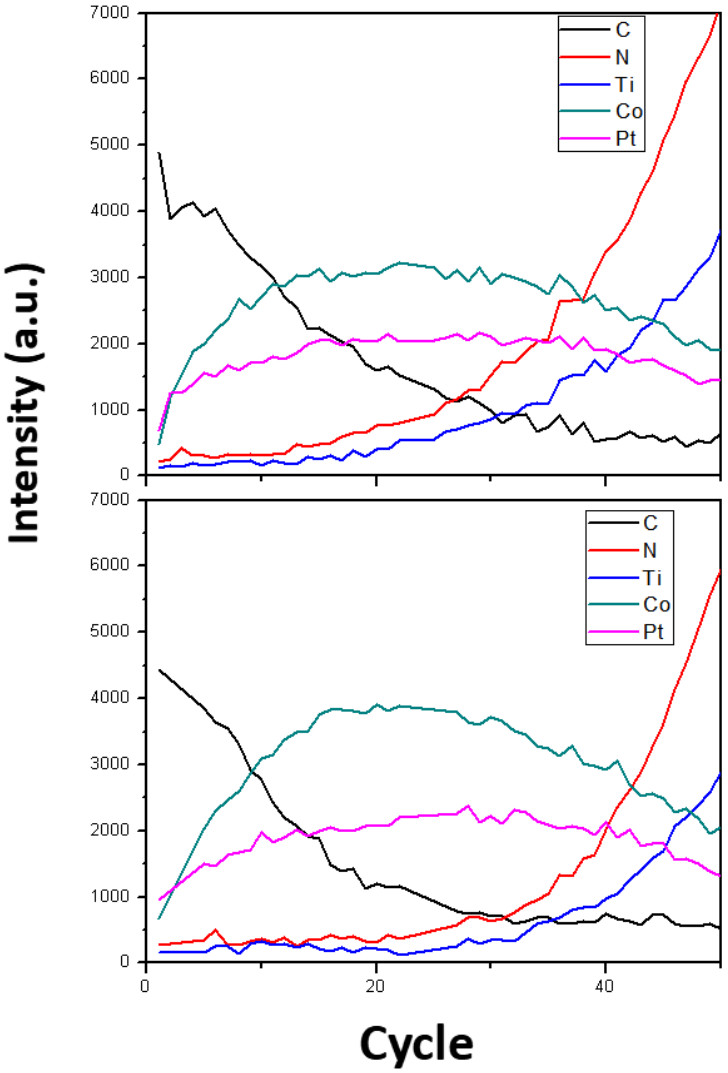

FIGURE 5.11: Auger results of 5 nm base layer with 2.5 nm soft layer of CoPt deposited at (top) room temperature, (bottom) 100 °C.

5.4 Intermediate layer effect

5.4.1 Magnetic Properties Measurement

Figure 5.12 exhibits the magnetic hysteresis loops of a 10 nm base layer coupled with 2.5 nm soft CoPt layer with TiN intermediate layer inbetween them. The intermediate layer thickness is varied from 0 to 4 nm in order to control the exchange coupling between the hard and soft layer. The strongest coupling occur when there

is no intermediate layer (Figure 5.12 (a.)) and a reduction in perpendicular coercivity is observed. The perpendicular coercivity decreases the most when a 1 nm TiN intermediate layer is inserted in order to weaken the exchange coupling between the hard and soft layer. However, as the intermediate layer thickness in increased to 2 nm, the magnetic hysteresis loop starts to show steps indicating that the hard and soft layer starts to decouple because the exchange coupling constant is weakened by the thick intermediate layer. The steps become even clearer as the intermediate layer thickness is doubled to 4 nm, where a step could be observed clearly in Figure 5.12 (d.).

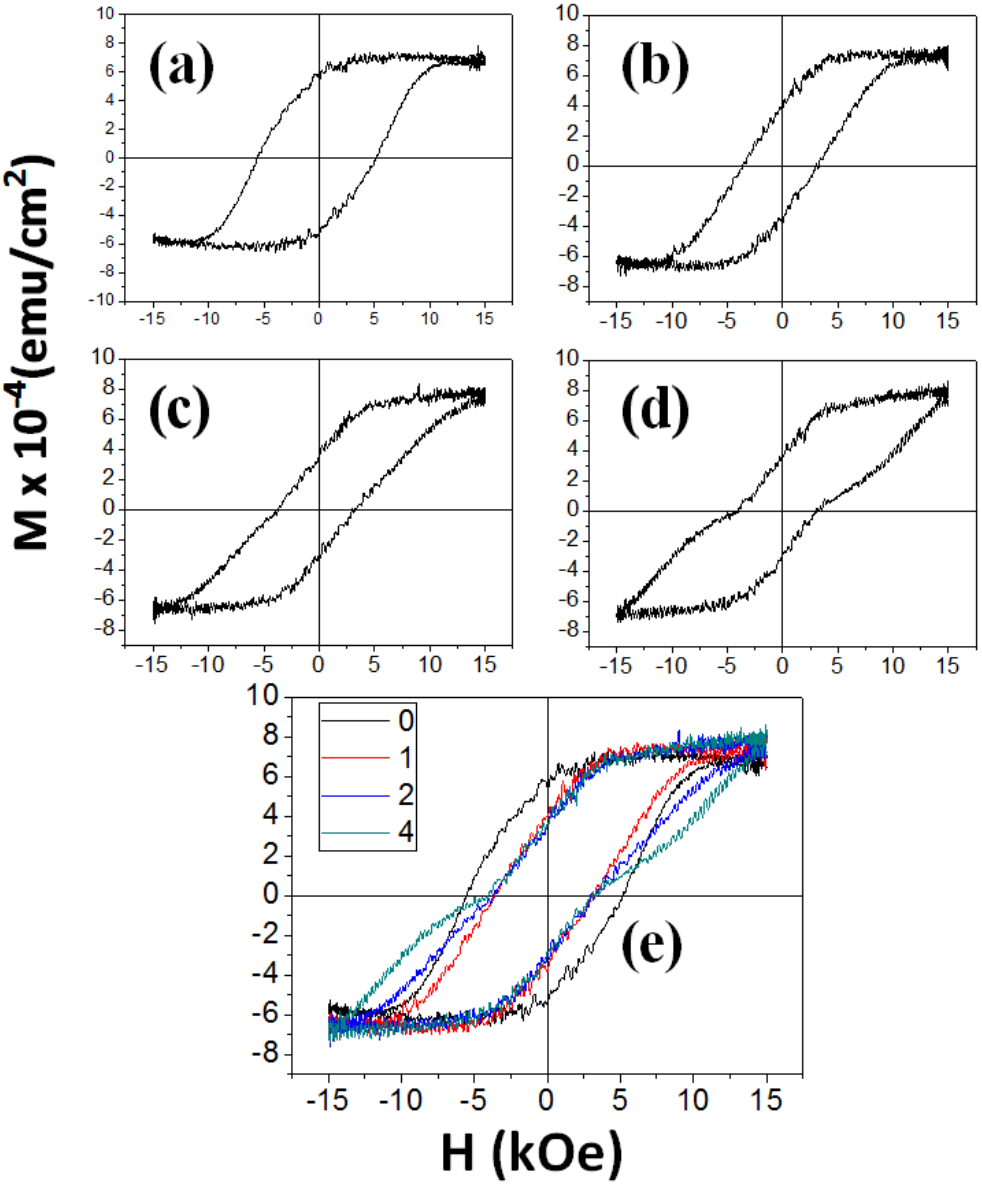

FIGURE 5.12: M-H curves of CoPt/TiN(x nm)/CoPt/TiN samples where x is (a) 0 nm, (b) 1 nm, (c) 2 nm, and (d) 4 nm. Figure (e) is the compilation of all samples in order to compare the shape visually.

An interesting point to note is that even though the H_c is similar for the samples with intermediate layer, the switching field of the hard layer is gradually changed with intermediate layer thickness. The similar value of H_c probably comes from the small part of the hard magnetic layer that is exchange coupled to the soft magnetic layer, and the increase in hard magnetic layer switching field could be imagines as an increase in ratio of decoupled hard magnetic layer thickness compared to the

exchange coupled magnetic layer thickness. As the intermediate layer thickness is increased, more and more part of the hard magnetic layer will be decoupled from the soft magnetic layer and eventually will return to its original switching field. Ferromagnetic coupling between a hard and soft layer in an ECC system are governed by two kinds of interactions.[12] The first one is termed exchange interactions, and it consists of direct exchange interactions (Heisenberg type) for the case of hard/soft layer coupling without interlayer, and the indirect exchange interaction, where an intermediate layer is inserted between the hard and soft layer (RKKY type). The second one is called magnetostatic interaction, and this includes dipolar interaction between the hard layer and soft layer, and the self-demagnetization interaction that occurs in the soft layer. The hard magnetic layer with easy axis of magnetization in the normal direction to the plane contributes little to the magnetostatic field, this is due to the assumption that the in-plane direction is infinitely larger compared to the thickness of the film. Then, by using the formula $H_{\text{demg}} = 4Ms$, we could estimate that the self-demagnetizing field coming from the soft magnetic layer is around 7.5 kOe for A1-CoPt with M_s of 600 emu/cm^3. This self-demagnetizing field is stronger than the dipolar field coming from the hard magnetic layer, thus it is energetically favorable for the magnetic moment in the soft magnetic layer to be aligned along the in-plane direction instead of the out-of-plane direction. Therefore, the general assumption here is that the magnetostatic interaction is negatively affecting the perpendicular ferromagnetic coupling and the only driving force for the perpendicular magnetic coupling comes from the Heisenberg exchange interaction for sample without intermediate layer and RKKY exchange interaction for the samples with intermediate layer.

In order to study how the perpendicular coercivity of the hard magnetic layer is affected by the intermediate layer thickness, the relationship between the switching field, H_{sw}, and the intermediate layer thickness is plotted in Figure 5.11. It could be observed that there is a local minimum point where the switching field of the hard magnetic layer is reduced the most when a 1 nm TiN layer is introduced as an intermediate layer. As the intermediate layer thickness is increased to 2 and 4 nm, the switching field of the hard magnetic layer grows even larger than when the hard/soft layer is directly exchange coupled. The switching field tends to return

to its original perpendicular coercivity of a single hard magnetic $L1_0$-CoPt in this experiment.

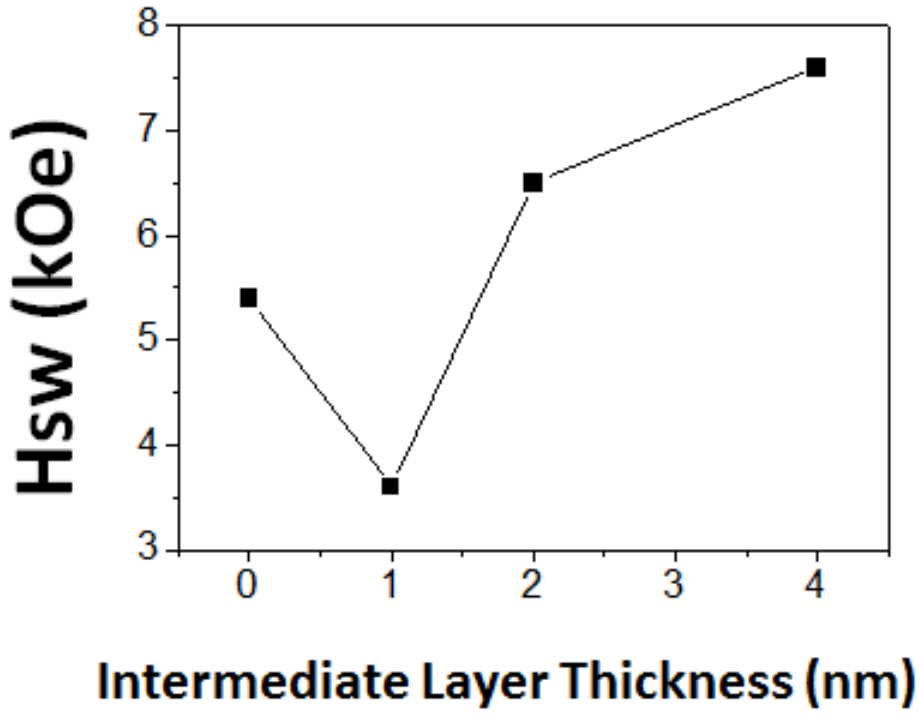

FIGURE 5.13: Switching field vs. intermediate layer thickness of TiN.

The behavior of the switching field when the interlayer thickness is changed could be described by the following concept. ECC media is greatly affected by the ferromagnetic coupling strength between the hard magnetic layer and the soft magnetic layer. The exchange coupling strength has a sweet spot where the magnetic moment in the soft magnetic phase switches earlier than the soft magnetic phase under the influence of an external magnetic field. As the spins in the soft magnetic phase is reversed, they began to exert a exchange coupling field to the spins in the hard magnetic phase along the direction of the external magnetic field, thus helping to reverse the hard magnet spins and a reduction in the switching field of the hard layer could be achieved. However, this sweet spot of the exchange coupling strength depends on a lot of parameters between the soft layer and the hard layer. This includes the ratio of saturation magnetization, ratio of volume, and the magnetic anisotropy constant of the hard magnetic phase. In this study, the exchange

coupling strength between the hard and soft CoPt layer seems to be stronger than the optimum exchange coupling strength. This could be seen from the larger switching field of the hard layer when no intermediate layer is inserted between the hard and soft layer. After 1 nm of TiN intermediate layer is introduced, the exchange coupling strength is weakened up to a certain optimum point where the spins inside the soft magnetic layer are reversed earlier than the spins in the hard magnetic layer and the additional exchange coupling field along the external magnetic field will make switching of the hard magnetic layer easier. However, when the TiN intermediate layer thickness is increased to 2 and 4 nm, the exchange coupling strength grows too weak and unable to overcome the demagnetizing field of the soft layer that the two layers eventually become decoupled from each other. The decoupling of these two layers lead to an increase in the switching field of the hard magnetic phase up to the original coercivity of the single layer hard magnetic phase layer.

5.4.2 Exchange Coupling Strength Calculation

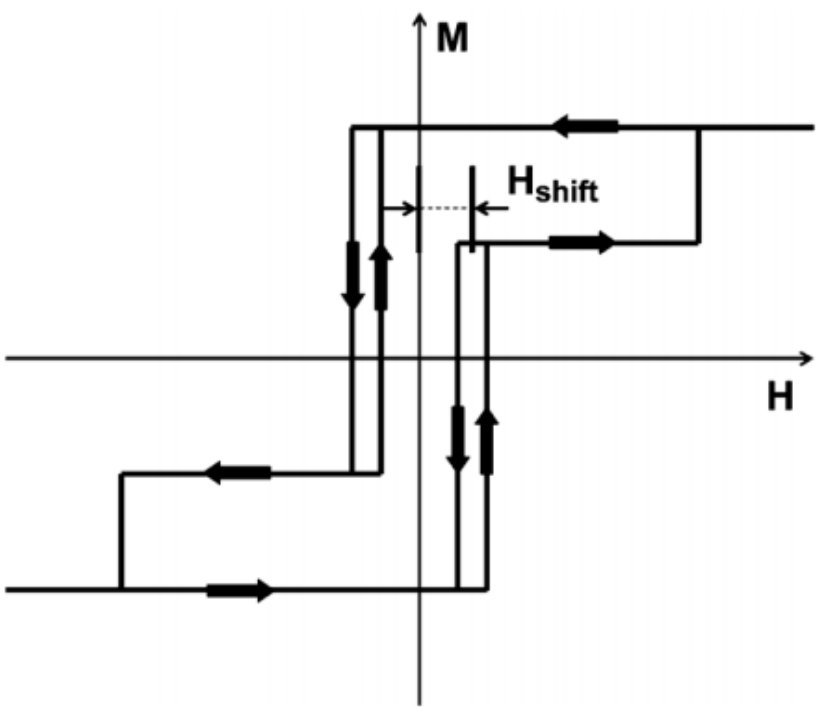

FIGURE 5.14: Illustration of an ideal M-H loop with a shift in the coercivity of the minor loop. Figure adapted from [13].

The exchange coupling strength could be estimated by calculating the interlayer exchange coupling energy, E_c. E_c is generally used in order to calculate the exchange coupling strength between two layers separated by a segregant layer as a function of segregant thickness and has been defined as [14]

$$\begin{aligned} E_c &= -J_1 \frac{M_1 \cdot M_2}{|M_1| \cdot |M_2|} - J_2 \left(\frac{M_1 \cdot M_2}{|M_1| \cdot |M_2|} \right)^2 \\ &= -J_1 \cos(\Delta\varphi) - J_2 [\cos(\Delta\varphi)]^2 \end{aligned} \tag{5.1}$$

where E_c is the interlayer exchange coupling energy and $\Delta\varphi$ is the angle between the magnetizations of the films in which an intermediate layer is inserted. J_1 and J_2 are variables that describe the strength and type of exchange coupling between the films. If J_1 is larger, then the coupling is ferromagnetic in nature when J_1 is positive and antiferromagnetic if J_1 is negative. Likewise if J_2 is larger, then the coupling is antiferromagnetic in nature when J_2 is positive and ferromagnetic if J_2 is negative. For a multi-layered structure coupled across a non-magnetic intermediate layer with two similar CoPt magnetic films of the same thickness d, magnetization M, and uniaxial anisotropy constant K_u, the total Zeeman energy is given by [4, 15]

$$\begin{aligned} E_{tot} = &-M_1 H d_1 \cos(\varphi_1) - M_2 H d_2 \cos(\varphi_2) + d_1 K_{u1} \sin^2(\varphi_1) \\ &+ d_2 K_{u2} \sin^2(\varphi_2) - J_{ex} \cos(\varphi_1 - \varphi_2) \end{aligned} \tag{5.2}$$

where subscript 1 represents the upper film and subscript 2 represents the lower film and φ_1 and φ_2 are the angles between the film magnetization and the field direction. For a given external field, we can find the orientation of the magnetization for the coupled structure by finding the minimum of (2) as a function of φ_1 and φ_2. If we minimize the total energy of the system and assume the top and bottom layers of CoPt are ferromagnetically coupled ($\varphi_1 = \varphi_2$), the dependence on an external field of the double layer with magnetic films of equal thickness d and magnetization M is

given by [14]

$$\frac{dE_{\text{tot}}}{d\varphi_1} = M_1 H d_1 \sin(\varphi_1) + 2 d_1 K_{\text{u1}} \sin(\varphi_1)\cos(\varphi_1)$$
$$\frac{dE_{\text{tot}}}{d\varphi_2} = M_2 H d_2 \sin(\varphi_2) + 2 d_2 K_{\text{u2}} \sin(\varphi_2)\cos(\varphi_2)$$

if $\varphi_1 = \varphi_2$ and $K_{\text{u1}} = K_{\text{u2}}$

$$M_1 H d_1 = M_2 H d_2 \tag{5.3}$$

If we define a coupling field H_{shift} which is related to the interlayer exchange coupling energy E_c, H_{shift} can be experimentally obtained by measuring the shift of the reversal field of the hysteresis loop from the top soft CoPt layer as seen in Fig. 4.14 The interlayer coupling energy is calculated according to [15–17]

$$\begin{aligned} E_{\text{c}} &= H_{\text{shift}} M_{\text{s, soft}} d_{\text{soft}} \\ &= (H_{\text{r}} - H_{\text{r,0}}) M_{\text{s, soft}} d_{\text{soft}} \end{aligned} \tag{5.4}$$

where $M_{\text{s, soft}}$ is the saturation magnetization (CoPt: 600 emu/ cc), $H_{\text{r,0}}$ is the coercivity of the top CoPt layer ($\sim$ 10 Oe) without interlayer coupling, H_{r} is the reversal field with the interlayer exchange coupling and d_{soft} is the thickness (2.5 nm) of the soft top CoPt layer. For each intermediate layer material, there is a particular critical thickness when the upper and lower layers have the same reversal field and measuring a shift in the minor loop becomes impossible. In this case, by using (3), the interlayer coupling energy can be estimated from the decrease in the reversal field of the major loop. If we equate the interlayer exchange coupling energy and the total Zeeman energy difference between the stepped hysteresis loops in the absence and presence of the interlayer coupling and neglect the uniaxial anisotropy term, can be calculated as [16–18]

$$E_{\text{c}} = (H_{\text{r, 0}} - H_{\text{r}}) M_{\text{s, hard}} d_{\text{hard}} \tag{5.5}$$

where $H_{r,0}$ is the coercivity of the bottom CoPt layer (5.5 kOe) without interlayer coupling and H_r is the reversal field with the interlayer exchange coupling.

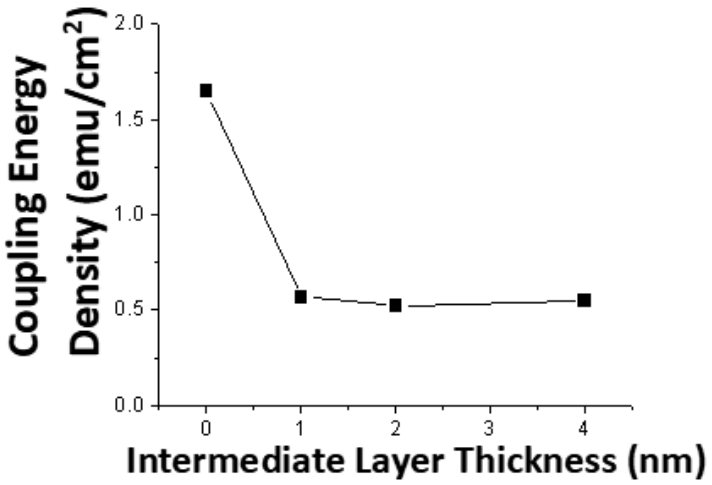

FIGURE 5.15: $L1_0$-CoPt/A1-CoPt exchange coupling energy density.

The dependence of the exchange coupling energy density on the intermediate layer thickness was illustrated by varying the thickness of the intermediate layer from 0 nm to 4 nm and is shown in Fig. 4.17. It is observed that as the thickness of the interlayer is decreased, the exchange coupling energy increased, which is consitent with the result of the M-H loops of $L1_0$-CoPt/A1-CoPt in Figure 5.12. When the intermediate layer thickness is 1 nm, the exchange coupling density reached its critical value at 0.57 emu/cm^2 as determined from equation 5.5.

5.4.3 Summary

Control of perpendicular coercivity of magnetically hard CoPt has been achieved by depositing a magnetically soft CoPt layer on top. It has been found that at the thickness of 5 up to 10 nm, the magnetically hard layer does not significantly affect the exchange coupling between the hard/soft layer, on the other hand it is apparent that the thickness of the soft layer is important in determining the exchange coupling of the hard/soft layer and thus controlling the perpendicular coercivity. By coupling a 2.5 nm soft CoPt layer on top of hard CoPt layer, the perpendicular coercivity could be reduced from around 11 kOe to around 6 kOe while maintaining a good M_r/M_s ratio. This study also noted that the depositing the soft layer at higher temperature

(100 ^{o}C) also affect the magnetic properties of the hard layer, even though when the temperature is increased further to 300 ^{o}C, the magnetic properties does not change significantly. Due to the high ordering temperature of CoPt, the soft layer should remain in the disordered state and the magnetic anisotropy would not change due to ordering transformation. However, at elevated temperature, the distribution of the Co and Pt atoms inside the film is found to be fundamentally different compared to room temperature samples. When deposited at 100, 200, and 300 ^{o}C, the Co atoms tend to be concentrated at the bottom of the soft layer and this difference in density distribution changed the magnetic properties of the soft layer, and hence the hard/soft exchange coupling. Finally, the hard/soft exchange coupling strength is controlled further with the introduction of a TiN intermediate layer. By introducing the intermediate layer it is observed that the exchange coupling energy is reduced from around 1.6 emu/cm^2 to a critical value of 0.57 emu/cm^2 when the intermediate layer is at 1 nm. Therefore, by varying the soft layer thickness, soft layer deposition temperature, and intermediate layer insertion the perpendicular coercivity of a magnetically hard CoPt layer could be controlled while maintaining the thermal stability.

Bibliography

[1]H. J. Richter, J. Phys. D: Appl. Phys. **40**, R149–R177 (2007).

[2]F. B. Hagedorn, J. Appl. Phys. **41**, 2491–2502 (1970).

[3]R. H. Victoria, and X. Shen, IEEE Trans. Magn. **41**, 537–542 (2005).

[4]J. P. Wang, W. K. Shen, and J. M. Bai, IEEE Trans. Magn. **41**, 3181–3186 (2005).

[5]D. Suess, T. Schrefl, S. Fahler, M. Kirschner, G. Hrkac, and F. Dorbauer, Appl. Phys Lett. **87**, 012504 (2005).

[6]A. Y. Dobin, and H. J. Richter, J. Appl. Phys. **101**, 09K108 (2007).

[7]F. Casoli, L. Nasi, F. Albertini, S. Fabbrici, C. Bocchi, F. Germini, P. Luches, A. Rota, and S. Valeri, J. Appl. Phys. **92**, 142506 (2008).

[8]D. Goll, and A. Breitling, J. Appl. Phys. **104**, 083903 (2008).

[9]J. F. Hu, J. S. Chen, Y. F. Ding, B. C. Lim, P. W. Lwin, and B. Liu, IEEE Trans. Magn. **44**, 3547–3549 (2008).

[10]T. J. Zhou, B. C. Lim, and B. Liu, Appl. Phys. Lett. **94**, 152505 (2009).

[11]Y. K. Takahashi, K. Hono, S. Okamoto, and O. Kitakami, J. Appl. Phys. **100**, 074305 (2006).

[12]W. K. Shen, and J. P. Wang, J. Appl. Phys. **100**, 096113 (2006).

[13]S. D. Granz, and M. H. Kryder, IEEE Trans. Magn. **48**, 2746 –2748 (2012).

[14]P. Grunberg, and U. Hartmann, *Magnetic multilayers and giant magnetoresistence* (Springer, 2000), p. 52.

[15]A. Yelon, *Physics of thin films*, Vol. 6 (New York: Academic, 1971), p. 216.

[16]V. Sokalski, D. Laughlin, and J. Zhu, Appl. Phys. Lett. **95**, 102507 (2009).

[17]V. Sokalski, D. Laughlin, and J. Zhu, IEEE Trans. Magn. **46**, 2260 (2010).

[18]P. Heijden, P. Bloemen, J. Metselaar, R. Wolf, J. Gaines, J. van Eemeren, P. Zaag, and W. de Jonge, Phys. Rev. B **55**, 11569 (1997).

Chapter 6

Conclusions

This thesis has described the study of the magnetic properties and microstructure of CoPt/TiN thin films deposited on glass and single crystal MgO (001) substrates under Nitrogen and Argon gas flow ratio. The experiments involve systematically varying the Nitrogen gas flow ratio, annealing temperature, and CoPt thickness to study their effects in both CoPt/TiN bilayer films and CoPt/TiN/CoPt trilayer films. Ordering transformation in CoPt films have been achieved at a lower temperature and at a higher level of ordering parameter by controlling the annealing temperature and the Nitrogen gas flow ratio during the deposition.

Ordering transformation of $L1_0$-CoPt occurs at higher temperature due to the slow diffusion speed of both the Co and Pt atoms that it requires higher energy in order to order the atoms. This diffusion speed is affected by both the post-deposition annealing temperature and the ease of diffusion of the atoms. By characterization of the magnetic properties through the use of vibrating sample magnetometer, the optimum condition for a $L1_0$-CoPt deposited on glass substrate has been determined. Post deposition annealing at 700^{o}C is needed in order to get a good ordering parameter, on the other hand the incorporation of 50% Nitrogen gas flow ratio during the deposition is crucial in order to lower the ordering temperature of the $L1_0$-CoPt.

By standardizing the deposition of the CoPt films on the previously mentioned parameters, the underlying effect of Nitrogen incorporation during the deposition on the ordering temperature of CoPt is studied by depositing the CoPt/TiN layer on MgO substrate. It is observed that the TiN under layer plays a huge part in determining the nature of nitrogen incorporation inside the CoPt film. Without TiN under layer, the CoPt grows coherently on top of the single crystal MgO substrate.

However the larger lattice parameter of the MgO induces a huge strain on the CoPt layer. The tensile strain that was introduced is beneficial for the $L1_0$-CoPt formation due to two reasons. The first one is that the as-deposited A1-CoPt will have its lattice size more similar to $L1_0$-CoPt due to in-plane tensile strain. The second one is due to the rotation of the $L1_0$-CoPt c-axis towards the perpendicular direction during the post-annealing process. The addition of Nitrogen gas flow during the deposition will worsen the magnetic properties mainly due to the relaxation of said tensile strain in the CoPt film. The Nitrogen atoms will be incorporated inside the thin film, enhancing the lattice parameter and reducing the lattice mismatch between the two film which is the main source of the tensile strain energy inside the film. For samples deposited on MgO with TiN intermediate layer, the growth method is mostly incoherent and the tensile strain would be non existent inside the CoPt film. However, in this case the introduction of Nitrogen gas flow during the deposition does increase the $L1_0$-CoPt ordering transformation during the post-deposition annealing process. This is due to the formation of superabundant vacancies due to incorporation of Nitrogen atoms inside the CoPt lattice. The bonds between Nitrogen atoms and vacancies will lower the total formation energy of new vacancies inside the lattice and hence, more vacancies are formed in CoPt lattice with Nitrogen compared to normal CoPt lattice. This lattice will improve the diffusivity of Co and Pt atoms and thus it would be easier for the A1-CoPt to transform into $L1_0$-CoPt.

The effect of CoPt thickness when deposited on MgO single crystal substrate with TiN under layer has also been investigated in this thesis. It has been observed in the previous chapter that the growth of CoPt on MgO single crystal substrate with TiN under layer is of the incoherent growth. This could be explained from two phenomena. The first one is the low contact angle between the TiN and CoPt that let the CoPt grows as a continuous thin film instead of the island growth. The second one is the large lattice mismatch between TiN and CoPt that leads to a high strain energy inside the film. The thickness of CoPt was fixed at 10 nm while the TiN was fixed at 40 nm, and the orientation of both is the same in the (001) direction. Thus, it could be assumed that the 10 nm of CoPt was too thick for the epitaxial growth to be sustained. The large thickness and the good wetting contact angle between CoPt and TiN will cause the CoPt film to grow incoherently to relax the tensile strain inside

the film. When the thickness of CoPt is reduced to 2.5 nm, it is more possible for the CoPt to sustain the coherent growth on top of the TiN layer. This coherent growth leads to tensile strain inside the CoPt layer and the A1-CoPt lattice will be strained in the in-plane direction such that the dimensions are similar to that of the $L1_0$-CoPt lattice. The formation of face centered tetragonal disordered lattice is observed to be sufficient to break the symmetry of the lattice and a magnetocrystalline anisotropy could be obtained from the disordered lattice.

From the previous two chapters, two methods of obtaining CoPt film with high magnetocrystalline anisotropy have been described. This CoPt film is a promising media to obtain stability in small magnetic bits, however the challenge to improve the writability still remains. In this study a method of using the same material in order to ease the writability of the hard CoPt phase has been systematically studied by depositing a magnetically soft layer of CoPt on top of a magnetically hard CoPt layer obtained from the previous two chapters. The experiment is done by changing the hard CoPt layer thickness, soft CoPt layer thickness, soft CoPt layer deposition temperature, and TiN intermediate layer thickness. When the hard CoPt layer thickness is set to 10 nm, part of the film stays in the disordered phase due to a change in growth orientation from (001) in the bottom part to (111) in the upper part of the film. As the thickness is reduced to 5 nm, most of the film is transformed into the $L1_0$-CoPt and thus it is easier to predict the reduction of switching field by calculation. The thickness of the soft CoPt layer has been found to affect the switching field significantly. When a 2.5 nm thick soft CoPt layer is deposited on top of a hard layer, the switching field is reduced roughly by half. Furthermore, this reduction keeps increasing as the soft layer thickness is increased up to 10 nm, over which the switching field reduction reaches a saturation point. The soft CoPt layer also gives the optimum switching field reduction when the deposition temperature is at an elevated temperature. The reason is due to an internal density change inside the elevated temperature deposited film that causes the soft layer to have lower anisotropy compared to the room temperature deposited soft CoPt layer. Finally, the addition of an intermediate TiN layer has been proven to be able to tune the exchange coupling energy between the hard/soft CoPt layer. When a 1 nm thick TiN intermediate layer is inserted between the hard/soft CoPt layer, the exchange coupling energy is

reduced to 0.57 emu/cm^2 and the switching field is reduced to around 3.5 kOe. This experiment proves that thermally stable and small magnetic bits are feasible by using CoPt thin films, while coupling it with a magnetically soft CoPt will ease the writability of the hard CoPt layer. Since only CoPt films are used as the base of the magnetic thin film, simple equipment is capable of reproducing our study, and this could be a good method to manufacture CoPt films for future high density magnetic recording media.